



NATIONAL AND KAPODISTRIAN UNIVERSITY OF ATHENS

**SCHOOL OF SCIENCE
DEPARTMENT OF INFORMATICS AND TELECOMMUNICATIONS**

**POSTGRADUATE PROGRAM
"SPACE TECHNOLOGIES, APPLICATIONS AND SERVICES"**

MSc THESIS

**Use and assessment of remote sensing for the safety of
maritime shipping**

Ioannis I. Venieris

Supervisor: Konstantinos Kartalis, Professor

ATHENS

NOVEMBER 2022



ΕΘΝΙΚΟ ΚΑΙ ΚΑΠΟΔΙΣΤΡΙΑΚΟ ΠΑΝΕΠΙΣΤΗΜΙΟ ΑΘΗΝΩΝ

**ΣΧΟΛΗ ΘΕΤΙΚΩΝ ΕΠΙΣΤΗΜΩΝ
ΤΜΗΜΑ ΠΛΗΡΟΦΟΡΙΚΗΣ ΚΑΙ ΤΗΛΕΠΙΚΟΙΝΩΝΙΩΝ**

**ΠΡΟΓΡΑΜΜΑ ΜΕΤΑΠΤΥΧΙΑΚΩΝ ΣΠΟΥΔΩΝ
"ΔΙΑΣΤΗΜΙΚΕΣ ΤΕΧΝΟΛΟΓΙΕΣ, ΕΦΑΡΜΟΓΕΣ ΚΑΙ ΥΠΗΡΕΣΙΕΣ"**

ΔΙΠΛΩΜΑΤΙΚΗ ΕΡΓΑΣΙΑ

**Χρήση και αξιολόγηση της δορυφορικής τηλεπισκόπησης
για την ασφάλεια της ναυτιλίας**

Ιωάννης Ι. Βενιέρης

Επιβλέπων: Κωνσταντίνος Καρτάλης, Καθηγητής

ΑΘΗΝΑ

ΝΟΕΜΒΡΙΟΣ 2022

MSc THESIS

Use and assessment of remote sensing for the safety of maritime shipping

Ioannis I. Venieris

S.N.: SR2190013

SUPERVISOR:

Konstantinos Kartalis, Professor

**EVALUATION
COMMITTEE**

**Alexandros Kolovos, Associate Professor
Konstantinos Filippopoulos, Professor**

November 2022

ΔΙΠΛΩΜΑΤΙΚΗ ΕΡΓΑΣΙΑ

Χρήση και αξιολόγηση της δορυφορικής τηλεπισκόπηση για την ασφάλεια της ναυτιλίας

Ιωάννης Ι. Βενιέρης

A.M.: SR2190013

ΕΠΙΒΛΕΠΩΝ:

Κωνσταντίνος Καρτάλης, Καθηγητής

ΕΞΕΤΑΣΤΙΚΗ ΕΠΙΤΡΟΠΗ:

Αλέξανδρος Κολοβός, Αναπληρωτής Καθηγητής
Κωνσταντίνος Φιλιππόπουλος, Καθηγητής

Νοέμβριος 2022

ABSTRACT

In recent decades there has been a growing interest in the use of satellite remote sensing to protect shipping from dangers that lie ahead and cannot be observed with the human eye. Its contribution is significant, considering the economic, (geo)political and social impact of shipping globally. In the context of this work, the applications and algorithms for processing satellite images are simulated through the functional program SNAP.

First, there is a historical review of the beginnings of commercial shipping until today and some of the difficulties facing shipping today are mentioned. The sensors on satellites used for satellite remote sensing and ESA's missions supporting marine remote sensing are analyzed, as well as the Copernicus program of the European Union.

Subsequently, an epigrammatic bibliographic description of SAR and optical data processing techniques is developed with a focus on innovative procedures and research.

Then, the simulation model is investigated and appropriate parameters and variables are defined in the SNAP software based on the references from the available literature. Some of the popular supervised and unsupervised classification algorithms are tested, as well as applications from the toolbox. At the end of each simulation, the QGIS program is applied to visualize the results on the Earth map.

Finally, based on the results of the simulation, the considered environments are analyzed, as well as observations and conclusions obtained during the preparation of this work, and we arrive at important conclusions for satellite remote sensing regarding its usefulness in maritime shipping.

SUBJECT AREA: Remote sensing and image processing

KEYWORDS: maritime shipping, data processing, simulation model, SNAP software, QGIS software

ΠΕΡΙΛΗΨΗ

Τις τελευταίες δεκαετίες υπάρχει αυξανόμενο ενδιαφέρον ως προς τη χρήση δορυφορικής τηλεπισκόπησης για την προστασία της ναυσιπλοΐας από κινδύνους που ελλοχεύουν και δεν μπορούν να παρατηρηθούν με το ανθρώπινο μάτι. Η συμβολή της είναι μεγάλη, αναλογιζόμενοι τον οικονομικό, (γεω)πολιτικό και κοινωνικό αντίκτυπο της ναυτιλίας στον κόσμο. Στο πλαίσιο της παρούσας εργασίας, προσομοιώνονται οι εφαρμογές και οι αλγόριθμοι επεξεργασίας δορυφορικών εικόνων μέσα από το λειτουργικό πρόγραμμα SNAP.

Αρχικά γίνεται μια ιστορική αναδρομή στις απαρχές της εμπορικής ναυσιπλοΐας μέχρι σήμερα και αναφέρονται κάποιες από τις δυσκολίες που αντιμετωπίζει η ναυτιλία σήμερα. Αναλύονται οι αισθητήρες των δορυφόρων που χρησιμοποιούνται για τη δορυφορική τηλεπισκόπηση και οι αποστολές της ESA που συνδράμουν στη θαλάσσια τηλεπαρατήρηση, καθώς και το πρόγραμμα Copernicus της Ευρωπαϊκής Ένωσης.

Εν συνεχεία, αναπτύσσεται επιγραμματική βιβλιογραφική περιγραφή των τεχνικών επεξεργασίας SAR και οπτικών δεδομένων με επίκεντρο μελέτης καινοτόμες διαδικασίες και έρευνες.

Έπειτα, ερευνάται το μοντέλο προσομοίωσης και ορίζονται κατάλληλες παράμετροι και μεταβλητές στο λειτουργικό SNAP βάσει των αναφορών από τη διαθέσιμη βιβλιογραφία. Δοκιμάζονται μερικοί από τους διαδεδομένους αλγορίθμους επιβλεπόμενης και μη επιβλεπόμενης ταξινόμησης, καθώς και εφαρμογές από την εργαλειοθήκη. Στο τέλος κάθε προσομοίωσης εφαρμόζεται το πρόγραμμα QGIS για την οπτικοποίηση των αποτελεσμάτων στον χάρτη της Γης.

Τελικά, βάσει των αποτελεσμάτων της προσομοίωσης, αναλύονται τα εξεταζόμενα περιβάλλοντα, όπως και παρατηρήσεις που προέκυψαν κατά την εκπόνηση της παρούσας εργασίας και καταλήγουμε σε σημαντικά για την δορυφορική τηλεπισκόπηση συμπεράσματα σχετικά με την χρησιμότητά της στη ναυτιλία.

ΘΕΜΑΤΙΚΗ ΠΕΡΙΟΧΗ: Δορυφορική Τηλεπισκόπηση και επεξεργασία εικόνων

ΛΕΞΕΙΣ ΚΛΕΙΔΙΑ: Ναυτιλία, λειτουργικό SNAP, QGIS τεχνικές επεξεργασίας, μοντέλο προσομοίωσης

*We dedicate this master thesis to our families that have supported us in every way
throughout our studies.*

ACKNOWLEDGMENTS

For the preparation of this Master Thesis, I would like to thank the supervisor Professor Konstantinos Kartalis, for his time and co-operation and Professor Antonis Paschalis for the valuable motivation that gave me to conduct this thesis. I would also like to thank ESA for the generous contribution of free access data.

CONTENTS

PREFACE	24
1. INTRODUCTION.....	25
1.1 The impact of maritime transport.....	25
1.2 The challenges of maritime trade in modern world	26
1.3 Major shipping obstacles.....	27
1.3.1 Wind speed and direction.....	27
1.3.2 Ice cover variability in navigation channels.....	28
1.3.3 Oil spill detection	29
1.3.4 Presence of dangerous cargoes	30
1.4 Purpose of this thesis	31
1.5 Remote sensing in general	31
1.5.1 Active sensors.....	31
1.5.2 Passive sensors	32
1.6 Remote sensing platforms.....	32
1.7 Space missions associated with ocean observation.....	34
1.7.1 GOCE and SMOS satellites	35
1.7.2 Cryosat.....	36
1.8 Copernicus program	37
1.8.1 Sentinel missions	37
1.8.2 The Copernicus services.....	40
2. LITERATURE REVIEW.....	42
2.1 Review of oil spill and remote sensing capabilities.....	42
2.1.1 Polarization modes.....	42
2.1.2 Approach 1: SNAP - Oil spill detection	43
2.2 Studying of sea ice variability and type	44
2.2.1 Methods for sea ice type examination	44
2.3 Literature review of wind direction and speed estimation	45
2.3.1 Approach with SNAP – Wind field estimation	46
2.4 Ship detection for identification of dangerous cargoes	47
2.4.1 Review of previous studies	47

2.4.2	Approach with SNAP – Ocean object detection tool.....	48
3.	1ST SIMULATION DESIGN	49
3.1	1st Scenario: Oil spill mapping	49
3.1.1	Data download – Onda Dias	49
3.1.2	Exploration of data and pre-processing	50
3.1.3	Image processing with graph builder	52
3.1.4	Speckle filtering and threshold method.....	54
3.1.5	Final step, color manipulation	56
3.1.6	Extra step – Visualization in QGIS.....	57
3.2	2st Scenario: Ice cover variability	59
3.2.1	Data download – Copernicus Open Access Hub.....	59
3.2.2	Exploration of data and pre-processing	60
3.2.3	Unsupervised Classification	64
3.2.4	Supervised Classification	65
3.2.5	Extra step – Visualization in QGIS.....	69
4.	2ND SIMULATION DESIGN	70
4.1	3rd Scenario: Ocean Wind Speed Estimation and Direction.....	70
4.1.1	Data download – Onda Dias	70
4.1.2	Data pre-processing.....	70
4.1.3	Image processing with graph builder	71
4.1.4	Adding the wind field data	73
4.1.5	Vector data visualization in QGIS	73
4.2	4th Scenario: Ship and object detection	76
4.2.1	Data download – Onda Dias	76
4.2.2	Data pre-processing.....	77
4.2.3	Ocean object detection algorithm	78
4.2.4	Vector data visualization in QGIS	80
5.	CONCLUSION	82
5.1	Results	82
5.2	Future studies and analysis	84
	TABLE OF TERMINOLOGY	86
	ABBREVIATIONS – ACRONYMS	87
	REFERENCES.....	89

LIST OF FIGURES

Figure 1: The growth of population, GDP and maritime trade by 2030 [6].	26
Figure 2: Spanish coastline affected by oil spill (Source: www.eea.europa.eu)	27
Figure 3: Wind speed and direction mapping on the Mediterranean Sea	28
Figure 4: Ice on the St Lawrence River, Canada at January 17, 2010 (Source: eoimages.gsfc.nasa.gov)	29
Figure 5: Satellite image of illegal discharge of oily bilge water (Source: www.dw.com)	30
Figure 6: Passive and active remote sensing	32
Figure 7: "Earth Explorers" satellite missions focus on the study of the atmosphere, biosphere, hydrosphere, cryosphere and interior of the Earth and their interactions (Source: www.esa.int)	35
Figure 8: ESA's SMOS mission for ocean salinity (Source: www.esa.int)	36
Figure 9: CryoSat: ESA's Ice Mission (Source: www.esa.int)	36
Figure 10: The six thematic streams of Copernicus services	41
Figure 11: Area of interest, central Persian Gulf southwest of Shiraz town of Iraq as a SAR image.	50
Figure 12: Same image as the previous one as shown with Google Terrain layer.	50
Figure 13: Products downloaded from catalogue.onda-dias.eu	51
Figure 14: Bands file containing the Amplitude VV (vertical-vertical beam), VH (vertical-horizontal beam) band and Intensity VV, VH band.	51
Figure 15: Two different images of Persian Gulf. The left image was taken on May 6, 2022 and the right one on April 24, 2022.	52
Figure 16: Same Images converted to dB to better visualize the extent of oil spill.	52
Figure 17: The completed graph that was used in the image processing toolbox for oil spill detection with 2 range looks.	53
Figure 18: The two images after calibration, ellipsoid correction and land-sea mask and speckle filtering	54
Figure 19: Profile Plot of a line across an oil spill.	55

Figure 20: Six different thresholds, -22dB upper left, -22.5dB upper center, -23dB upper right,	55
Figure 21: The image after the application of an arithmetic mean 5x5 filter.	56
Figure 22: The final product of oil spill mapping.	56
Figure 23: Histogram of pixels with the value of 1.	57
Figure 24: Projected image in the Google terrain map.	57
Figure 25: A closer look to understand the extension of pollution.....	58
Figure 26: Gulf of Bothnia, the narrow shipping route that is used to transfer goods is the area of interest.....	59
Figure 27: Exploring the bands of the 2 products	61
Figure 28: Satellite image of the gulf of Bothnian with 2 different channel combinations. Upper and lower left images are set to B8, B4 and B4 for red, green and blue respectively while upper and lower right images are set to B4, B3 and B2 for red, green and blue respectively. Top images correspond to 22/02/2022 while lower images correspond to 13/10/2021.....	62
Figure 29: The expression that was used in very single band	63
Figure 30: Sentinel 2 MSI False-color Infrared RGB (left), Sentinel 2 MSI Natural Colors RGB (right)	63
Figure 31:EM Cluster Analysis upper left (with 5 clusters), upper mid (with 6 clusters) and upper right (with 7 clusters). K-Means Cluster Analysis lower left (with 5 clusters), lower mid (with 6 clusters) and lower right (with 7 clusters).	64
Figure 32: Histogram of the 2 types of Cluster Analysis for different number of clusters as described for “water”, “new ice”, “thin layer of ice”, “thick ice” and “land” classes.....	65
Figure 33: Different color of polygons reflect different surface type. Brown, Purple, Fern, Red and Green for Water, New Ice, Thin Ice, Thick Ice and Soil respectively.....	66
Figure 34: Color manipulation tab for KNN Classifier	67
Figure 35: KD (upper left), KNN (upper mid), MD (upper right), ML (lower left), RF (lower right)	68

Figure 36: New ice with teal color (upper left), thin layer with blue color (upper right), thick ice with white color (lower left) and the union of the 3 different types of ice (lower right)	69
Figure 37: Strait of Gibraltar as the area of interest.....	70
Figure 38: The SAR image before the batch processing.....	71
Figure 39: A complete graph that was used during the image processing for wind field estimation with a window size of 10.....	72
Figure 40: The final output image for the wind field estimation with 10 km window size on the left and 20 km window size on the right.....	72
Figure 41: Wind direction and speed estimation data presented with red arrows and numeric values for the area of interest in SNAP	73
Figure 42: Vector points projected on a Google Satellite map.....	74
Figure 43: Classified wind speed values	74
Figure 44: The wind field estimation (speed and direction) in QGIS.....	75
Figure 45: Saronic Gulf as the main area of interest of the wider region of Central Greece	76
Figure 46: Four bands available for pre-processing, 2 amplitude VH and VV and 2 Intensity VH and VV respectively.....	77
Figure 47: Specified product subset is selected due to the large processing time that would be needed	77
Figure 48: The result of the ocean object detection algorithm along with the terrain-correction. The red circles represent ships or boats with a target window size of 30. The ship detection points are available only after we add them through the layer manager tool window on the right.....	79
Figure 49: The graph builder tool illustrates the steps and the functions that were used in object and ship detection simulation.....	79
Figure 50: Vector points projected in QGIS on a Google Satellite map. Upper image shows the layer of vector points in a terrain corrected way while the bottom image is a combination of the google satellite map and the vector points.	80
Figure 51: Classified ship size values.....	81

Figure 52: The graduated points were added in the Google Map Terrain to provide the best possible visualization of the detected ships.81

LIST OF TABLES

Table 1: Advantages and disadvantages of remote sensing platforms (Source: astron.com.au).....	34
Table 2: Mission details of Sentinel-1A and Sentinel-1B	38
Table 3: Backscatter values of water, oil-covered water and the SAR noise floor illustrating the improved contrast for oil slick detection (Source: www.nrcan.gc.ca).....	43
Table 4: Product types and processing levels of Sentinel-1A and Sentinel-1B mission.	49
Table 5: Sentinel-2 product types	60
Table 6: Percentages of surface type coverage for different classifier along with the average percentage value	67
Table 7: Distance from average percentage value for KD, KNN and RF.....	68
Table 8: Advantages and disadvantages of each SNAP algorithm.....	83

PREFACE

The current MSc thesis was implemented in the context of the graduate course of studies of the Department of Informatics and Telecommunications of National and Kapodistrian University of Athens, with MSc specialization in Space Technologies, Applications and Services, during the academic year 2021-2022. The scope of this work is the implementation of satellite remote sensing for the calculation and estimation of physical parameters associated with risk for maritime shipping. In particular, through the use of satellite imagery in different spectral regions and the exploitation of the advantages of passive and active remote sensing, the appropriate parameters will be extracted, in order to study the wind speed and direction, the variability of sea ice coverage in marine channels, oil spillages and the presence of dangerous cargoes. As part of the work, Sentinel Application Platform (SNAP) and QGIS will be configured, which based on satellites observations, will contribute to marine navigation. Finally, the thesis will evaluate the applicability of the toolbox to business function depending on the available satellite data and the future satellite missions.

1. INTRODUCTION

The art of navigation was developed from the first western civilizations about 4,000 years ago intended to migrate people to other continents as well as finding a better quality of life. Early sailors used primitive maps in order to guide themselves and observed the position of the Sun and stars to determine their route. They had to rely on those methods to get from A to B while at sea. Another method was to stay close to the shore and follow the shoreline. Seafarers would detect prominent landmarks to determine their progress at sea [1].

Until about the 15th century AD, people were traveling coastal as they could easily predict the course of the winds, calculate the depth of the sea and follow the continental shelf. Techniques and tools of navigation improved after that century and civilizations began to use ships not only for colonization but also for the transportation of goods and materials. They used special patented tools such as astrolabe, sextant, and chip log to calculate latitude and longitude [2], [3].

After World War II, the development of electronic navigation aids progressed quickly. Captains had access to electronic calculators and computers to perform the necessary calculations, and they started to use satellite navigation or global positioning systems to determine their location at sea. Today, navigating during sea voyages is a lot easier than back then. With access to these advanced technological developments, it is much harder for a ship to get lost at sea. Gyroscopic compass, radar, loran and GPS are some of the important navigation advances that were brought in the twentieth century and improved maritime shipping even further [4].

1.1 The impact of maritime transport

Maritime shipping is a fundamental part of world trade that makes its presence felt every day in our lives. Almost the entire economy of our planet is based on the transport of goods and raw materials through commercial sea channels. For the prosperity and sustainable development of economies, efficient shipping mechanisms have been used for decades by most countries, especially in the developing world. It is estimated that about 90% of the global supply chain is supported by the international shipping industry while the remaining 10% is based on rail, air and road transport [5].

Throughout the last three decades, the shipping industry has experienced a flourishing growth in total trade volume. This growing industrialization and liberalization of national economies have fueled free trade and brought a galloping demand for consumer products. Advances in technology have also made shipping an increasingly efficient and fast method of transportation. Numerous benefits of shipping can be listed, but the most important advantage lies in the large capacity of the ships used to transport materials. That being said, many products can be transported at the same time, saving time and money. Figure 1 below shows that seaborne trade is an important factor of world economy, GDP and world population [6].

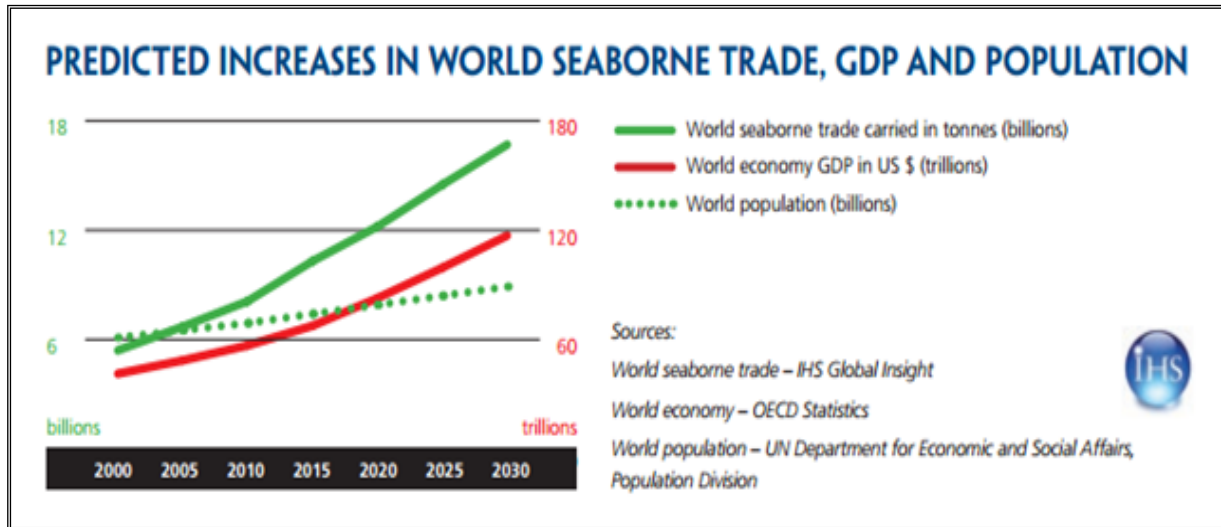


Figure 1: The growth of population, GDP and maritime trade by 2030 [6].

Every day about 55 thousand merchant ships transport their goods to different countries, traveling thousands of miles around the globe. Their technology has been developed so that they can withstand long journeys and have a total capacity of approximately 12,000 TEU (Twenty-foot Equivalent Unit). Their protection is of the utmost importance, for that reason they possess a special automatic identification system (AIS), a tracking system that uses transceivers on ships and is used by vessel traffic services (VTS). Shipping companies in collaboration with telecommunication companies such as exactEarth, ORBCOMM, Spacequest and also government programs, collect data, analyze and process it in order to acquire knowledge about the traffic on the sea routes. They make modifications to voyages, giving shipowners and operators guidance on the most economical voyage, increasing efficiency and reducing voyage time [7].

1.2 The challenges of maritime trade in modern world

Transporting products by sea can be quite difficult, without doubt. Items are often stacked on top of each other, receiving significant pressure and turbulence during the voyage, much more than they receive on planes or trucks. Natural disasters, accidents due to human error or pandemics are non-controllable incidents that cause additional delay and discomfort.

The challenges and the complications are often catastrophic for both shipping and the global economy. For example, Evergreen, one of the largest container ships on March 23, 2021, stuck in the Suez Canal [8], one of the world's most important trading routes, obstructed 300 vessels at both ends of the canal causing decline in the global market. Another instance was the Prestige oil spill that occurred off the coast of Galicia, Spain, caused by the sinking oil tanker MV Prestige in November 2002 (Figure 2). The tanker was hit by a severe storm and was cut in half and as a result, 60,000 tons of oil spilled into the sea, polluting thousands of kilometers of Spanish coastline [9].

Taking into account such serious events, it is necessary to continuously monitor, record and study the course of the vessels as an established method of shipping companies.

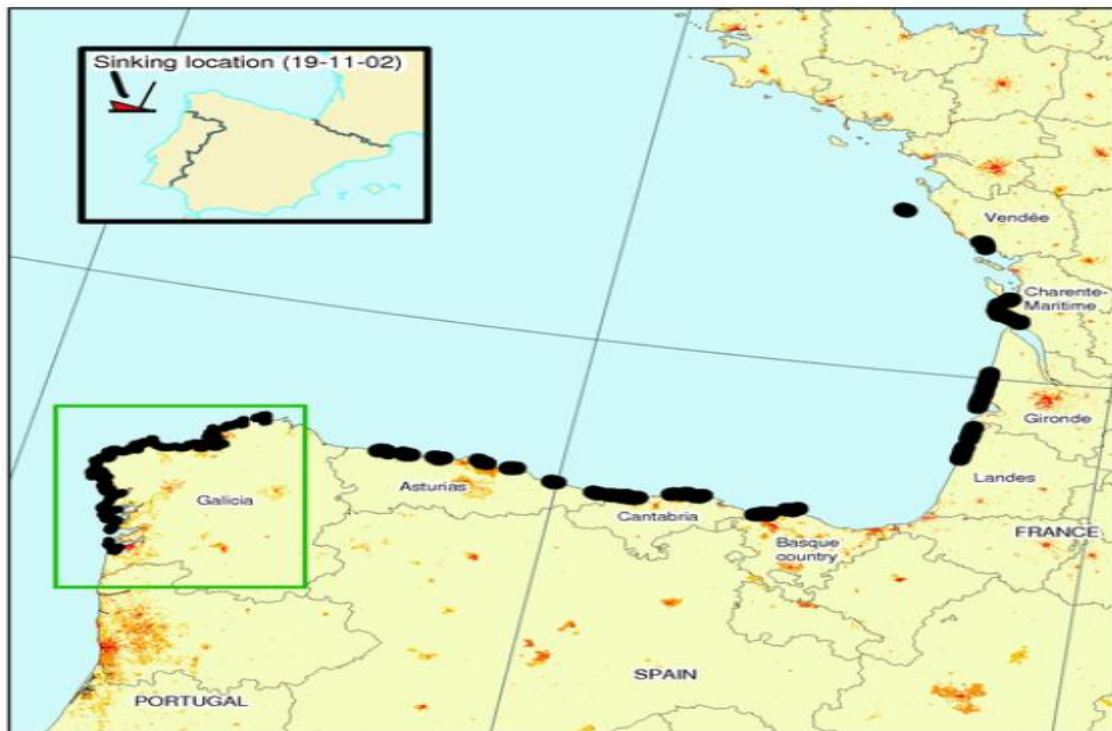


Figure 2: Spanish coastline affected by oil spill (Source: www.eea.europa.eu)

1.3 Major shipping obstacles

In fact, the above accidents could have been avoided by using remote sensing. Processing satellite or aerial images, provides important information about the area of interest, which is none other than maritime transport channels. In this chapter we will mention some of the most important obstacles of navigation and in the following chapters we will learn how to deal with these obstacles using a special toolbox specialized for the processing of satellite and aerial images.

Our contemporary objectives are:

- Wind speed and direction
- ice cover variability in navigation channels
- oil spill and licks
- presence of dangerous cargoes

1.3.1 Wind speed and direction

Near-surface wind speed and direction variability, in particular, are highly related to wind energy applications, coastal erosion where wind changes play a dominant role, the design and construction of buildings where, in addition to the speed of wind, its direction is an

important design parameter, wave propagation patterns, assessment of local extreme oceanic conditions, etc.

Also assessing wind climatology is important for a wide variety of research fields, such as dispersal patterns, air pollution, bird migration routes, biological mechanisms and patterns, weather forecasting along shipping lanes and ship routing optimization, and issues and implications of climate change [10].

Analysis and variability of climate, frequency and intensity of extreme wind events are also important, while linear trends in wind speed can be used as indicators of atmospheric circulation patterns. The composite image in Figure 3 provides examples of satellite-derived maps (of the Mediterranean Sea), in which remote sensing has been used to outline wind speed and direction, pointing to atmospheric forcing of the sea.

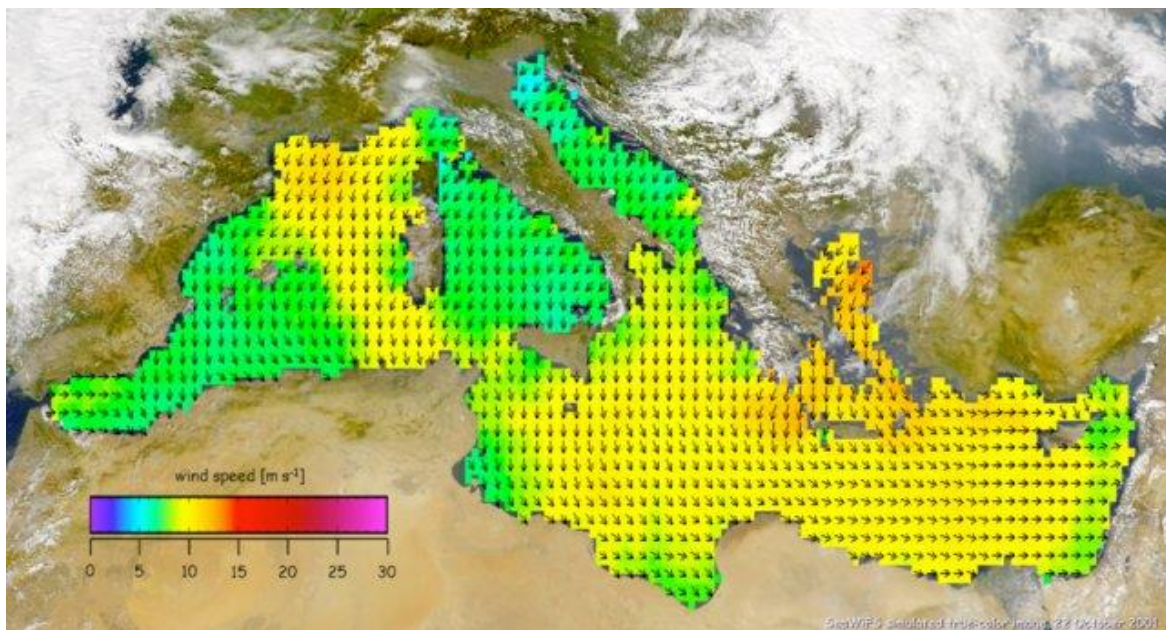


Figure 3: Wind speed and direction mapping on the Mediterranean Sea

1.3.2 Ice cover variability in navigation channels

Sea Ice (SI) is an element of the cryosphere that interchangeably interacts with the ocean and atmosphere. The SI coverage considerably fluctuates within a year. SI monitoring is essential for many environmental applications. Particularly, SI can affect the global climate by altering the surface albedo and reducing solar radiation absorbed by the ocean surface water [11]. Additionally, melting SI, as a freshwater source, changes water constituents and, thus, influences the ocean circulation patterns. SI presence and movement can threaten vessel navigations and impose severe limitations on vessel traffic. Moreover, SI collisions with marine facilities, coastal ports, and oil platforms lead to considerable infrastructure damages.

Freshwater SI also has positive effects on the environment, society, and the economy, particularly along river systems and deltas. Frozen rivers are valuable recreational and cultural resources, for activities such as ice fishing and ice skating, and create important transportation networks among remote communities. Unfortunately, river-ice events, such as ice jams and floods caused by ice cover, can be costly to society and the economy in

many regions throughout the Northern Hemisphere. For example, an ice jam on the St. Lawrence River (QC, Canada) in 1993 lasted for 40 days and cost the Port of Montréal an estimated CDN \$200 million due to the halting of commercial navigation. Figure 4 below shows a thin layer of new ice formed over Québec, Canada's St. Lawrence River in mid-January 2010 [12].



Figure 4: Ice on the St Lawrence River, Canada at January 17, 2010 (Source: eoimages.gsfc.nasa.gov)

1.3.3 Oil spill detection

Ocean Oil Spill (OOS) is a significant environmental problem that endangers the ocean ecosystems through multiple adverse effects. Oil pollution in open waters can be caused due to the ship colliding with obstacles, oil leakage from petroleum tankers, effluents from offshore platforms, industrial plants, pipelines, and refineries [13]. However, OOS is also encountered because many ships illegally dump their used engine oils at night (Figure 5). Despite the primary source of the oil leakage, it is highly required to inspect OOS for further environmental management. In particular, OOS can negatively alter the ocean ecosystem, water quality, and human food chain, as well as bringing economic and environmental damages [14].

In this regard, Ocean Remote Sensing Systems (ORSS) can be an efficient tool because they provide multitemporal observations with broad coverage that can enhance OOS detection and tracking. Spectral information of ORSS data can be integrated with image processing techniques and machine learning algorithms to take the essential information about the OOS [15]. The impact of these daily small oil spills on marine life remains under investigation, as recurrent spills create a form of chronic pollution that can have severe effects on the environment.

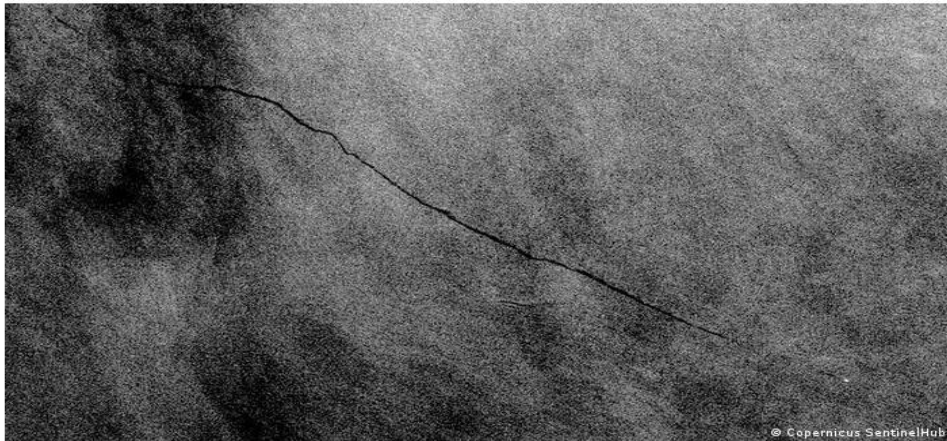


Figure 5: Satellite image of illegal discharge of oily bilge water (Source: www.dw.com)

When oil spills into water, it often interferes with sea shipping routes. The oil from the spill can damage the ships and spread even further. In many cases, ships are ordered to bypass areas affected by spills, but in some others, operators are forced to keep the ship's course unchanged to avoid additional delays.

1.3.4 Presence of dangerous cargoes

Bulk cargoes are a daily challenge for merchant ships, which are obliged to care for their storage in an expert manner to ensure it is discharged in the same state in which it was loaded. The most common loads, such as carbon, sulfur, cotton and fishmeal are easily heated due to the oxidation process that takes place in them, causing unwanted self-ignition. The carbon emits methane, which is flammable and when it comes in contact with air it can form an explosive mixture. Dust generated by certain loads, such as sulfur, poses a risk of explosion. Finally, friction between the cotton bales generates heat and causes spontaneous heat and combustion.

For the safe storage and shipment of solid bulk cargoes, good naval knowledge and ability to minimize and deal with hazards is required, as well as strict fire precautions following the IMSBC (International Maritime Solid Bulk Cargoes) code must be observed. The ships carrying each of these cargo groups are special container vessels, tankers and bulkers respectively. In terms of volumes, dry bulk cargoes represent the largest group estimated to be over 50% of all loaded goods [16] (30% for liquid cargoes and 16% for containers).

The most recent incident during the transport of hazardous materials included but was not limited to, fire and explosion at the Tianjin port that resulted in 165 deaths, 565 injuries, 17000 households being damaged, 779 businesses affected and an estimated total loss of 1.5 billion US dollars. The eruption in Sea Eagle ship which resulted in a mortality and the detriment of the ship in 2003, the burst of Hyundai Fortune in 2006, and a fire and blast on Zim Haifa in 2007. Accidents like these have diverted the government and general public attention to research on risk assessment and accident prevention [17].

1.4 Purpose of this thesis

In this thesis we will assess the obstacles one by one that cause difficulties in maritime shipping to specific areas of interest within specific time intervals. For this purpose, images freely accessible by various organizations and remote sensing companies will be used and the contribution of modern development tools of Earth Observation (EO) in the recording of these phenomena will be studied.

In the next chapter we will conduct a literature survey to scrutinize the studies that have been made on the existing obstacles mentioned above which are the wind speed and direction, ice cover variability in navigation channels, oil spill and leaks, presence of dangerous cargoes. The research that we will conduct is necessary to be placed in the scope together with other relevant research or otherwise to highlight its relation with the existing relevant bibliography.

1.5 Remote sensing in general

Remote sensing is a technique of monitoring the Earth by collecting data to determine the nature and properties of one or more objects in an area of interest, remotely, without physical contact with the objects. This is done either by satellite or by an airplane with integrated sensors, which collect data for the object to be studied. Satellite remote sensing is performed using satellites, and depending on the mission and the nature of the data received, is divided into active and passive. The two main categories are distinguished based on radars and radiometric characteristics that are integrated [18].

1.5.1 Active sensors

When a sensor broadcasts a directed pattern of energy to illuminate a portion of the Earth's surface, it receives the portion scattered back to the instrument. Sensors of that kind are called active microwave sensors, a radar device that records electromagnetic waves emitted from another external source or from the recorder itself. Usually, the recording system is what generates its own energy, so the use is subjected to fewer constraints and under a wider range of operational conditions [19].

The reflected electromagnetic radiation depends on the geometric and dielectric properties of the surface or volume being studied and the phenomenon of reflection is called backscattering. Backscattering depends on the roughness of the surface, the type of material (e.g., whether it is iron, cement, wood or organic material) as well as the moisture content.

Their advantages are that they can penetrate the clouds, the relatively low rain and snow and therefore do not depend on weather or sunlight conditions. They also have the ability to penetrate vegetation and ground to a depth of about one meter. With methods quite complex and expensive, they can assess the moisture of the surface layer of the soil.

Finally, used in various applications such as agriculture and forestry, geology, hydrology, oceanography and recording; and study of ice on the earth's surface. Also, the counting

of the time difference between the transmitted and return signal is used to calculate distances (and altitude differences). Of course, the main drawbacks of radars are that due to the low emitted radiation the signal they record can be distorted by interference and in addition their signal has no multispectral characteristics

1.5.2 Passive sensors

Remote sensing systems which measure energy that is naturally available are called passive sensors. They depend on two sources of radiation, the radiation that has been reflected from the earth's surface originating from the sun and the thermal radiation emitted directly by materials on the earth combined with self-emitted thermal radiation in the atmosphere as it propagates upward. Figure 6 presents the difference between active and passive sensor systems [20].

Most satellites - including Landsat, one of the most representative satellites - are equipped with a multispectral scanner which records the electromagnetic signal coming from the same area of the earth's surface, the same time but at different wavelengths, thus providing different spectral channels of a multispectral satellite image.

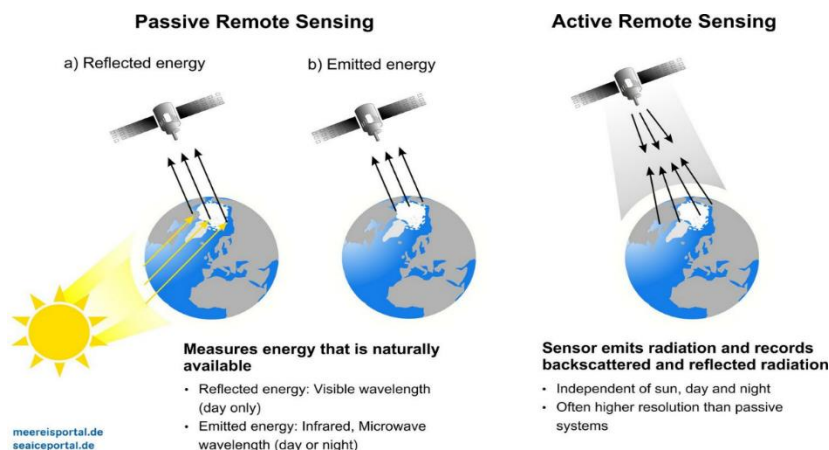


Figure 6: Passive and active remote sensing

1.6 Remote sensing platforms

The traffic on the navigation lines consists of a huge number of ships that cause concern every day and raise important issues around remote sensing and surveillance of the sea. There are a variety of remote sensing platforms and data available which can be used for a variety of applications. Choosing the most appropriate platform to utilize will usually depend on both the application of the data and the scale of the area.

- Satellite missions carried out to monitor the Earth in a timely manner involve low-orbit missions in order to provide data of its surface on a daily basis. The data and information extracted are mainly related to the location of ships and the monitoring of traffic. Satellite imagery is best suited for projects which require a large spatial area (> 100 km²) to be monitored and assessed from a consistent position and time of day. It is not suitable for applications that require very high-resolution

imagery as the best resolution currently available is around 30 centimeters for panchromatic values, and around one meter for multispectral data. Examples of applications for satellite imagery with different spatial resolutions are provided in the table below.

- Unmanned Aerial (UAV) imagery is obtained from compact sensors mounted on unmanned aircraft. Most UAVs have significant payload restrictions both from an operational limits and licensing perspective. As a result, there are limitations in the types of sensors available. However, there is a rush of manufacturers developing small lightweight sensors for the burgeoning UAV market. Imagery from UAV mounted sensors typically has a spatial resolution between one and eight centimeters and currently suits survey areas less than 20 km². UAVs have advantages over manned flights including safety, lead time, simplicity of mobilization, spatial resolution and cost. However, these must be considered in light of disadvantages such as payload limitations, sensor availability, flight endurance and stability in windy conditions. For some applications UAVs have unique capabilities, and Astron is excitedly pursuing the innovations that UAV data are enabling.
- Aerial imagery is obtained from sensors on manned aircraft. Without the payload weight restriction of most UAVs, manned flights can incorporate very sophisticated sensors, including hyperspectral cameras capable of recording hundreds of very narrow wavebands, or lidar, which uses laser technology to map surface height to millimeter precision. This allows a high sensitivity to different spectral signatures which enable us to classify features. The proximity to the ground not only means a higher spatial resolution, but also less atmospheric effects (such as clouds). Aerial imagery has a typical spatial resolution greater than five centimeters and suits survey areas from tens of square kilometers to hundreds of square kilometers [21].

The key advantages and disadvantages of the three platforms are summarized in the table 1 below.

Table 1: Advantages and disadvantages of remote sensing platforms (Source: astron.com.au)

Platform	Advantages	Disadvantages
Satellite	<ul style="list-style-type: none"> • Low cost over large areas (some satellite data is free) • Sensors are consistent (position and time) and accurate • No mobilisation requirements • Systematic acquisition provides data legacy and rich time series • Thermal and hyperspectral sensors available • A wide range of radar data readily available • Captures the broad picture • Atmosphere and weather can be measured • Gravity anomalies can be measured 	<ul style="list-style-type: none"> • Limited to > 1.2 m spatial resolution (multispectral bands) • Can be affected by cloud and atmospheric conditions • Capture times restricted to a fixed satellite orbit path • Failure of a satellite or sensor may inhibit a chosen method by many months • Sometimes there is a delay in the provision of data
Manned Aerial	<ul style="list-style-type: none"> • Flexible flight planning (capture time, resolution, survey area shape) • High quality, sophisticated sensors and typically very high quality data • Lidar, thermal and hyperspectral sensors available • Synthetic Aperture Radar data available 	<ul style="list-style-type: none"> • Generally more expensive • Mobilisation to remote areas can increase the cost greatly • Consistency between different data providers can be an issue
Unmanned Aerial (UAV)	<ul style="list-style-type: none"> • Easy mobilisation to any site • Capable of resolutions of less than 1 centimetre • Can be highly accurate – becoming very popular in the survey industry • Allows almost instant feedback • Can provide oblique imagery for enhanced 3D modelling 	<ul style="list-style-type: none"> • Typically more expensive than aerial imagery for areas > 20 km² • It is cutting edge technology and some operators are still learning how to deliver acceptable data quality • More susceptible to wind condition • Generally restricted in operations over urban areas and controlled airspace.

The SNAP platform is used for examination and study, responsible for the processing of images of collective data available from remote sensing missions of multiple sources and sensors for specific marine areas of interest. High-resolution data is provided by missions currently in orbit, such as the constellation ESA (European Space Agency) Copernicus Sentinel, ISI-IMAGESAT EROS-B and ISA (Italian Space Agency) COSMO-SkyMed. This data is processed to detect and locate obstacles in the area of interest and to evaluate important features, such as shape and kinematic parameters [22].

1.7 Space missions associated with ocean observation

The oceans cover about 70% of the entire surface of the Earth and are vital to all of us. Pollution, sea acidification and climate change are affecting ecosystems and biodiversity. Sustainable Development Goal (SDG), aims at the conservation and sustainable use of the oceans, seas and marine resources.

The European Space Agency (ESA), with its observation satellite fleet, monitors the ocean to support humanity and their missions to take place in a protected environment and to adapt to any requirements and changes. From temperature to sea level, sea ice

cover, salinity and phytoplankton, these satellites record the ocean in many different ways every day.

1.7.1 GOCE and SMOS satellites

The first two satellites of the "Earth Explorers" (Figure 7), were launched in 2009: the GOCE (Gravity field and steady-state Ocean Circulation Explorer) satellite for the study of the gravitational field and the SMOS (Soil Moisture and Ocean Salinity) in Figure 8 satellite for the study of water reserves on the planet, the salinity of the oceans, as well as soil moisture - which is particularly important for countries suffering from water scarcity - but also for improving the weather forecast on a seasonal scale and for extreme weather events. SMOS sensors and data analysis methods have previously been used to find water on Mars, but this is the first time they have been used to measure the Earth by a satellite. The measurements are based on an innovative 2-D interferometer that makes observations of thermal brightness in the L band (1.4 GHz) of the electromagnetic spectrum. These observations are translated into information about soil moisture and salinity in the surface layers of the oceans, both of which are necessary for a further understanding of the Earth's hydrological cycle [23], [24].

Earth Explorers



- **GOCE** (2009–13) studying Earth's gravity field
- **SMOS** (2009–) studying Earth's water cycle
- **CryoSat-2** (2010–) studying Earth's ice cover
- **Swarm** (2013–) three satellites studying Earth's magnetic field
- **ADM-Aeolus (2018)** studying global winds
- **EarthCARE (2019)** studying Earth's clouds, aerosols and radiation (ESA/JAXA)
- **Biomass** (2021) studying Earth's carbon cycle
- **FLEX** (2022) studying photosynthesis
- **Earth Explorers 9 & 10** to be selected



Figure 7: "Earth Explorers" satellite missions focus on the study of the atmosphere, biosphere, hydrosphere, cryosphere and interior of the Earth and their interactions (Source: www.esa.int)



Figure 8: ESA's SMOS mission for ocean salinity (Source: www.esa.int)

1.7.2 Cryosat

The Ice Study CryoSat-2 (Figure 9) satellite was launched in April 2010. After SMOS, it is the second in a series of Opportunity satellites and is the successor to CryoSat, which was lost after a failed launch in 2005. It has been orbiting since April 8, 2010, providing important information on the state of ice in the polar oceans, Greenland and Antarctica. With increasing global warming, changes in ice thickness are major because melting glaciers and polar ice caps can cause significant ocean levels to rise, threatening coastal areas around the world. Ice still plays an important role in the complex process of climate change, reflecting sunlight. Therefore, close and accurate monitoring of ice features by the CryoSat-2 satellite is extremely important [25].



Figure 9: CryoSat: ESA's Ice Mission (Source: www.esa.int)

1.8 Copernicus program

The Copernicus program was established by the Regulations (EU) No 377/2014 in 2014, building on the formerly known as Global Monitoring of Environment and Security (GMES), is an EU program aimed at developing European's information services based on an e-satellite and in situ (non-empty) data (<http://www.copernicus.eu/>). The Copernicus program implemented by the European Commission (EC) with European Space Agency (ESA) support and European Environment Agency (EEA) for the terrestrial component, monitors our planet and its many ecosystems while ensuring that its inhabitants are prepared for and protected against crises and natural or man-made disasters Copernicus's goal is to observe the environment, collect, store and analyze data and provide products to enable effective decisions to be made [30].

The information services are based on data from a constellation of 6 families of satellites, known as the "Sentinels", and dozens of third-party satellites known as "contributing space missions". These measuring devices in orbit sometimes operate alone and sometimes combined with sensors placed on the seas, land or in the air. Copernicus then stores the data and helps to provide a large amount of reliable and up-to-date information on the status of our planet. This data can be used to create different kinds of products such as statistics and topographic maps. The data is analyzed in a way that generates indicators useful for researchers and end users, providing information on past, present and future trends. Copernicus contributes not only to European scientific and technical excellence, but is part of a public service framework, allowing full, free and open access to all data collected. Anyone, scientists, policy makers, entrepreneurs and ordinary citizens - can use this data.

1.8.1 Sentinel missions

ESA developed a series of next-generation EO missions, on behalf of the joint ESA/European Commission initiative Copernicus (ECC). The goal of the Sentinel program is to replace the older EO missions which have retired, such as the ERS and Envisat missions, or are currently nearing the end of their operational life span. This will ensure a continuity of data so that there are no gaps in ongoing studies. Each mission focuses on a different aspect of EO; Atmospheric, oceanic, land monitoring and the data is of use in many applications.

1.8.1.1 Sentinel-1

The Sentinel 1 missions are supported by the ESA and Copernicus program and consist of two active remote sensing satellites, in opposite orbits 180°, equipped with C channel radiation radar. The two satellites cooperate and record the entire surface of the earth every 6 days [26]. Table 2 shows the details of Sentinel-1A and Sentinel-1B missions.

The radar sensors integrated in the mission satellites Sentinel 1 export satellite products with different physical and digital parameters. Some of these satellite products are press products broadband interferometry (IW) which supports recording of reflected polarized

signals (VH -Vertical Horizontal & VV -Vertical Vertical) while at the same time it has good spatial resolution (5 X 20 m). The polarization refers to the direction of linear polarization of the signal during broadcast and download. So, if the satellite is transmitting and receiving signal with vertical linear polarization, the product is denoted as VV (Vertical Vertical) as respectively for horizontal polarization (HH- Horizontal Horizontal). Also, for more extensive interpretation of the signal there are sensors of complex polarization, such as that of Sentinel 1, which emit radiation at a specific polarization and record the backscattered signal to another. The various combinations of complex polarization are denoted by two capital letters, symbolizing broadcast polarization and recording polarization such as for example, the combination of VH (Vertical Horizontal) & HV (Horizontal Vertical) [26].

Table 2: Mission details of Sentinel-1A and Sentinel-1B

Mission Details	
Launch	Sentinel-1A on 3 April 2014, Sentinel-1B on 25 April 2016
Orbit	Polar, Sun-synchronous at an altitude of 693 km
Revisit Time	Sentinel-1 is a constellation of two satellites orbiting 180° apart, so the mission images the entire Earth every six days (at the equator).
Instrument	C-band Synthetic Aperture Radar (SAR)
Main applications	Monitoring Sea ice, oil spills, marine winds, waves & currents, land-use change, and emergency management (e.g., for floods and earthquakes).

1.8.1.2 Sentinel-2

The Copernicus Sentinel-2 mission comprises a constellation of two polar-orbiting satellites placed in the same sun-synchronous orbit, phased at 180° to each other [27]. It aims at monitoring variability in land surface conditions, and its wide swath width (290 km) and high revisit time (10 days at the equator with one satellite, and 5 days with 2 satellites under cloud-free conditions which results in 2-3 days at mid-latitudes) will support monitoring of Earth's surface changes.

SENTINEL-2 mission objectives are to provide:

- systematic global acquisitions of high-resolution, multispectral images allied to a high revisit frequency

- continuity of multi-spectral imagery provided by the SPOT series of satellites and the USGS LANDSAT Thematic Mapper instrument
- observation data for the next generation of operational products, such as land-cover maps, land-change detection maps and geophysical variables.

1.8.1.3 Sentinel-3

The main objective of the Sentinel-3 mission is to measure sea surface topography, sea and land surface temperature, and ocean and land surface color with high accuracy and reliability to support ocean forecasting systems, environmental monitoring and climate monitoring.[28]. The Sentinel-3 Mission Guide provides a high-level description of the mission objectives, satellite description and ground segment. It also covers an introduction to heritage missions, thematic areas and services, orbit characteristics and coverage, instrument payloads and data products. The Sentinel-3 mission is jointly operated by ESA and EUMETSAT to deliver operational ocean and land observation services.

1.8.1.4 Sentinel-4-5-5P

The Copernicus Space Component comprises a series of space-borne missions called 'Sentinels' that are developed and procured by the European Space Agency. The missions Sentinel-4, -5 and -5 precursor (S4, S5, S5P, respectively) are conceived as complementary elements of a constellation serving the specific needs of the Copernicus Atmospheric Monitoring Services (CAMS). These services will provide coherent information on atmospheric variables in support of European policies and for the benefit of European citizens and will cover ozone and surface UV, air quality, and climate applications. Sentinel-5 is focused on air quality and composition-climate interaction with the main data products being O₃, NO₂, SO₂, HCHO, CHOCHO and aerosols. Additionally, Sentinel-5 will also deliver quality parameters for CO, CH₄, and stratospheric O₃ with daily global coverage for climate, air quality, and ozone/surface UV applications.[29].

The Space Segment of the Sentinel-4 mission consists of an Ultraviolet-Visible-Near-Infrared (UVN) light imaging spectrometer instrument embarked on the Meteosat Third Generation Sounder (MTG-S) satellite.

The Sentinel-5 mission consists of high-resolution spectrometer system operating in the ultraviolet to shortwave infrared range with 7 different spectral bands: UV-1 (270-300nm), UV-2 (300-370nm), VIS (370-500nm), NIR-1 (685-710nm), NIR-2 (745-773nm), SWIR-1 (1590-1675nm) and SWIR-3 (2305-2385nm). The instrument will be carried on the MetOp-SG A satellite.

The Copernicus Sentinel-5 Precursor mission reduces gaps in the availability of global atmospheric data products between SCIAMACHY/Envisat (which ended in April 2012), the OMI/AURA mission and the future Copernicus Sentinel-4 and Sentinel-5 missions.

The results of the missions are expected to be used in large numbers applications and environmental studies such as Arctic ice monitoring and available ice in the oceans, recording accidents, oil spills and the detection of ships for maritime safety.

1.8.1.5 Sentinel-6

Copernicus Sentinel-6 Michael Freilich includes two satellites that will fly sequentially, launched in 2020 and 2025, carrying a state-of-the-art optimized payload. Copernicus Sentinel-6 Michael Freilich is an Earth Observation satellite mission developed to provide enhanced continuity to the very stable time series of mean sea level measurements and ocean sea state that started in 1992, with the TOPEX/Poseidon mission, then continued by the Jason-1, Jason-2 and Jason-3 satellite missions. The mission was designed, built and operated by European organizations, while NASA provided the launch vehicle, and the LRR, AMR-C and GNSS-RO payloads.

The threat of sea level rise to coastal communities is an important global concern for governments and policymakers. The well-being and security of future generations in coastal regions and small low-lying island states depends on actions and decisions on environmental policies. Sea level rise is a powerful climate indicator, since it is the result of changes occurring in Earth's climate system, in response to unforced climate variability and forcing factors from both natural and artificial sources

In addition to observing sea level rise, Copernicus Sentinel-6 Michael Freilich will provide near-real-time measurements of sea surface height, significant wave height, and other products tailored to operational services in the ocean, meteorology and hydrology domains. Copernicus Sentinel-6 Michael Freilich will thus monitor sea level change and guarantee the continuity of the historic altimeter sea level record.

1.8.2 The Copernicus services

Copernicus missions also include essential interrelated themes, incorporating six sets of services: Atmosphere Monitoring, Marine Environment Monitoring, Land Monitoring, Climate change, Emergency Management and Security that translate into concrete and effective areas of application as shown in figure 10 below.

With regards to the environment, Copernicus detects the content of aerosols that destroys the ozone layer, analyzing atmospheric composition and biodiversity. It is regularly evaluating the melting of the polar ice cap in the Arctic as a result of temperature increases due to global warming. It determines the quality of air and water that affects our health, it monitors ocean levels coastal areas and forests in order to limit the damage from the threat of earthquakes floods and fires to ensure our safety.

In the energy sector, Copernicus promotes the use of hydraulic and wind power plants, promising clean, eco-friendly alternatives to fossil fuels. This will allow for renewable energy to account for up to 27% of our total energy consumption by 2030.

Copernicus also supports the monitoring of the external borders of the EU, using space data merged with other sources of information to increase situational awareness and improve assessment of risk at the external borders. Serving the marine world, Copernicus tracks marine pollution affecting aquatic ecosystems and the fishing industry. As part of a development cooperation policy, Copernicus warns of early signs of deforestation and desertification in order to avoid the problems of loss of biodiversity and food shortages. It oversees the irrigation of fields and monitors crops for better food management. It is also instrumental in tracing outbreaks of diseases such as EBOLA in West Africa.

Further to these examples, Copernicus can serve the tourism industry, urban development, archeology, oil and gas and the insurance sector (<https://www.copernicus.eu/en/about-copernicus>).

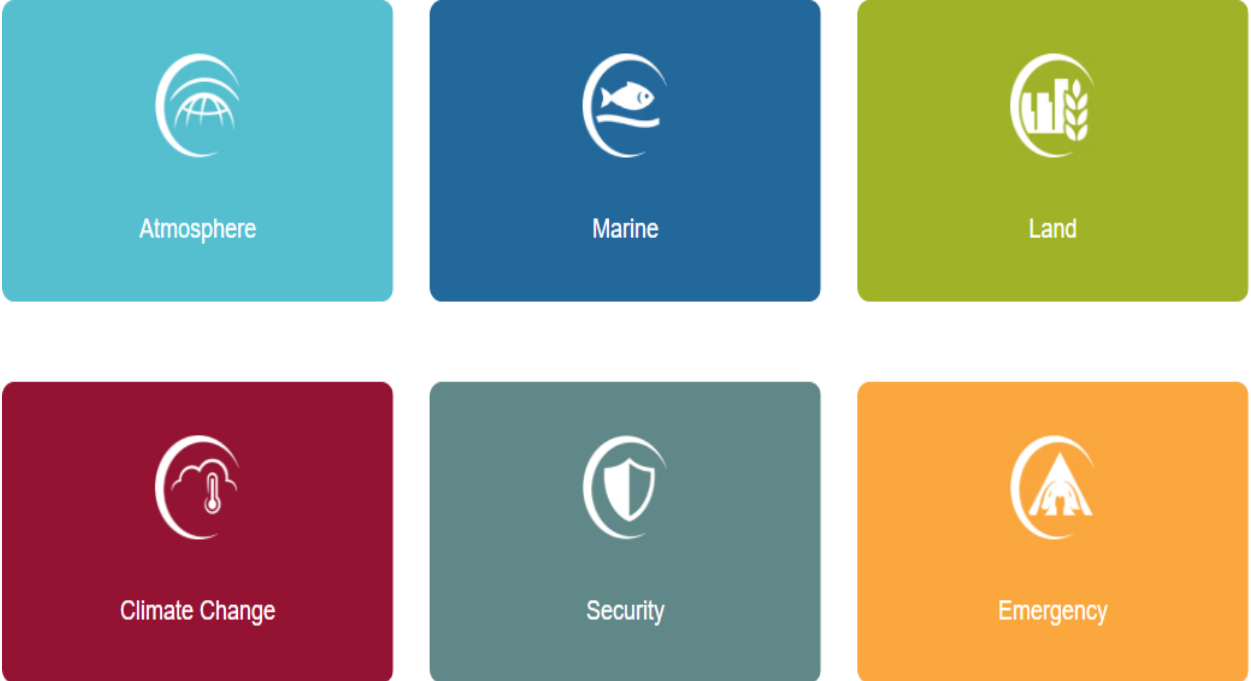


Figure 10: The six thematic streams of Copernicus services

2. LITERATURE REVIEW

In this chapter, a literature review will be applied to the current subjects that have been published and which concern the four topics of the dissertation. There will be an analysis of the theoretical background, some necessary introductory concepts of the subjects as well as the techniques used for the needs of the present study.

2.1 Review of oil spill and remote sensing capabilities

According to several surveys the most widespread method for finding oil spills is the Synthetic Aperture Radar (SAR) [31]. Oil spills are easily detected by radar images because they can distort the waves on the sea surface and smooth them creating detectable areas of low backscatter. Although these areas appear in SAR images as dark spots, they may not always come from oil spills [32]. These may originate from natural surface films produced by plankton or fish, low winds that are often encountered on leeward islands, raindrops impinging on the sea surface creating turbulence in the upper water layer, discharged sewage from land-based industrial or urban facilities, water flowing from land into the sea after heavy rains, vegetable oil spilled into the sea during the cleaning of tanks of ships carrying palm oil etc.

The real challenge was how satellite remote sensing would be able to detect dark areas of crude oil and distinguish it from oils of biogenic origin. Algorithms based on different criteria have been tested in the past without much success [33]. They first used radar images acquired with single polarization and developed discrimination algorithms based on the degree of NRCS (normalized radar cross section) reduction, the location or shape of the area, and the texture of the dark feature. It turned out, however, that algorithms based on these properties often gave unsatisfactory results (false alarms). Their main shortcoming was that they failed to distinguish between seepage of mineral oils and biogenic surface oils [32].

2.1.1 Polarization modes

In the last few decades there have been studies that utilize the use of single frequency, as it appeared that the use of multi-frequency did not help and satisfactory results were not obtained since 1994 during the space shuttle mission [34]. Since then, satellites have carried single polarimetric frequency (SAR) sensors that have the ability to transmit and receive radar signals in different polarizations. Such as the German TerraSAR-X, the Italian Cosmo-SkyMed satellite, the Canadian Radarsat-2, the Japanese ALOS-2 and the European Sentinel-1 satellites. TerraSAR-X, Radarsat-2 and ALOS-2 satellites in particular have the capability to operate in fully polarimetric mode. During this operation, two orthogonally polarized radar signals (horizontal and vertical) are transmitted and received in both polarizations. However, when using multi-polarization for oil spill detection, we have to keep in mind that the bandwidth it records is quite narrow, which is not favorable for operational oil pollution monitoring, which needs to have a large coverage. Also, the use of multiple SAR channels increases the cost of the systems and their operation. It has been shown that although SAR images in both VV and HH polarizations can be used for grinding detection, VV imagery is preferred as it offers a better signal-to-clutter ratio than other polarization options (i.e., HH, VH or HV) [35]. This can be best seen in Table 3 below that although VV is more sensitive than HH for oil spill detection there may be no advantage in using the co-polarized or cross-polarized

signatures as oil-free and oil-covered surfaces as they tend to have similar ratios of contrast and polarization [36].

Table 3: Backscatter values of water, oil-covered water and the SAR noise floor illustrating the improved contrast for oil slick detection (Source: www.nrcan.gc.ca).

Polarization	Water	Oil-covered Water	SAR noise floor	Contrast
VV	-20 dB	-28 dB	-30 dB	8 dB
HH	-24 dB	-32 dB	-30 dB	6 dB
HV	-30 dB	-38 dB	-30 dB	0 dB

2.1.2 Approach 1: SNAP - Oil spill detection

For oil spill detection, several studies have been made on pre-processed images analyzed using the SNAP tool. The steps usually followed are:

- Multi-look: to improve image interpretability by reducing inherent speckles that appear in SAR images
- Speckle Filtering: Unlike optical remote sensing images, SAR images have an inherent salt and pepper like texture called speckle that degrades image quality and makes interpretation of features difficult.
- Radiometric Calibration: The product does not include radiometric correction and therefore significant radiometric partiality remains which needs correction.
- Ellipsoid Correction: Due to satellite sensor tilt and topographic variations, distances in a SAR image are distorted. So, in order to ensure that the geometric representation of the image is close to the real one, ground correction is applied to compensate for the distortions.

The order can be altered and Calibration may be applied before the multi-look function. In other applications, only the speckle filtering method is preferred and then the ellipsoid correction [37].

As a final step for oil spill detection, Misra and Balaji R. in [38] used the SNAP SAR utility. Based on the principle of recognizing a dark region, which is oil spills, using an adaptive threshold followed by a classification, they defined the dimension of the minimum cluster size. They tested two cases with a window size of 61, a threshold shift (dB) of 2, and a minimum cluster size of 0.1 square kilometers. Unfortunately, the first case did not yield satisfactory results. The output only marked ship locations as well as some traces of oil.

The second case however, managed to detect the oil spill but also some ship tracks as oil slicks.

In the next chapter, the oil spill detection method will be implemented with the applications of the above algorithms. An improvised implementation will be preferred depending on the location and size of the dark area and the appropriate parameters will be chosen as each oil spill may differ.

2.2 Studying of sea ice variability and type

Shipping in the Arctic regions experienced a great bloom after 1980 when icebreaker investments were developed and many new ports were established and used for trade operations. Over the years and due to the reduction of ice fields during the summer seasons in the Arctic, many traders have chosen to use the Arctic Ocean as a shortcut between the Pacific and Atlantic Oceans. The cost savings due to reduced fuel consumption were large in proportion to the increased frequency of travel [39].

Arctic sea ice variability has changed considerably over the past 3 decades [40]. This brings the need for the scientific community primarily to analyze and interpret sea ice observations. Thanks to satellite remote sensing of various properties of sea ice, including ice thickness, it is possible to investigate surface features, the relationship between thickness and various sea ice parameters such as type etc. [41], [42].

2.2.1 Methods for sea ice type examination

There are several algorithms in the literature that contribute to the detection of different types of sea ice from sensors operating in the visible and near-infrared spectrum. The products used in studies and algorithms to find these ice types are usually derived from satellite sensors or from aerial photographs and videos [43], [44]. For example, Rosel and Kaleschke [45], proposed an automatic method for principal component analysis in optical satellite remote sensing (Landsat) based on spectral information.

Pedersen [46] applied a neural network to retrieve the fractions of snow-covered ice, bare ice, brash ice and open water in a continuous series of photographs. By using two successive images overlapping each other, they were able to standardize the images. The neural network features used to synthesize it were selected based on FDA (Fisher Discriminant Analysis) and were both texture and spectral data. Pedersen compared their classification results with EM-bird ice thickness measurements; however, the data and photographs were not taken on the same flight and therefore did not cover exactly the same ice.

Nicholas C. Wright and Chris M. Polashenski [47], were asked to make a decision whether to analyze the image into individual pixels or to analyze objects made of the same neighboring pixels and also which classification algorithm to use for these image units. In previous work in terrestrial remote sensing applications, object-based classifications have been shown to be more accurate than single-pixel classifications when analyzing high-quality imagery [48], [49]. They examined a wide range of algorithms for image object classification. They first examined the use of supervised versus unsupervised schemes. Unsupervised designs were rejected because they produced inconsistent, non-comparable results. These schemes, like classification algorithms, group observations into a predetermined number of categories even if not all types of

features of interest are present in an image. In contrast to these, supervised classification schemes use a set of known examples (called training data) to assign classification to known objects based on similarity to user-recognized objects. They chose a random forest classifier over other supervised learning algorithms for its ability to handle nonlinear and categorical training input, robustness to outliers in the training dataset, and relative ease of implementation.

Khaleghian, S.; Ullah, H.; Kraemer, T.; Hughes, N.; Eltoft, T. [50], explored new and existing convolutional neural network (CNN) architectures for sea ice classification using Sentinel-1(S1) SAR products. They identified difficulties and challenges in analyzing ice types in SAR images due mainly to thermal noise but also to radar backscatter ambiguities for certain conditions involving complex information reflection from the sea ice surface. They used images containing various types of ice to generate a dataset for Deep Learning (DL) analysis. To avoid cross-class interaction they used a combination of near-simultaneous SAR images from S1 and fine-resolution Sentinel-2 optical data (S2), without the presence of clouds. For classification they used data augmentation to adjust the imbalance of sea ice type classes in the training data. The SAR images were divided into small patches which were processed one at a time. They found that the combination of data augmentation and training of a proposed modified Visual Geometric Group 16-Layer (VGG-16) network, trained from scratch, significantly improves the classification performance, compared to the original VGG-16 model and an ad hoc CNN model alone. Their experimental results showed, both qualitatively and quantitatively, that the models produced accurate classification results.

In the next chapter, a demonstration of supervised and unsupervised classification will be conducted using SNAP software and data from Sentinel-2's optical sensor. According to the previous studies SAR images require a more sophisticated approach along with texture analysis that will not be included in this particular thesis.

2.3 Literature review of wind direction and speed estimation

Ocean images recorded by SAR systems consist of data and information on the geophysical parameters of the marine environment. More specifically, microwave sensitivity to surface roughness allows SAR images to be exploited for accurate estimation of surface wind (direction and speed). These satellite-based radars allow the investigation of atmospheric and marine processes on a spatial scale not achieved by other space-based sensors. Satellite wind mapping is a useful tool for quick assessments of wind conditions.

In a 20-year-old survey, Yon Du, Paris W Vachon and John Wolfe presented a method for the automatic estimation of wind directions from SAR images of the ocean [51]. Based on wave analysis, the method assumes that the wind direction is aligned with boundary layers of atmospheric eddies (which often appear as kilometer-scale streaks in SAR images of the ocean) and measures the orientation of streaks. Unlike estimation methods using Discrete Fourier Transform (DFT), bands in SAR images are quantitatively described as a physical output of this method.

A method of estimating the annual average wind speed at a selected site using neural networks was presented in the article of P. Lopez, R. Velo, F. Maseda [52]. The method that was proposed, uses only a few measurements taken at the selected site in a short time period and data collected at nearby fixed stations. The neural network used in this study is a multilayer perceptron with one hidden layer of 15 neurons, trained by the

Bayesian regularization algorithm. The number of inputs that were used in the neural network was analyzed in detail, and results suggested that only wind speed and direction data for a single station were required. In sites of complex terrain, direction is a very important input that can cause a decrease of 23% in root mean square (RMS).

The results obtained by simulating the annual average wind speed at the selected site based on data from nearby stations were satisfactory, with errors below 2%. Therefore, it was concluded that direction is an input of major importance in complex terrain with considerable changes in roughness and with the presence of obstacles. This was the case of the Galician region, where the measuring stations considered in the study are located.

Haoyu Jiang at [53] managed to measure ocean wave spectra and use it to estimate sea surface winds. In the study he used two deep neural networks (DNNs) to estimate the wind speed and direction from the first five Fourier coefficients from buoys. The wind and wave measurements from more than 100 meteorological buoys during 2014-2018, trained the DNNs. It was found that the wave measurements could best represent the wind information about 40 min previously because the high-frequency portion of the wave spectrum integrates preceding wind conditions.

2.3.1 Approach with SNAP – Wind field estimation

S F James at [54] proposes Sentinel Application Platform (SNAP) which provides the tools needed to calibrate Sentinel-1 L1 data products and describes the method for processing multiple SAR images to extract wind speed maps. The steps used on the L1-GRD (ground range detected) data are orbit correction, thermal noise removal, radiometric calibration (to calculate Sigma0), application of a land mask, and multi-looking to smooth out the inherent speckle noise in the radar data. Results were tested against the coincidence of offshore mast data.

Alexandre Corazza, Ali Khenchaf and Fabrice Comlbet [55], focused on three methods to estimate wave direction from a sea surface SAR image in order to evaluate which one offers the best performances and to estimate the wind direction and wind speed. They performed a pre-processing step chain through SNAP in order to enhance the usability of a SAR image in the context of marine remote sensing. They first masked the land out to avoid any unfortunate estimation of wind direction or speed values on these areas. Then they calibrated the data to provide it with a more independent incidence angle and get the NRCS values. The third processing was speckle filtering by choosing a Lee filter which uses the local statistical characterization to smooth homogenous areas and keep the

edges information. The three wave direction estimation methods that they abbreviated were:

- **HOG** for the Histogram of Oriented Gradient computed with the Improved Local Gradient
- **WVT** for the wavelet method with the extraction on the 2DFT by linking the dominant pair of maxima
- **WVT Radon** for the wavelet method with the extraction on the 2DFT masked with Otsu by taking the maximum of the Radon projection.

Finally, the image was projected into the Earth's coordinates by making a range-Doppler terrain correction.

2.4 Ship detection for identification of dangerous cargoes

Remote sensing is a very useful tool for ship detection as well. It offers security at sea which includes, among other things, the maintenance of sea traffic, protection against illegal fishing, maritime border activity or the detection and monitoring of oil spills and marine pollution. Combined with the use of an Automated Identification System (AIS), which uses VHF radio frequencies to wirelessly transmit the ship's location, destination and identity to nearby receiver devices on other ships and ground systems, continuous and all-weather, ship information and motion can be provided from the surface of the sea [56].

SAR technology, as one of the most active telescopic tools, provides signals that penetrate clouds giving the advantage to space agencies and organizations to use it in areas with intense weather conditions or in areas with heavy cloud cover. In particular, ship detection plays an increasingly essential role in both the political and military regimes. However, a small (few pixels) ship rendering is still a challenge. In addition, the various complex background conditions make the method for their detection even more difficult when, for example, ships are in a highly cluttered area.

2.4.1 Review of previous studies

Authors J. Zhao, Z. Zhang, W. Yu and TK. Truong [57], used convolutional neural networks (CNNs) to increase the performance in SAR ship detection. They proposed a new method, which was composed of two stages: ship proposal generation by using a newly presented 3C2N (Cascade Coupled Convolutional Neural Network) model and followed by a PCT-based visual attention model to discriminate ship targets. Their model was trained with a fairly large number of Sentinel-1 images and could adequately characterize testing images in the space domain more sufficiently.

Another comparison study, presented by P. Lervolino, R. Guida, P. Lumsdon, J. Janoth, M. Clift, A. Minchella and P. Bianco [58], compared datasets in terms of probability of detection (PD), probability of false alarm (PFA) and Target-to-Clutter Ratio (TCR). The Generalized Likelihood Ratio Test (GLRT) was tested on a couple of SAR images acquired over the Solent Channel in UK by the European Sentinel-1 (operating at C-band) and the German TerraSAR-X (operating at X-band) sensors on the same area at the same time. Outcomes showed that the GLRT presents a much higher TCR (21.7 dB in the worst-case scenario) than the original SAR intensity and that X-band showed better results with a higher increment of the TCR than the C-band. In addition, the novel GLRT

algorithm performed better than CFAR showing a higher detection and lower false alarm rate at X-band.

An article published in EUSAR 2021, the 13th European Conference on Synthetic Aperture Radar by M. Tsvetkova, N. Kolev, A. Hristov and C. Alexandrov discusses an algorithm for processing complex SLC (Single Look Complex) images of marine targets obtained at the output of Sentinel-1 [59]. The article focuses on AIS data for marine target detection and SLC target chips are extracted with ESA SNAP. Processing and evaluation of the ship's course and speed was performed in MATLAB. At first, they identified regions with targets and exported complex images through ESA SNAP into appropriate format for MATLAB. To do that, the operator must define two thresholds - *Pixel Threshold* through constant – times STD added to 2D mean and *Area Threshold* for target detection. The images were binary segmented with the *Pixel threshold* and later with MATLAB, image processing region properties, target detection and parameters were estimated. The results from the investigation and processing of SAR SLC images were positive.

2.4.2 Approach with SNAP – Ocean object detection tool

One of the studies published in 2018 on the 3rd International Conference on Science and Technology, was conducted by F. Bioresita, C.B. Pribadi and H. S. Firdaus [60]. They used two different methods and compared them using the Sentinel-1 IW GRDH data set. The first method was an ocean object detection algorithm and the second was a manual processing chain to extract ship objects using manual threshold extraction. The pre-processing chain for both methods included:

- Apply Orbit File
- Calibration
- Multi-Look
- Speckle Filtering
- Sigma nought image
- Land Sea Mask

The land-sea mask is used to reduce the area of the detection and reduce the processing time. The operation can be achieved using Digital Elevation Model (DEM) which in their study used SRTM (Shuttle Radar Topography Mission) data which is downloaded automatically while processing in SNAP. Afterwards they performed a terrain correction for geometric correction and image data was exported to GeoTIFF format to facilitate the next process. Their next step was using threshold (0.2) to extract a ship object.

Their results from the rapid method process were compared with manual ship extraction method indicated 34% false alarm estimation after visual observation. Compared with manual ship extraction, some artificial objects were classified as ships with a 45% false alarm. Based on the findings they concluded that rapid ship extraction produces less false alarm with minimal time-consuming process than manual ship extraction. Thus, in the case of Sentinel-1, ocean object detection in SNAP tools is suitable for rapid mapping.

In the next chapters, a similar approach will be performed with the SNAP tool using these thresholds techniques with automated rapid mapping.

3. 1ST SIMULATION DESIGN

3.1 1st Scenario: Oil spill mapping

3.1.1 Data download – Onda Dias

In this simulation we used Sentinel-1 SAR data as shown in Figure 10 to map the oil spill of the Persian Gulf from April to May 2022. We used the website <https://catalogue.onda-dias.eu> which in collaboration with the Copernicus program, offers free data on a 24-hour basis to users giving them the option to download as many images as they want throughout the day. Search filters included Sentinel-1A or Sentinel-1B products (table 4), remote sensing period from 20/4/2022 to 16/5/2022, GRD product type and IW sensor function. Several results were returned but only 2 were selected. Image ID:

S1A_IW_GRDH_1SDV_20220424T023119_20220424T023144_042909_051F4C_A9BA

and

S1A_IW_GRDH_1SDV_20220506T023119_20220506T023144_043084_052513_71AA

Table 4: Product types and processing levels of Sentinel-1A and Sentinel-1B mission.

Mission ^	Spatial Coverage ^	Instru... ^	Application Domain ^	Proces... level(s) ^	Product type(s) ^	Availabil... ^
Sentinel-1A	Global	SAR-C	Land, Marine	L0, L1, L2	RAW, SLC, GRD, OCN	Full Archive
Sentinel-1B	Global	SAR-C	Land, Marine	L0, L1, L2	RAW, SLC, GRD, OCN	Full Archive

This place (Figure 11) was chosen because there is a daily illegal transportation of oil to Shatt Al Arab which is owned by Iraq. They discharge in ship-to-shore operations within the Iranian 12-mile limit close to shore and try to keep clear of the various offshore oil fields in that area. The vessels normally run down the Gulf using the 12-mile limit as much as possible. They also proceed without deck and navigation lights or radar, to avoid detection by the MIF (Maritime Interdiction Forces) [61]. Due to this, vessels impact other vessels or hit rocks or even ports, as a result of which a significant amount of crude oil is spilled into the sea.



Figure 11: Area of interest, central Persian Gulf southwest of Shiraz town of Iraq as a SAR image.



Figure 12: Same image as the previous one as shown with Google Terrain layer.

3.1.2 Exploration of data and pre-processing

If we have a look at the data (Figure 12), we have 2 images, each one has a spatial resolution of 20 meters and below we can see the acquisition date which was 06/05/2022 for the first one and 24/04/2022 for the second one.

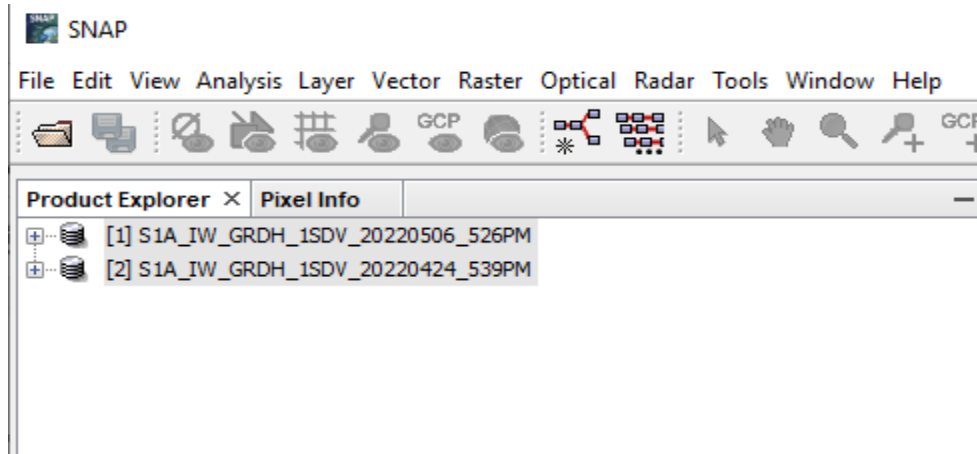


Figure 13: Products downloaded from catalogue.onda-dias.eu

The reason we downloaded 2 images is to compare these two in terms of the amount of oil spilled in the Persian Gulf from April 24 to May 6, 2022. Expanding them we will see the Band file inside the main product with the *Amplitude VV*, *VH* and the *Intensity VV*, *VH* bands, as shown in Figure 13.

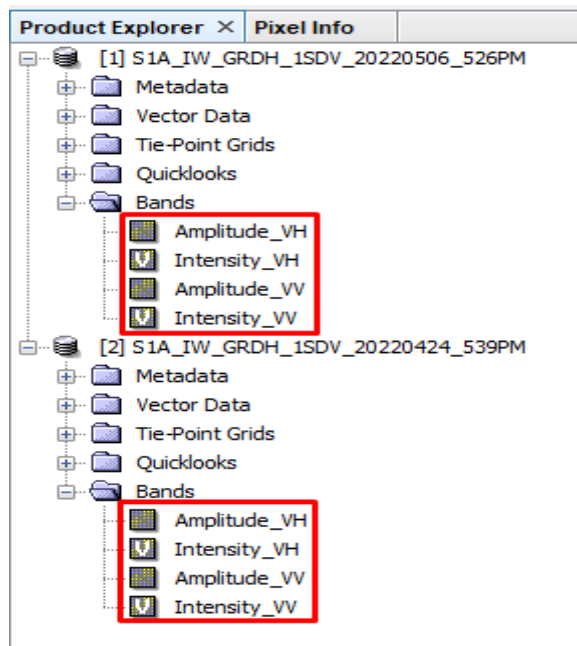


Figure 14: Bands file containing the Amplitude VV (vertical-vertical beam), VH (vertical-horizontal beam) band and Intensity VV, VH band.

The extent of the oil spill is quite clear in Figure 14 below, however we converted the Amplitude band to dB to have a more visible look of the extent in Figure 15.

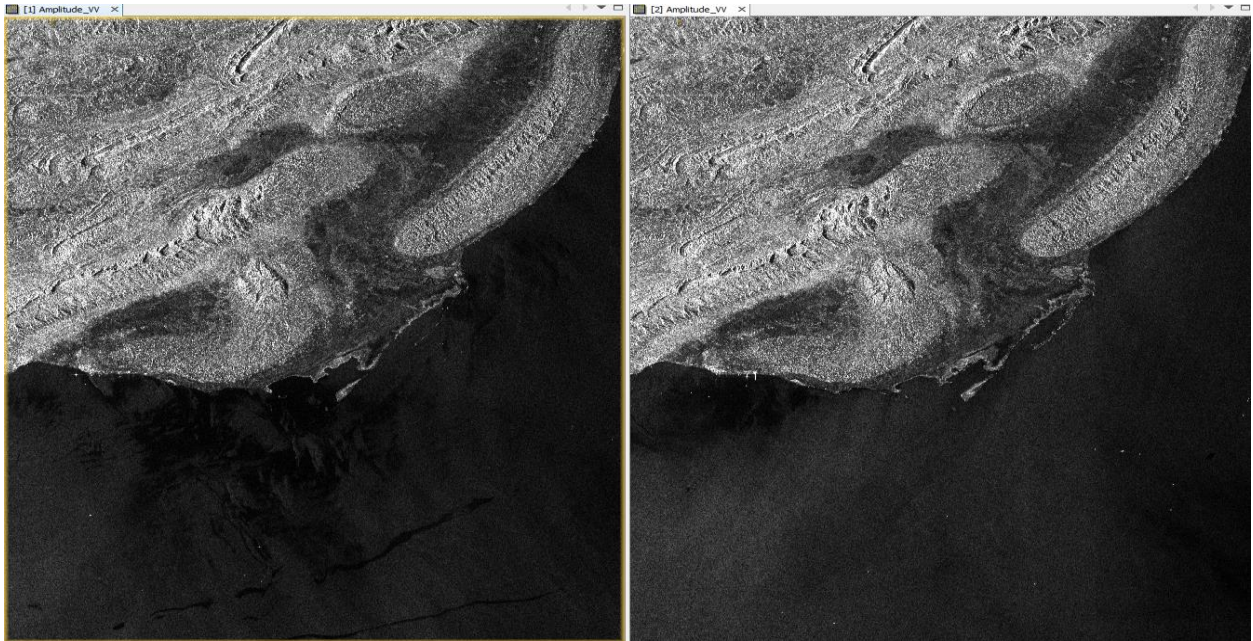


Figure 15: Two different images of Persian Gulf. The left image was taken on May 6, 2022 and the right one on April 24, 2022

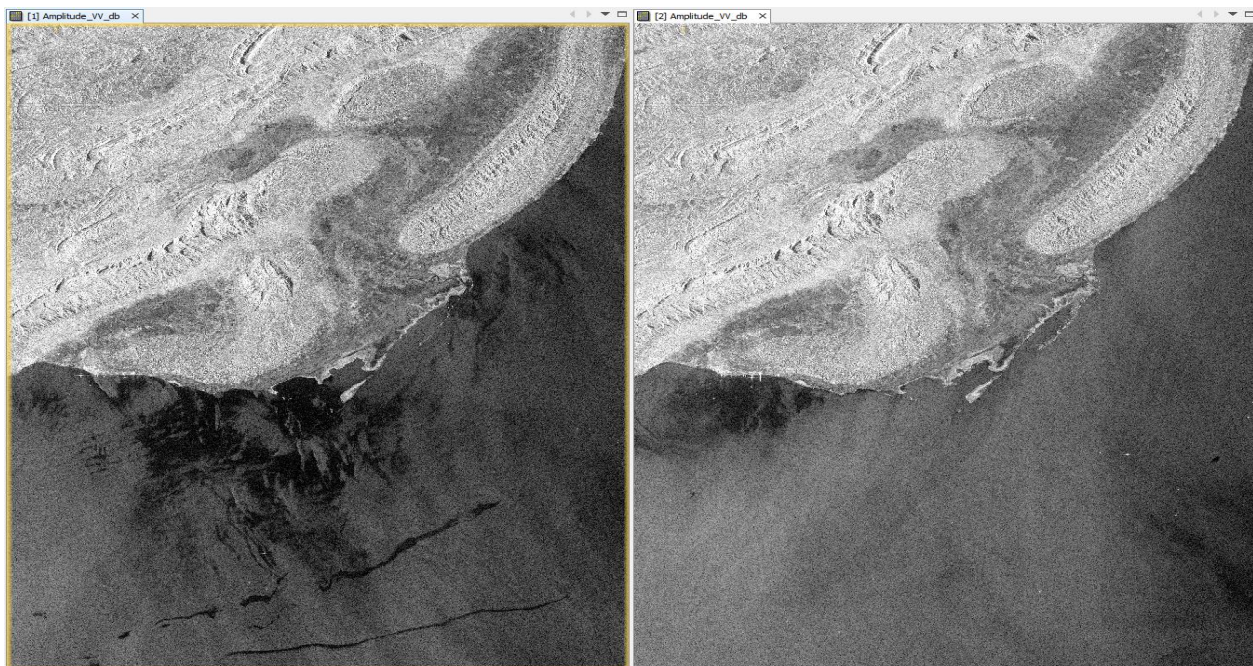


Figure 16: Same Images converted to dB to better visualize the extent of oil spill.

3.1.3 Image processing with graph builder

The next steps were calibration, geometrical correction and subtraction of the land area. Both images were processed along with the graph processing tool and batch processing

function. From the SNAP window on the upper bar **Tools** -> **Graph Builder** various functions were selected and placed on the graph builder window as shown in Figure 16.

Firstly, we added the *calibration* function and then the *multilook* function with a number of range looks equals 2. We reduced the dimensions of the image by a factor of 2 in order to smooth out the speckles and also to decrease the processing time. The next step was an *Ellipsoid-Correction-GG* and not a terrain correction because we were not interested in the land area where there is only a small amount of terrain. Finally, our graph was completed with the implementation of *Land-Sea-Mask* function.

Once the creation of the graph builder was completed, we saved it in an xml file and deleted the linear to decibel conversions of the images because our final result would contain a decibel band in any case.

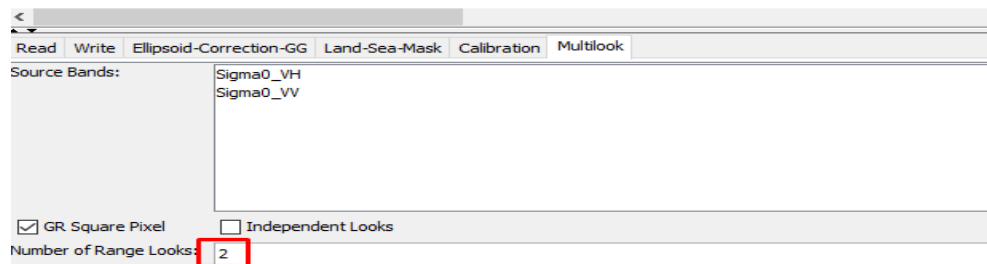
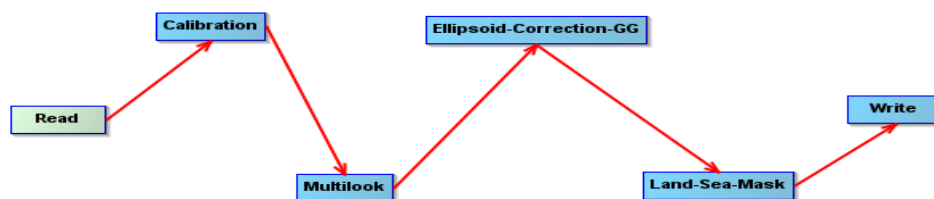


Figure 17: The completed graph that was used in the image processing toolbox for oil spill detection with 2 range looks.

The two images were produced with an average processing time of 5 minutes (in a faster system the speed increases significantly). Afterwards they were geographically corrected, and unnecessary land section was masked out, as shown in Figure 17.

The last part of our simulation concerns the detection of the pixels representing the oil spill. If we observe the pixels, their values range from 14dB to -28dB. Creating a profile plot of a random line that passes through the pixels of the oil slick we found that at about minus 23 dB we can detect oil. At the range of -22dB to 0dB, the image is mainly occupied by the sea while the white speckles are vessels with the range value of 5 to 14dB.

3.1.4 Speckle filtering and threshold method

To reduce the usual salt and pepper like texturing of SAR images, a speckle filter was needed. Speckle noise-like feature is a common phenomenon in SAR systems. It confers to SAR images a granular aspect and random spatial variation. The source of this noise is attributed to random interference between the coherent returns. The principle of speckle filtering is to reduce the variance of the complex speckled scattering and improve the estimate of the unspckled scattering coefficient. After the pre-processing steps which include calibration, ellipsoid correction, land-sea mask and speckle filtering we can produce the image below in Figure 17.

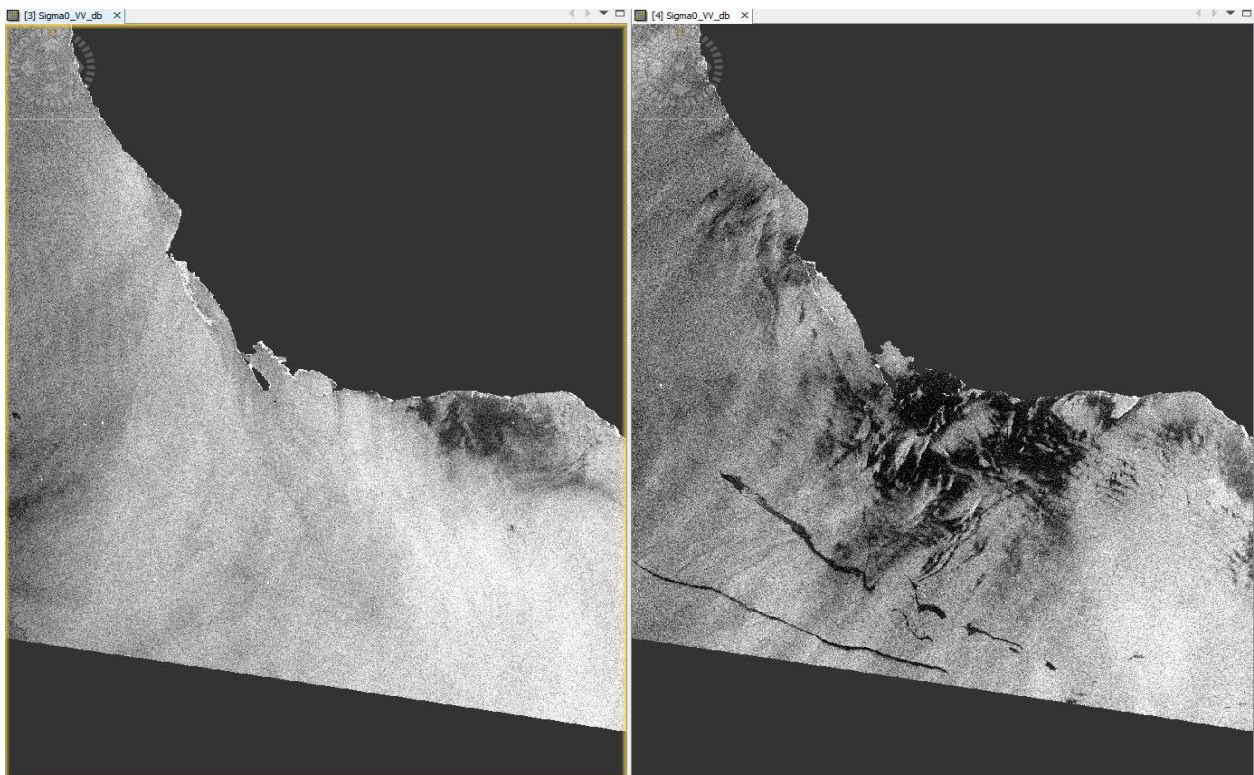


Figure 18: The two images after calibration, ellipsoid correction and land-sea mask and speckle filtering.

After that, we applied a simple threshold method which, although it's not always as effective as the SAR application for oil spill detection, it satisfied the condition for detecting them. To better visualize how an oil spill affects the reflectance of the SAR signal, we displayed a profile of the sigma nought (σ^0) value. The profile plot in Figure 18, with a box size of 21, shows what are the values that represent an oil spill. From **Raster -> Bandmath** we created a mask that excludes all the pixels that have a value below a specific threshold.

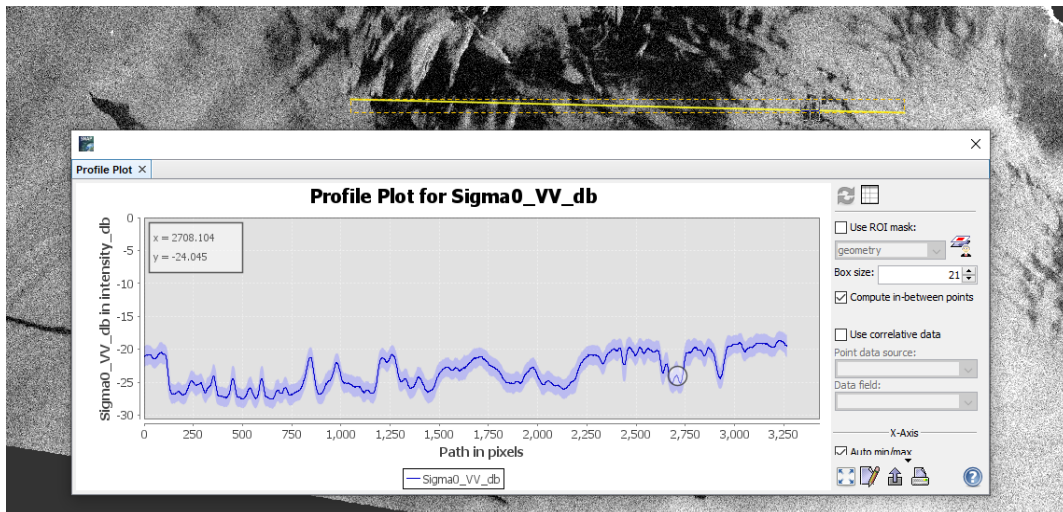


Figure 19: Profile Plot of a line across an oil spill.

In the pictures below (Figure 19), 6 different thresholds are introduced, corresponding to minus 22 to minus 24.5dB. The -23dB threshold was chosen as the most efficient and safest because it rejected the backward scattering radiation from the wave, which it was mistakenly considered as oil from higher thresholds, and at the same time it incorporated all the pixels that could cause true alarm detection. In order to exclude some pixels that had been incorrectly given the value 1, an arithmetic mean filter 5x5 was used, that smoothed the image considerably (Figure 20).

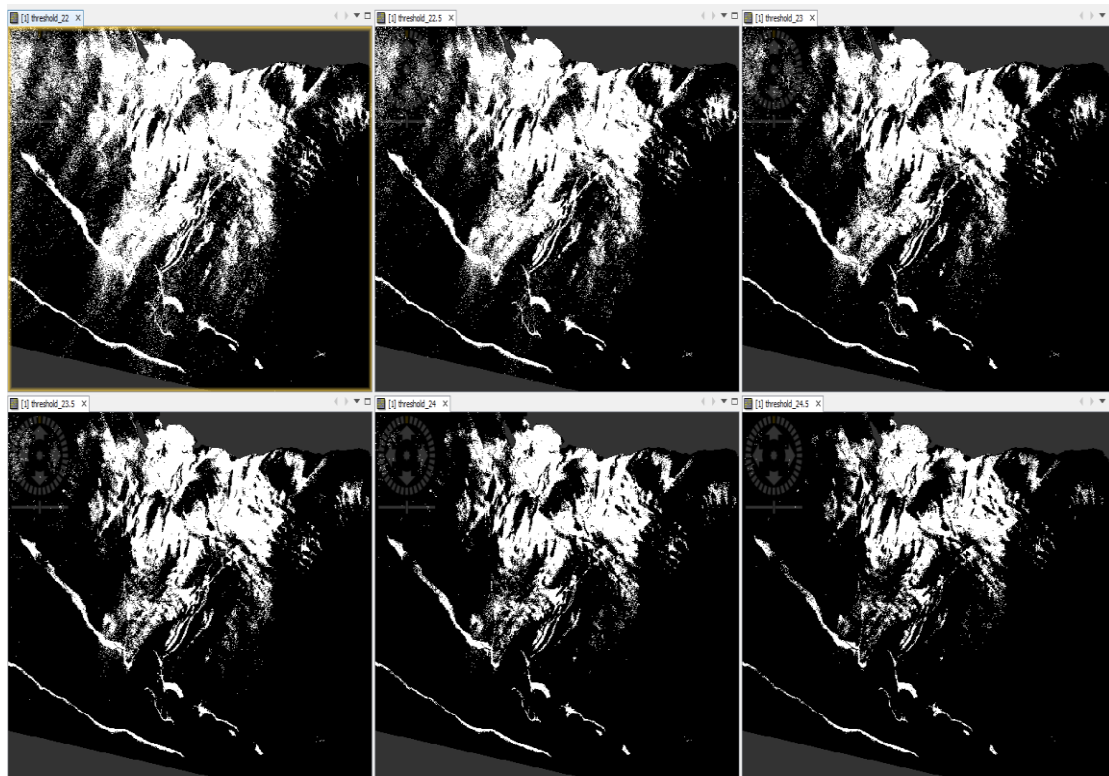


Figure 20: Six different thresholds, -22dB upper left, -22.5dB upper center, -23dB upper right, -23.5dB lower left, -24dB lower center, -24.5dB lower right.

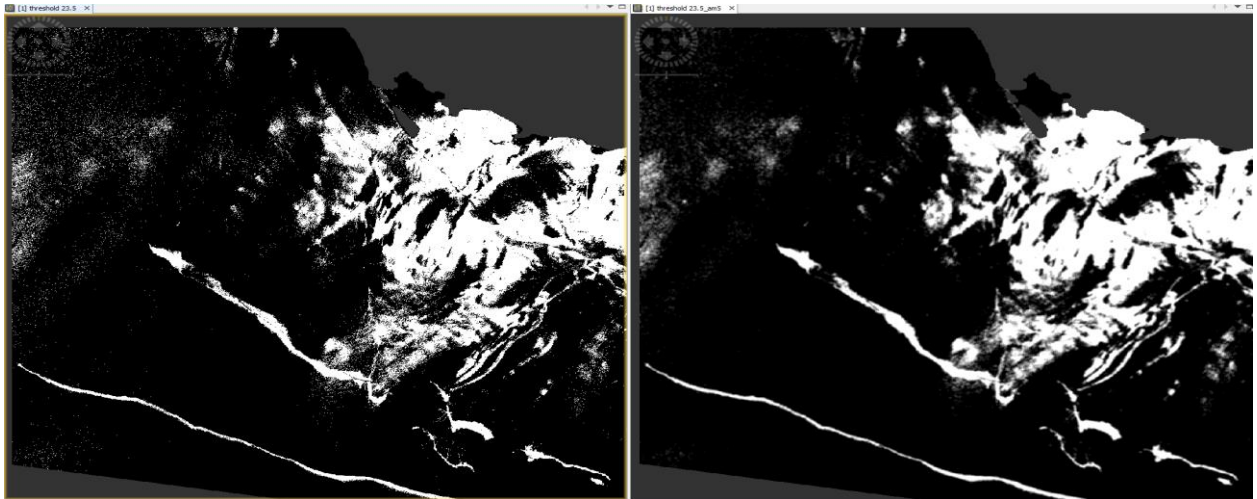


Figure 21: The image after the application of an arithmetic mean 5x5 filter.

3.1.5 Final step, color manipulation

The last step required a color manipulation to classify all the pixels and produce our final product as shown in Figure 21. To quantify the area covered by oil spill, a histogram was also used.

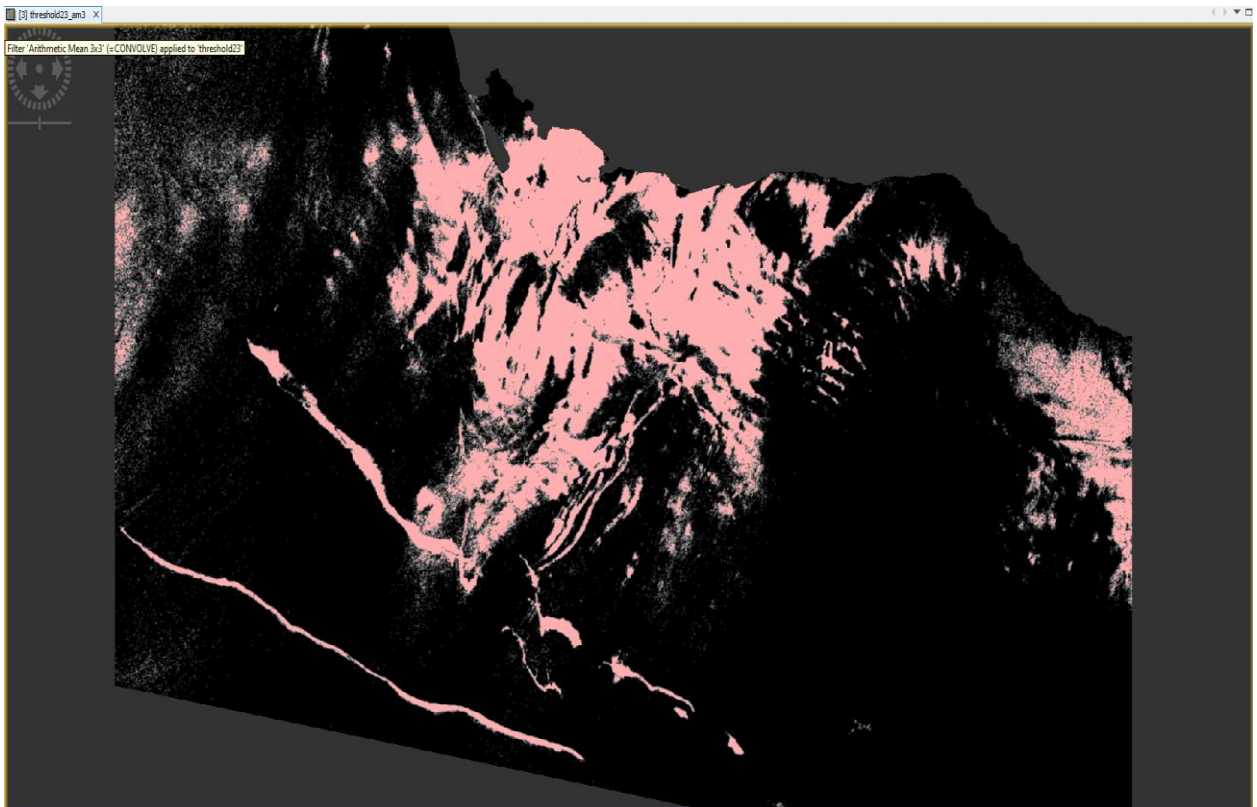


Figure 22: The final product of oil spill mapping.

The number of pixels with the value of 1 in the mask image of -23.5Db is 4,877,000 approximately (Figure 22). The original pixel spacing was 10 m, but we applied a multilook function, thus the pixel spacing ended up being 20 m. Knowing the pixel dimension which is $20 \times 20 = 400 \text{ m}^2$ and knowing the number of pixels covered by oil spill, we estimated the polluted area.

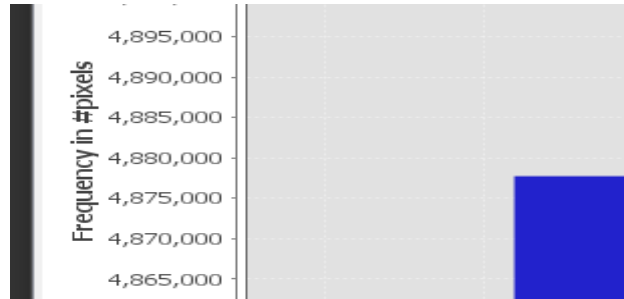


Figure 23: Histogram of pixels with the value of 1.

3.1.6 Extra step – Visualization in QGIS

For further analysis, the final image was exported as geotiff file and then was inserted in QGIS on Figure 23. By adding layers such as ocean, land and highways, we produced a realistic scenery. In other words, the results of the simulation, were projected in a Google terrain map in order to evaluate the environmental damage that has been done through April to May 2022.

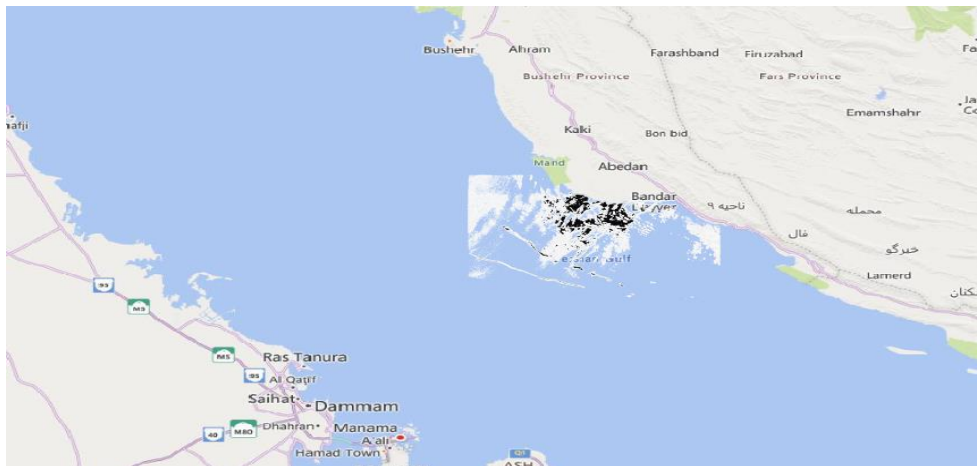


Figure 24: Projected image in the Google terrain map.

That scenario was a mapping for an incident that caused large scale damage to maritime environment. It is estimated that roughly 1,950 square kilometers of crude oil were spilled into the Persian Gulf (Figure 24).

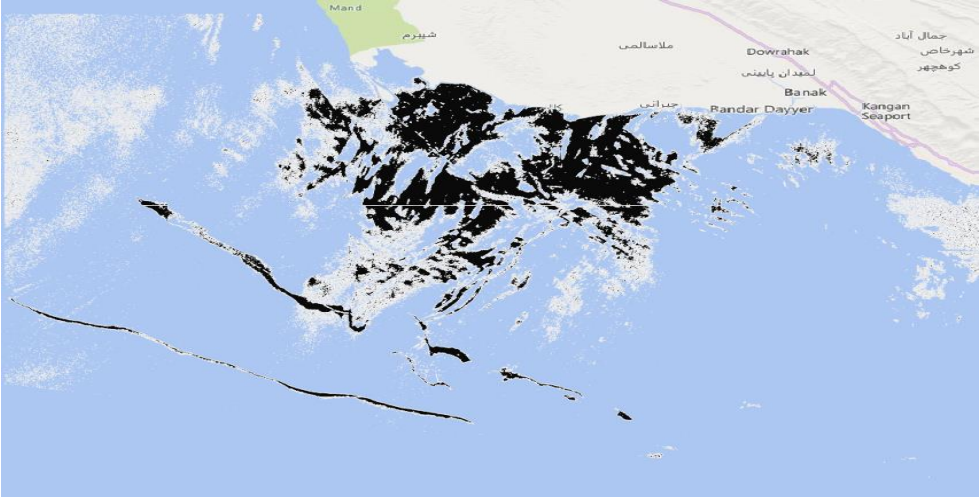


Figure 25: A closer look to understand the extension of pollution.

3.2 2st Scenario: Ice cover variability

3.2.1 Data download – Copernicus Open Access Hub

The second scenario of the simulation was the mapping of the sea ice variability in the Gulf of Bothnia (Figure 25). The gulf is very important for transporting oil to coastal cities and transporting ore to steel mills, for example in Raahé. In terms of capacity in international traffic, the largest ports on the Finnish side are Rauma, Kokkola and Tornio.

The main ports on the Swedish side are in Luleå, Skellefteå, Umeå, Sundsvall, Gävle and Hargshamn. Gävle is Sweden's third-largest container port and also ships forest products and oil. Icebreakers are required to assist port operations in the Gulf of Bothnia which lasts an average of up to six months while in the Gulf of Finland the period is only three months.

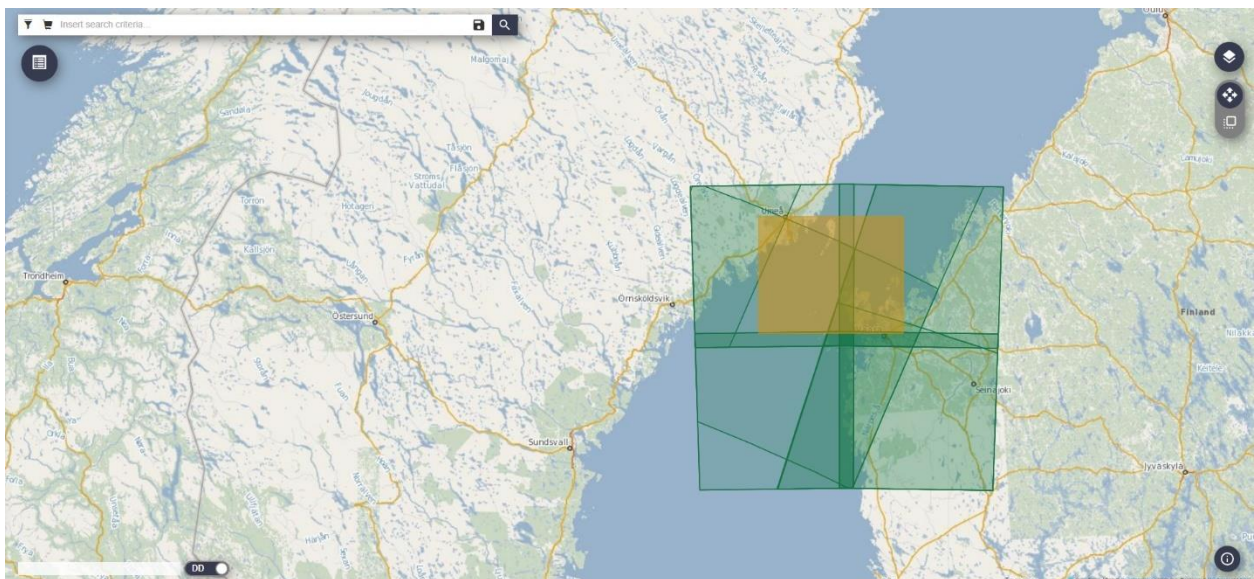


Figure 26: Gulf of Bothnia, the narrow shipping route that is used to transfer goods is the area of interest.

In this simulation we are going to use Sentinel-2 Optical data to map the sea ice variability of the Gulf of Bothnia from October 2021 to February 2022. **Some sources and reports on the classification and detection of different types of ice cover used neural networks and machine learning algorithms on SAR images combined with optical data. Optical data was acquired instead, because the use and the application of classification algorithms on those products are more efficient than they are on SAR products.** We use the Copernicus Open Access Hub for that purpose. Search filters only include Sentinel-2A or Sentinel-2B data, remote sensing period from 01/10/2022 to 25/2/2022 and S2MSI1C or MSIL2A product type. Finally, 2 products were selected as shown below.

Image ID:

S2A_MSIL1C_20211013T101951_N0301_R065_T34VDR_20211013T104044

and

S2B_MSIL2A_20220222T101019_N0400_R022_T34VDR_20220222T120120

3.2.2 Exploration of data and pre-processing

The Level-2A processing includes a scene classification and an atmospheric correction applied to Top-Of-Atmosphere (TOA) Level-1C orthoimage products. Level-2A main output is an orthoimage Bottom-Of-Atmosphere (BOA) corrected reflectance product. Table 5 presents the Sentinel-2 product types while Figure 26 shows the different spectral bands for each product.

Standard distributed products contain the envelope of all resolutions in three distinct folders:

- 10 m: containing spectral bands 2, 3, 4, 8, a True Color Image (TCI) and an AOT and WV maps resampled from 20 m.
- 20 m: containing spectral bands 2 – 7, the bands 8A, 11 and 12, a True Color Image (TCI), a Scene Classification map (SCL) and an AOT and WV map. The band B8 is omitted as B8A provides more precise spectral information.
- 60 m: containing all components of the 20 m product resampled to 60 m and additionally the bands 1 and 9. The cirrus band 10 is omitted, as it does not contain surface information.

Table 5: Sentinel-2 product types

Name	High-level Description	Production and Distribution	Data Volume
Level-1B	Top-of-atmosphere radiances in sensor geometry	Systematic generation and online distribution	27 MB (each 25*23 km ²)
Level-1C	Top-of-atmosphere reflectances in cartographic geometry	Systematic generation and online distribution	500 MB (each 100*100 km ²)
Level-2A	Bottom-of-atmosphere reflectances in cartographic geometry	Generation on user side	600 MB (each 100*100 km ²)

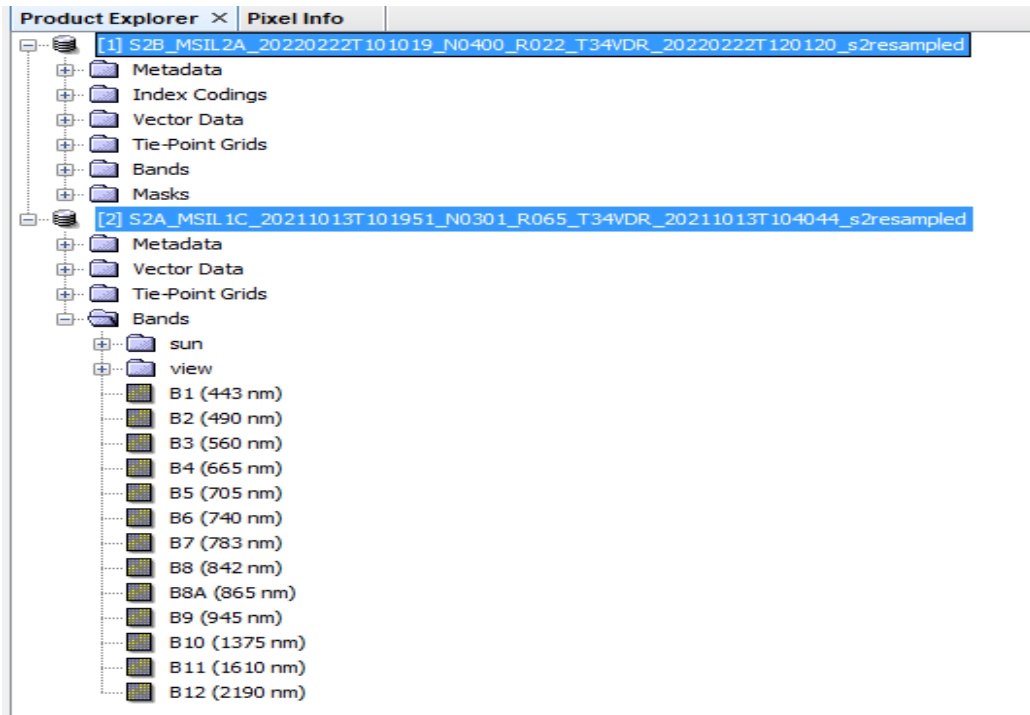


Figure 27: Exploring the bands of the 2 products

The spatial resolution of all satellite bands should be resampled to a unique size (60m to simplify the processing workflow). From the SNAP window on the upper bar we apply **Optical -> Geometric -> S2 Resampling Processor**.

Processing Parameters are set as below:

Output resolution: 60

Upsampling method: Bilinear

Downsampling method: Mean

Flag downsampling method: First

The composite RGB (color) image to be created is using the B4 channel for red, B3 for green and B2 for blue. We can also produce a False-color Infrared image for better contrast, using B8 channel for red, B4 for green and B3 for blue in Figure 27.

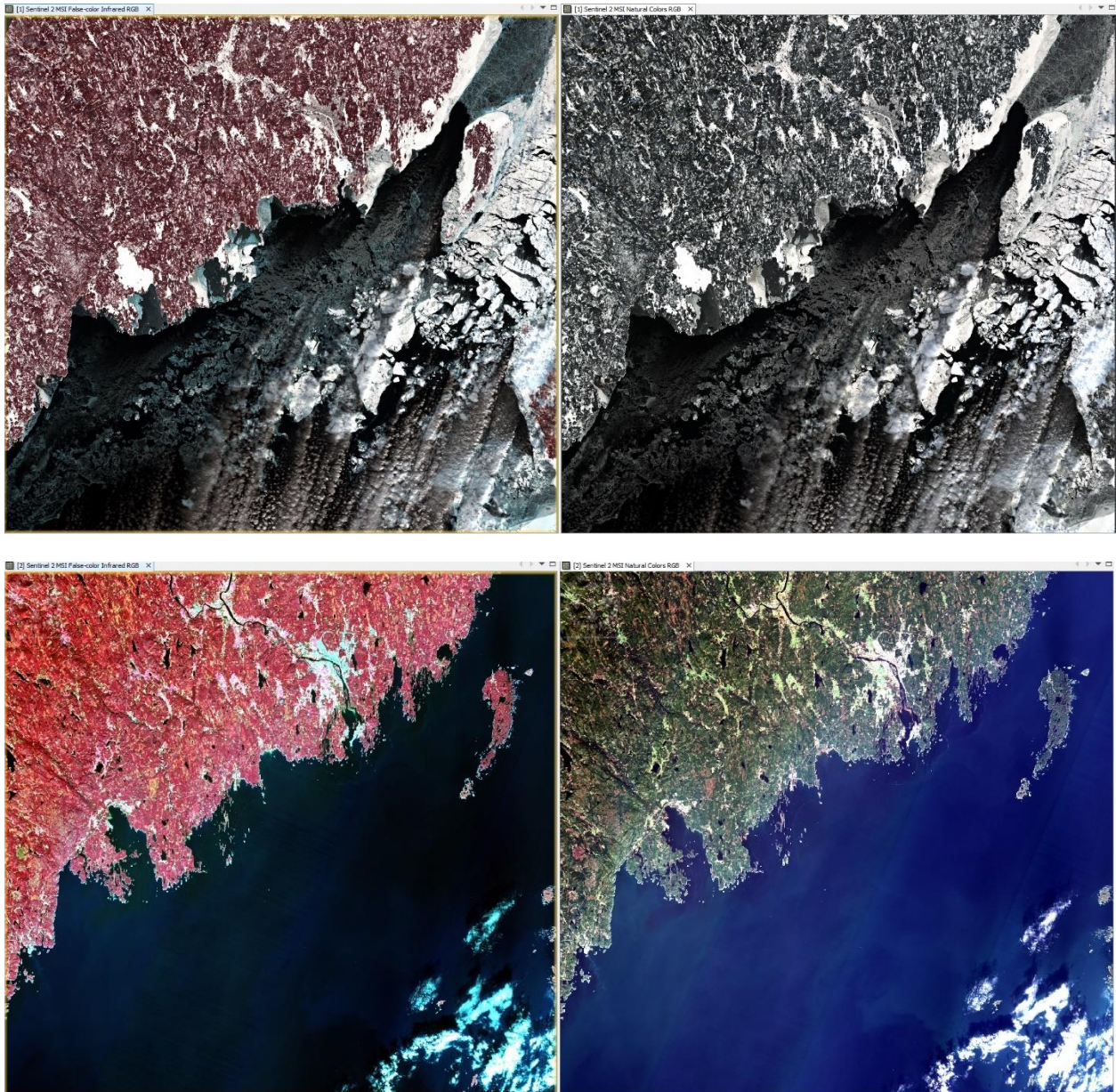


Figure 28: Satellite image of the gulf of Bothnian with 2 different channel combinations. Upper and lower left images are set to B8, B4 and B4 for red, green and blue respectively while upper and lower right images are set to B4, B3 and B2 for red, green and blue respectively. Top images correspond to 22/02/2022 while lower images correspond to 13/10/2021.

The Level-2A prototype product is an orthorectified product providing Bottom-of-Atmosphere (BOA) reflectance and basic pixel classification (including classes of different types of cloud).

In order to remove the impact of clouds we will apply a simple band math expression in all bands except B11 and B12. Bands from B1-B9 will be recreated with the subtraction of B11 or B12 (Figure 28).

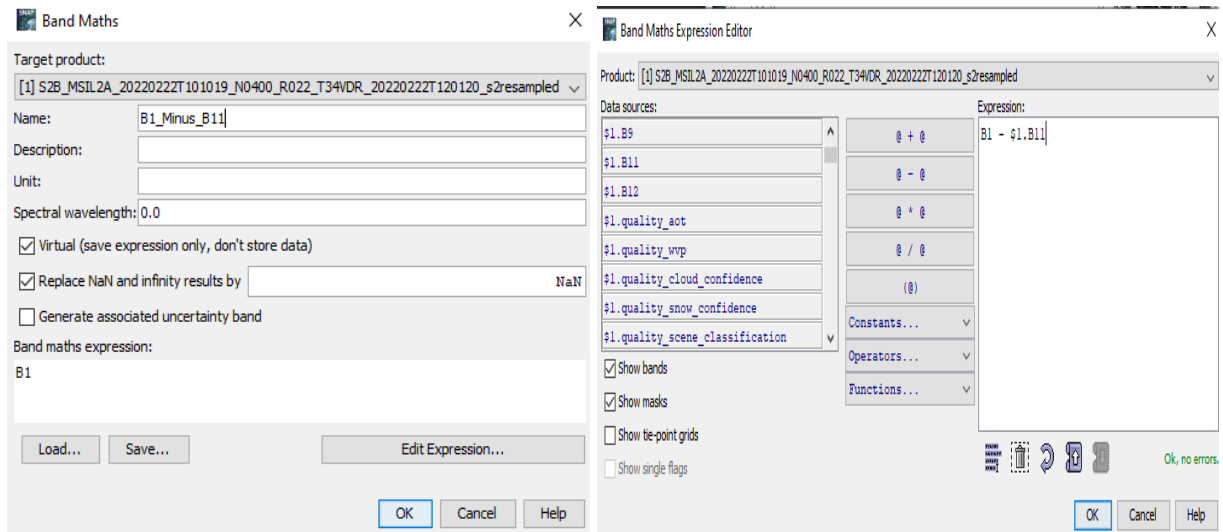


Figure 29: The expression that was used in very single band

After we apply the expressions, 2 new composite RGB images are produced with the modified channels B8, B4, B3 and B4, B3, B2 respectively. The difference is obvious in Figure 29 with the cloud coverage being reduced significantly.

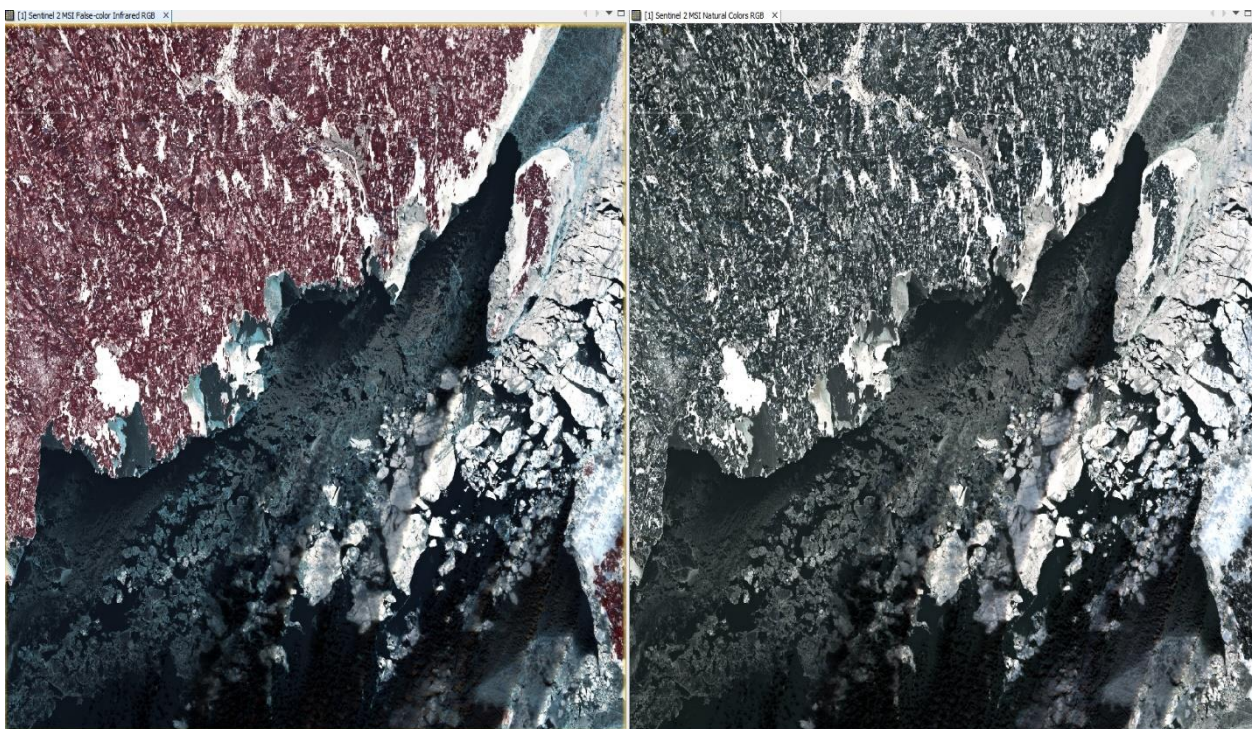


Figure 30: Sentinel 2 MSI False-color Infrared RGB (left), Sentinel 2 MSI Natural Colors RGB (right)

3.2.3 Unsupervised Classification

The next stage of the simulation consists of an unsupervised classification of the different types of sea ice, as each type differs in thickness and size. In addition to the floating ice, the image consists of urban areas, lakes, soil and snow. However, the urban area is not taken into account and instead is considered as an icy field. To perform the classification, we follow the path **Raster -> Classification -> Unsupervised Classification -> K-Means Cluster Analysis** in the SNAP toolbar.

The classification is performed 3 times with the number of clusters as 5, 6 and 7 respectively (Figure 30). After selecting the new bands without the cloud interference, we run the algorithm. The color of each class depends on our personal taste and approach. For example, even if the classification does not categorize the thick ice correctly, we can manipulate the color palette and homogenize it with a different misclassified ice.

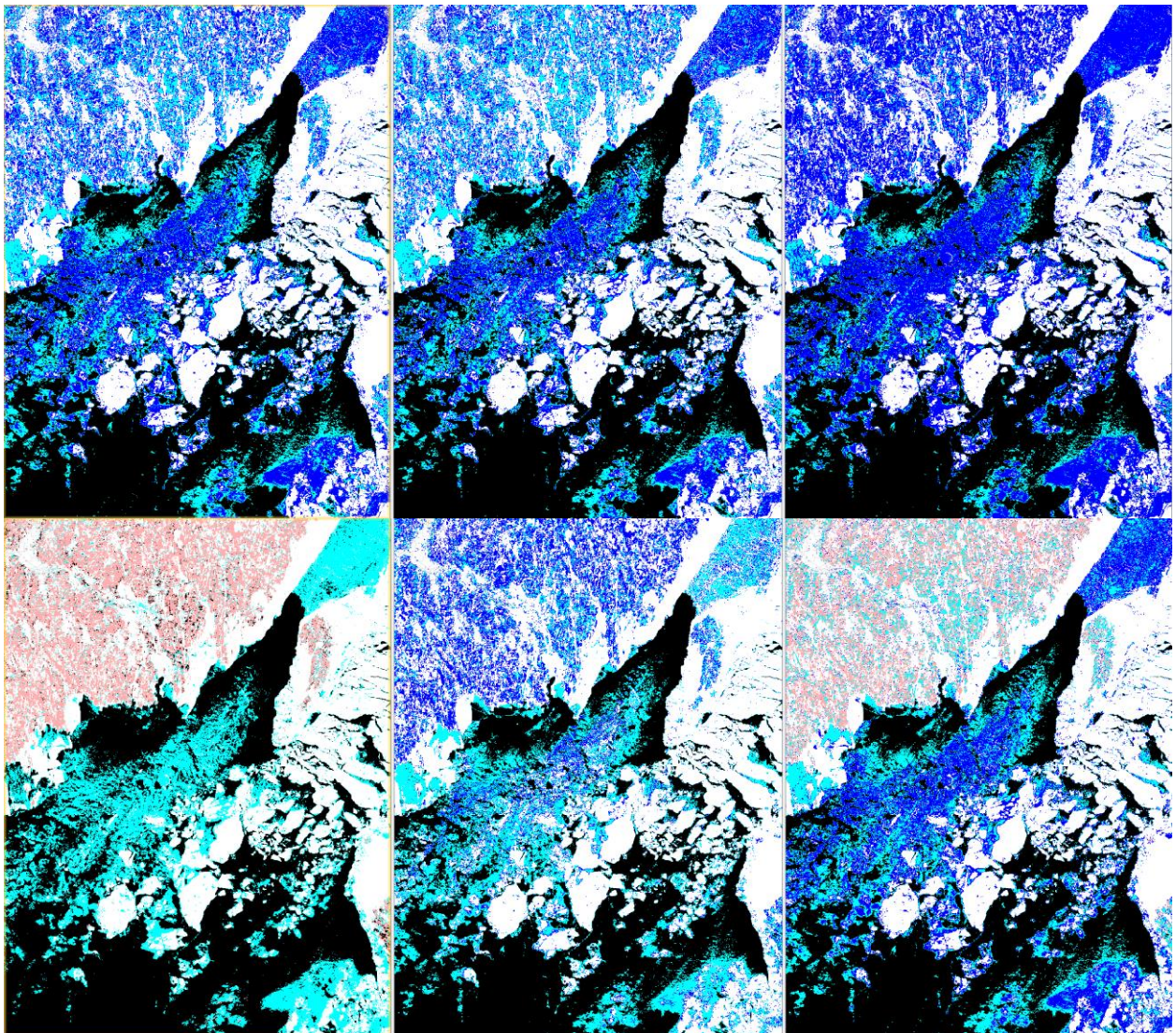


Figure 31:EM Cluster Analysis upper left (with 5 clusters), upper mid (with 6 clusters) and upper right (with 7 clusters). K-Means Cluster Analysis lower left (with 5 clusters), lower mid (with 6 clusters) and lower right (with 7 clusters).

The next classification we apply in the product is the **EM Cluster Analysis**. We repeat the steps 3 times with the number of clusters 5, 6 and 7. The histogram in Figure 31 clearly shows the percentage of coverage of each layer of ice with the addition of land and water. Only **K-Means** with 5 or 7 clusters seems to identify the land. With 6 clusters, the algorithm perceives the soil as a thin layer of ice.

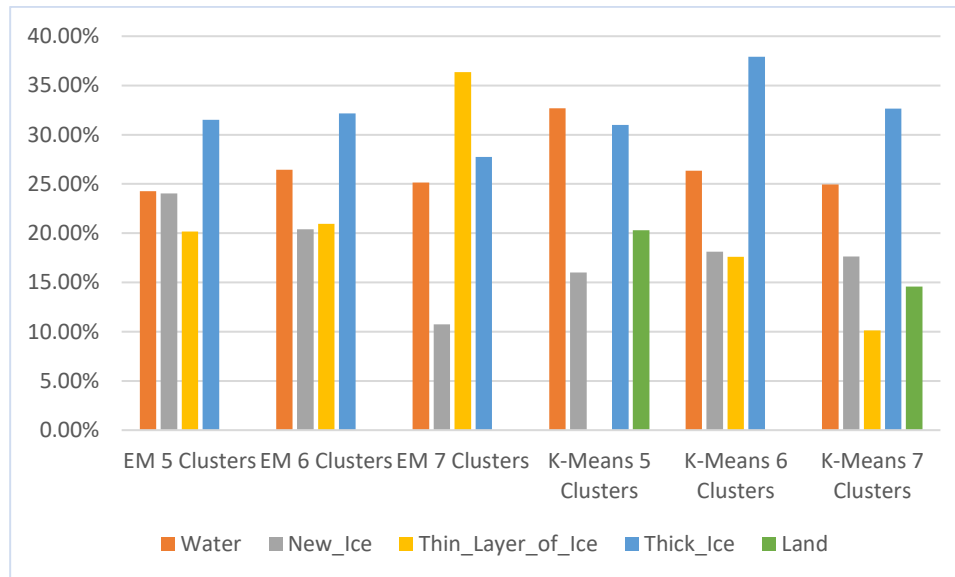


Figure 32: Histogram of the 2 types of Cluster Analysis for different number of clusters as described for “water”, “new ice”, “thin layer of ice”, “thick ice” and “land” classes.

The results are interesting but not overly useful, even though it looks promising for distinguishing water and thick ice. There is definitely some confusion with the thin layer and the new ice but the important thing is that this step helps us target areas that need more attention and, in this case, distinguishing water from thick ice is a key parameter.

Obviously adding in some better training data, actual field or ground verified training data would help but that would move us into supervised image classification which is the next subchapter.

3.2.4 Supervised Classification

In order to classify the image through a supervised classification approach, a training data set is needed by making the use of on-screen digitization to define learn areas. The tools for on-screen digitization will be the *polygon drawing tool*. Also, for the new vectors' data container, we add *Water*, *New_Ice*, *Thin_Layer*, *Thick_Layer* and *Land*. Our object is to be able to separate the water satisfactorily from the land and then to make a proper assessment of the different types of ice that float in the sea.

At this point, five vector samples are gathered corresponding to each type of surface. The goal of the machine learning model is to generalize well the training data. If the model learns the detail and noise of ice to the extent that it negatively impacts the performance of the new data, overfitting will happen and is more likely to apply ice coverage to new data.

On the other hand, if less than five vector samples are selected, the machine learning model will have poor performance on the training data, consequently it will fail to generalize ice type variability to the new data set. Below in Figure 32, we classify each surface type with different colored polygons.

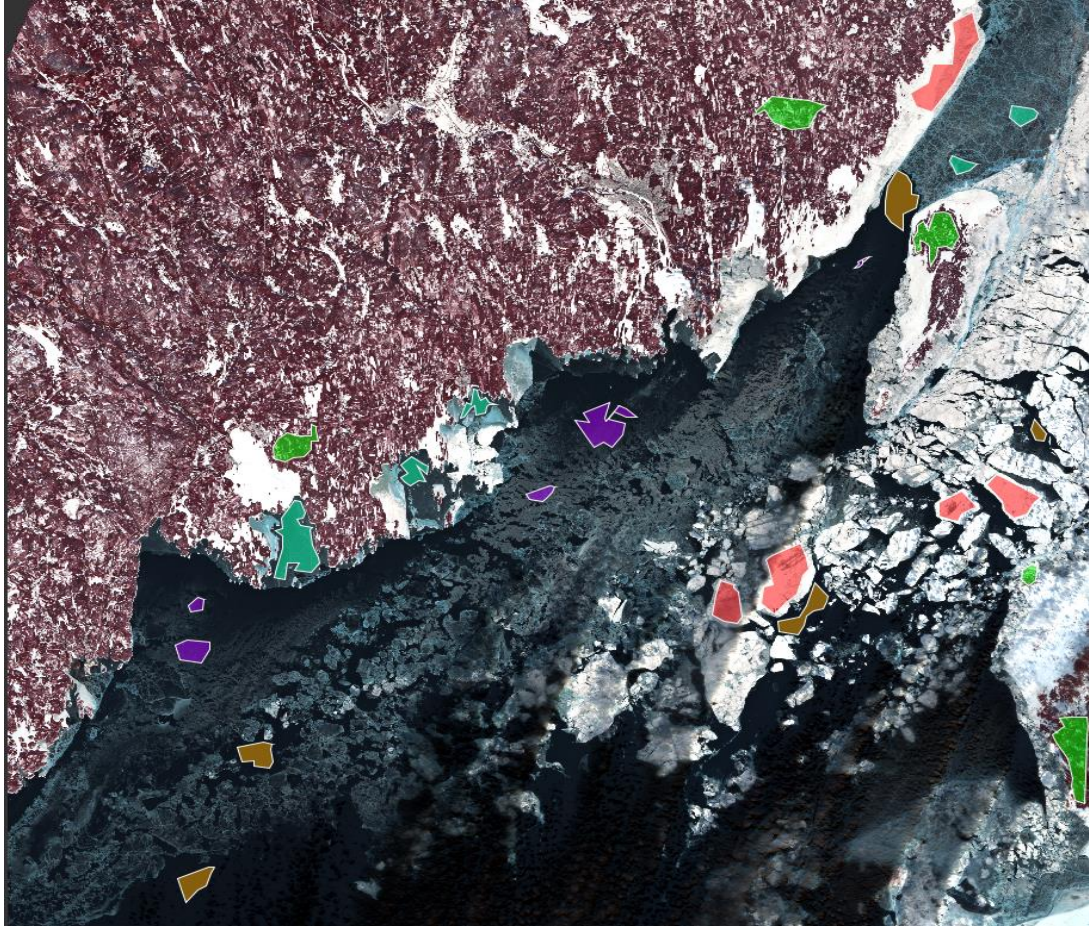


Figure 33: Different color of polygons reflect different surface type. Brown, Purple, Fern, Red and Green for Water, New Ice, Thin Ice, Thick Ice and Soil respectively

In the final step, the collected training areas which represent homogeneous areas of the scene of different ice cover types, will be used to perform 5 different supervised classifications. Those are: *Random Forest*, *KNN*, *KDTree KNN*, *Maximum Likelihood* and *Minimum Distance Classifiers*. The feature bands we choose for the previous mentioned classifiers are the new bands from B1-B9 with the absence of clouds.

The classifier identifies the five given classes and assign to each one of them a different color. The color manipulation tab provides us with a list of color assignments and the frequency of occurrence in the processed image. An appropriate label recoloring to more meaningful intuitive matching colors is necessary to achieve a better understanding of the ice cover variability (Figure 33). Table 6 below contains the results for different classifiers and represent how much of each type of has been identified with percentage numeric values.

Table 6: Percentages of surface type coverage for different classifier along with the average percentage value

	<i>KD</i>	<i>KNN</i>	<i>MD</i>	<i>ML</i>	<i>RF</i>	Average
<i>Water</i>	16.92%	17.05%	19.63	1.51%	14.35%	13.89%
<i>New_Ice</i>	10.57%	10.15%	14.44%	5.88%	15.03%	11.21%
<i>Thin_Layer</i>	20.36%	20.05%	17.96%	27.49%	17.40%	20.65%
<i>Thick_Layer</i>	12.47%	14.80%	22.07%	9.22%	16.39%	14.99%
<i>Land</i>	39.68%	37.95%	25.90%	55.90%	36.83%	39.25%
Sum	100%	100%	100%	100%	100%	100%

Label	Colour	Value	Frequency	Description
no data		-1	0.000%	no data
Water		0	17.045%	
New_Ice		1	10.157%	
Thin_Layer		2	20.047%	
Thick_Layer		3	14.803%	
Land		4	37.948%	

Figure 34: Color manipulation tab for KNN Classifier

Of all the classification algorithms applied in Figure 34, the top 3 classifiers are **KD**, **KNN** and **RF Classifiers**. KD excels at classifying new ice, thin layers of ice and land while KNN can produce better results on identifying thick layers which is crucial for maritime shipping. Last but not least, RF has better performance on classifying water. Table 7 shows the performance of the classifiers. The closer to 0 the better we consider the algorithm to have performed in detecting and classifying a land or sea type. The numbers with bold text belong to the classifier with the best performance for identifying each type.

Table 7: Distance from average percentage value for KD, KNN and RF.

	KD	KNN	RF
Water	+ 3.03%	+ 3.16%	+ 0.46%
New_Ice	- 0.64%	- 1.06%	+ 3.82%
Thin_Layer	- 0.29%	- 0.60%	- 3.25%
Thick_Layer	- 2.52%	- 0.19%	+ 1.40%
Land	+ 0.43%	- 1.30%	- 2.42%

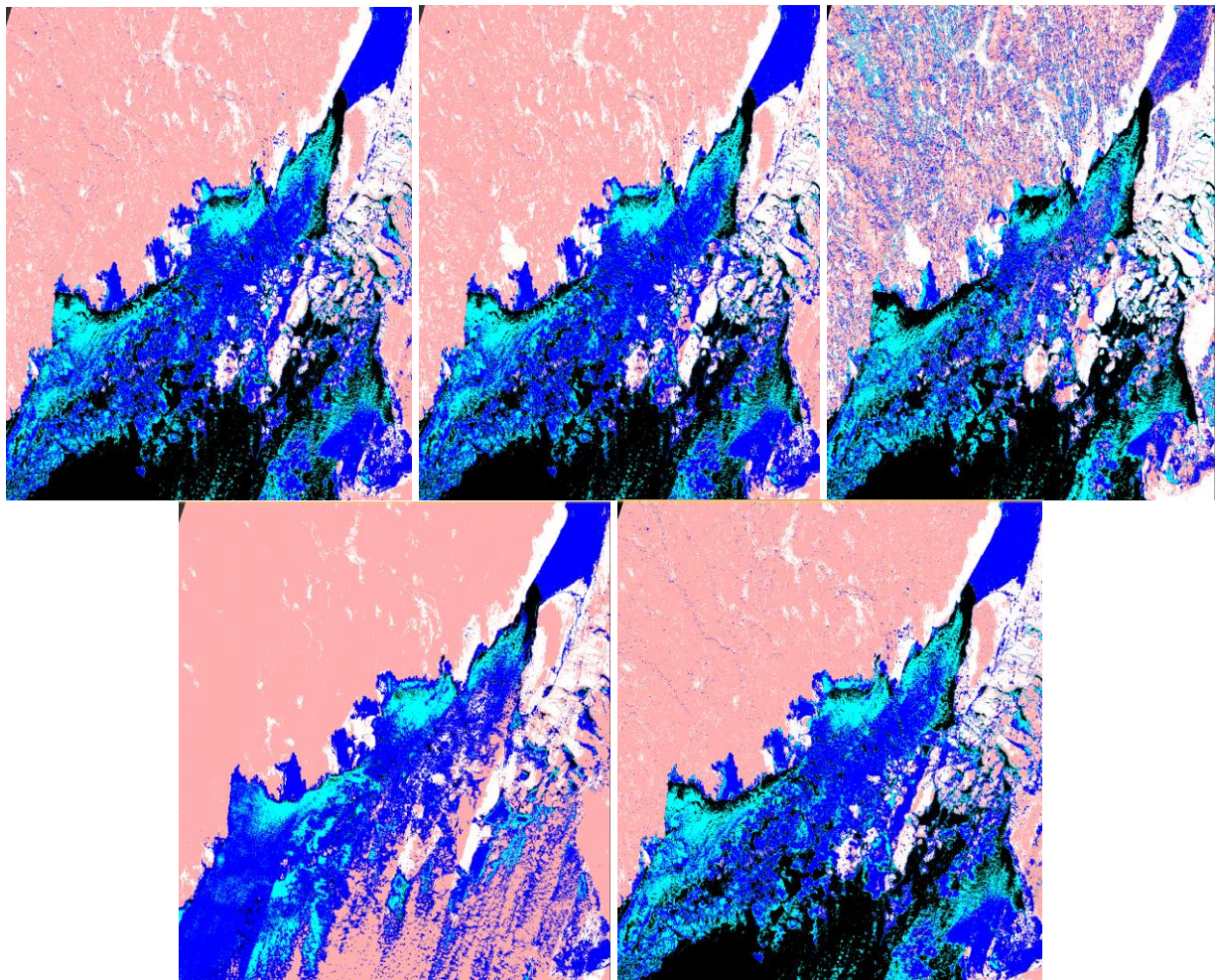


Figure 35: KD (upper left), KNN (upper mid), MD (upper right), ML (lower left), RF (lower right)

3.2.5 Extra step – Visualization in QGIS

The combination of SNAP and GIS is an excellent practical tool that can project the extent of ice cover on the Earth map and capture the magnitude of the hazard on important maritime shipping lines. By separating the different types of ice with colors such as teal, blue and white, we can create layers, each of which is shown in Figure 34. Teal is the type of ice that can be easily penetrated by ships with an average thickness of 10cm, blue is potentially dangerous between 10-30cm but has high permeability with icebreakers while white is considered dangerous for navigation with an average of 120-200cm thickness.

The last category of ice flows varies considerably in size, thickness and roughness depending on their growth history. Many of these characteristics can be seen in the satellite image of a typical multi-year floe, presented in Figure 35. Thick ice is the stronger and hardest form of the sea ice and represents a serious impediment, indeed a danger to all ship, as even the most powerful icebreakers will avoid contact with it if at all possible.

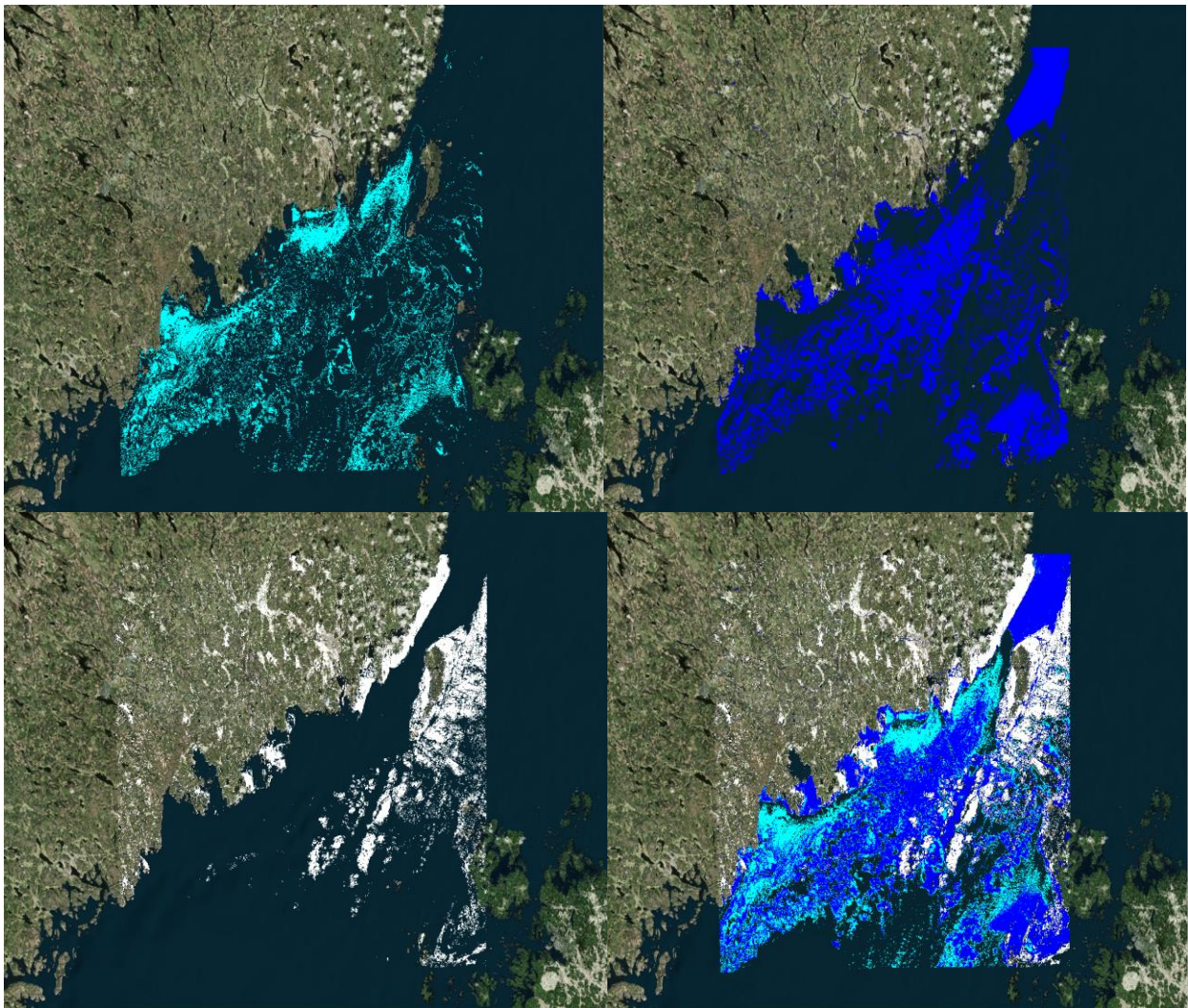


Figure 36: New ice with teal color (upper left), thin layer with blue color (upper right), thick ice with white color (lower left) and the union of the 3 different types of ice (lower right)

4. 2ND SIMULATION DESIGN

4.1 3rd Scenario: Ocean Wind Speed Estimation and Direction

4.1.1 Data download – Onda Dias

In the 3rd scenario, Sentinel-1 SAR data will be used for the data processing which is Level 1 SAR image of the Strait of Gibraltar (Figure 36). Search filters include Sentinel-1A or Sentinel-1B products, remote sensing period from 01/05/2022 to 31/05/2022, GRD product type and IW sensor function. The image ID is:

S1A_IW_GRDH_1SDV_20220525T181822_20220525T181847_043371_052DE0_BA96.

The Strait is an important shipping route from the Mediterranean to the Atlantic. There are ferries that operate between Spain and Morocco across the Strait, as well as between Spain and Ceuta and Gibraltar to Tangier, passing through the straits once every five minutes with countless smaller boats and yachts passing through frequently.

This strategic position is a globally important shipping lane and is considered to be one of the busiest waterways across the globe.

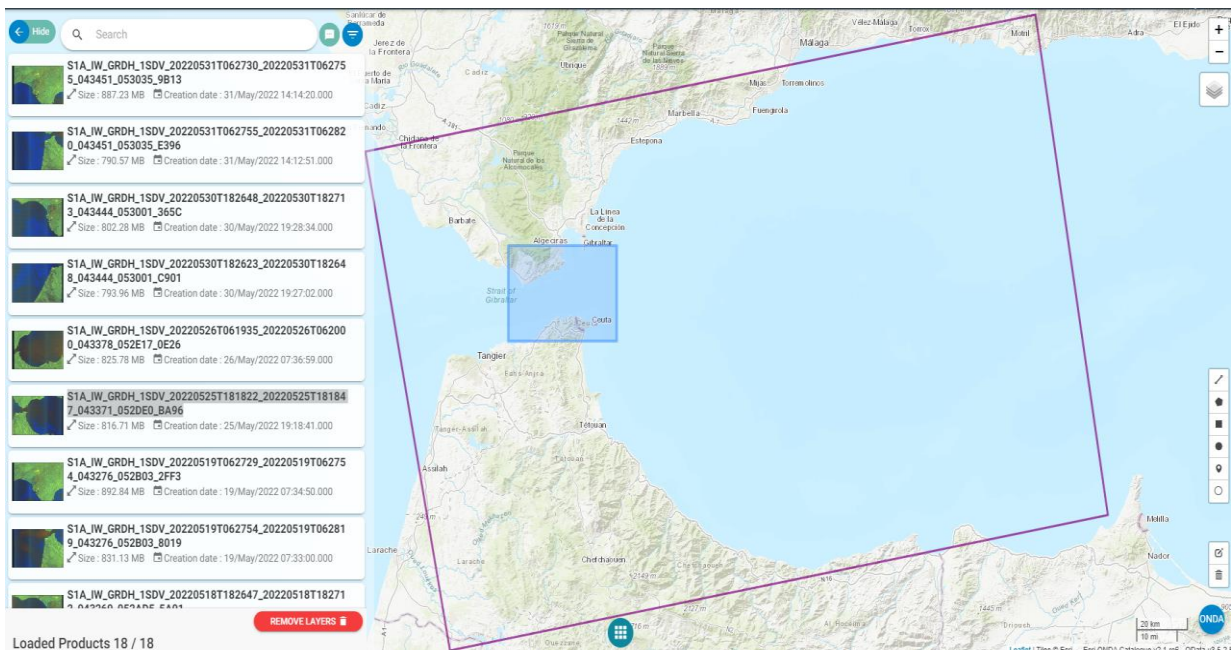


Figure 37: Strait of Gibraltar as the area of interest.

4.1.2 Data pre-processing

The first step incorporates the pre-processing of the data by applying a precise orbit file and a thermal noise removal operator. The precise orbits of satellites are determined after several days and are available days-to-weeks after the generation of the product. In that case, the operation allows the automatic download and update of the orbit state vectors for each SAR scene, providing an accurate position and velocity information. From the SNAP window on the upper bar **Radar -> Apply Orbit File** we produce the image with the precise orbit values.

The thermal noise removal reduces noise effects in the inter-sub-swath texture normalizing the backscatter signal within the entire Sentinel-1 data. So, the next step requires the path **Radar -> Radiometric -> S-1 Thermal Noise Removal** in order to continue in the batch processing through a graph builder. Below in Figure 37 we can see the image before any pre-processing function is applied.

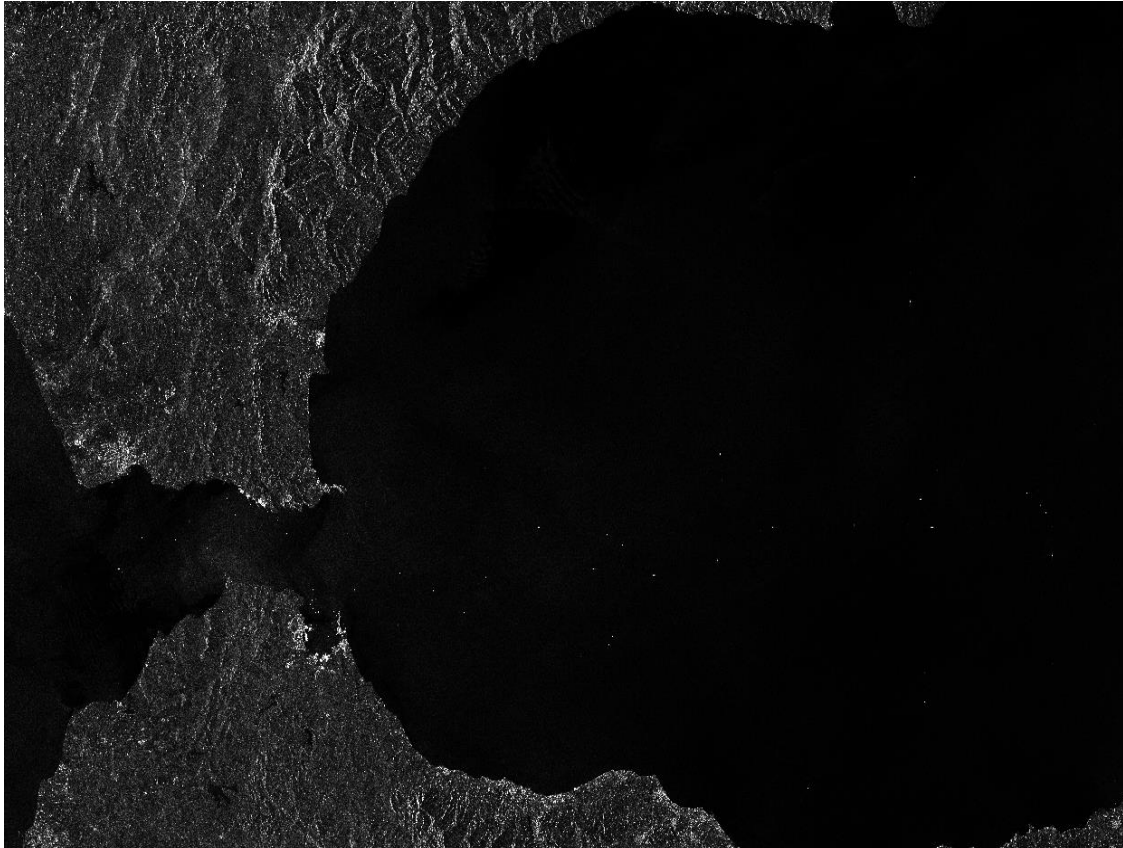


Figure 38: The SAR image before the batch processing.

4.1.3 Image processing with graph builder

After the precise orbits file and the thermal noise removal implementation, the data has the appropriate values to receive the next processing chain, which will estimate and evaluate the wind speed and direction. The graph builder that will be used, consists of *Land-Sea-Mask*, *Calibration*, *Wind-Field-Estimation* and *Range-Doppler Terrain-Correction* algorithms. For the Land Sea Mask, we extend the shoreline by 5 pixels, for the calibration we use the default parameters while in the Wind Field Estimation we use Sigma Nought input, followed by a 10 km window size. The window size setting is the most important setting because this will affect the wind field point density output. For the last algorithm, we perform the terrain correction to make the output data following a true map projection. The checkbox “Mask out areas without elevation” stays unchecked since we have already mask out land area. The final graph builder is shown in Figure 38.

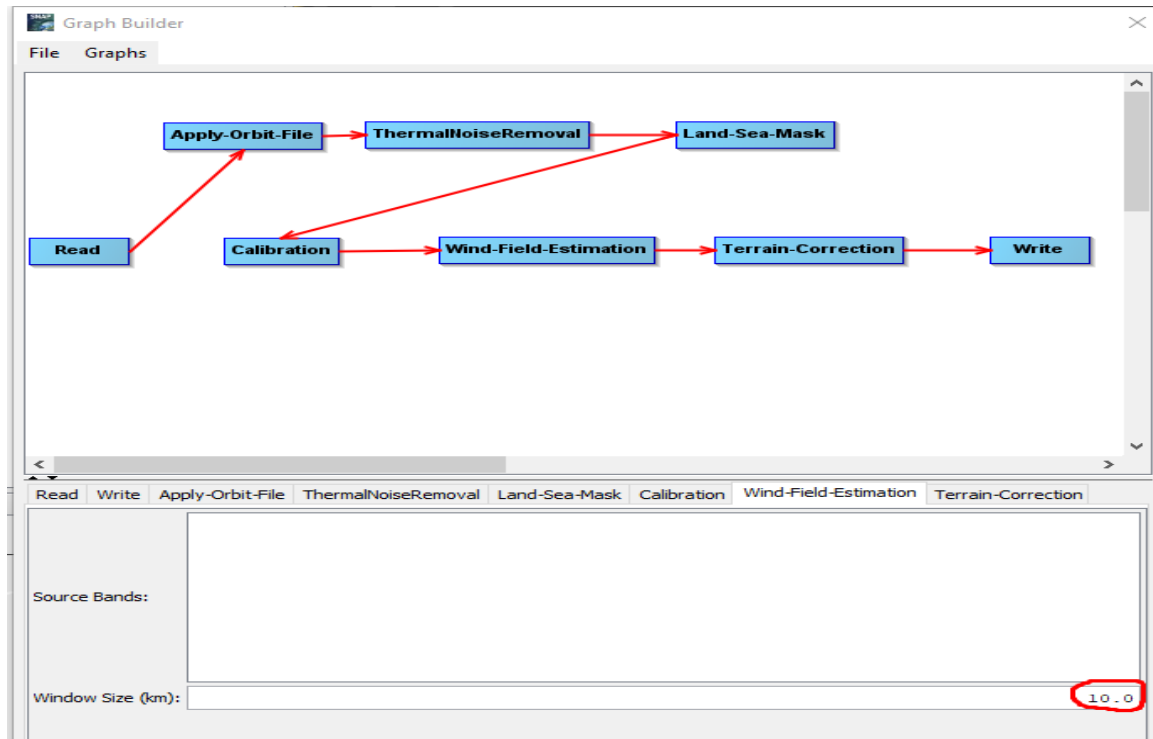


Figure 39: A complete graph that was used during the image processing for wind field estimation with a window size of 10

The final output image for the wind field estimation has regular points symbolized with red tic marks. We run the batch processing chain twice with different window size. The first one has a 10 km window size while the second has a 20 km window size, in order to compare the difference in the concentration of the wind marks. The smaller the size of the window, the denser the wind field values resulting in more information but additional delay in image processing. Below in Figure 39 the final geocoded images are shown which represent the two different size windows in each case.

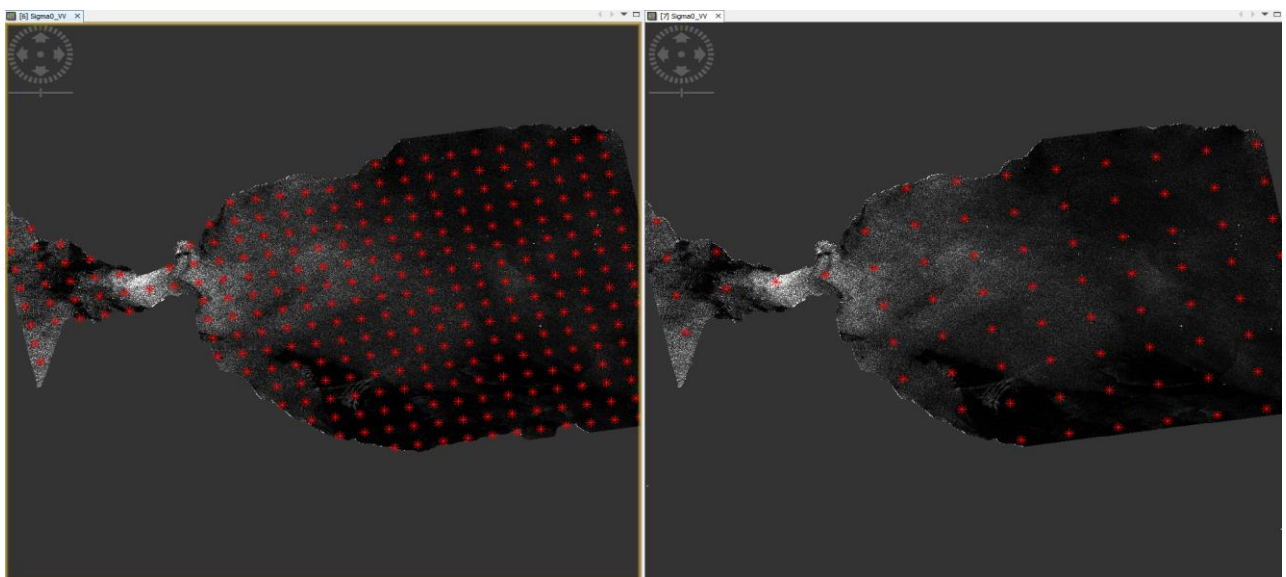


Figure 40: The final output image for the wind field estimation with 10 km window size on the left and 20 km window size on the right

4.1.4 Adding the wind field data

The values from the wind field data can be placed in the image through the layer manager. By adding the wind field estimation results we can produce the wind direction data recorded from the SAR imagery, along with its speed estimation for the current area. The output wind direction and speed points data are stored in the vector data folder (in CSV format) for every product and the export of the data to shapefile format is available for further processing in QGIS software (Figure 40).

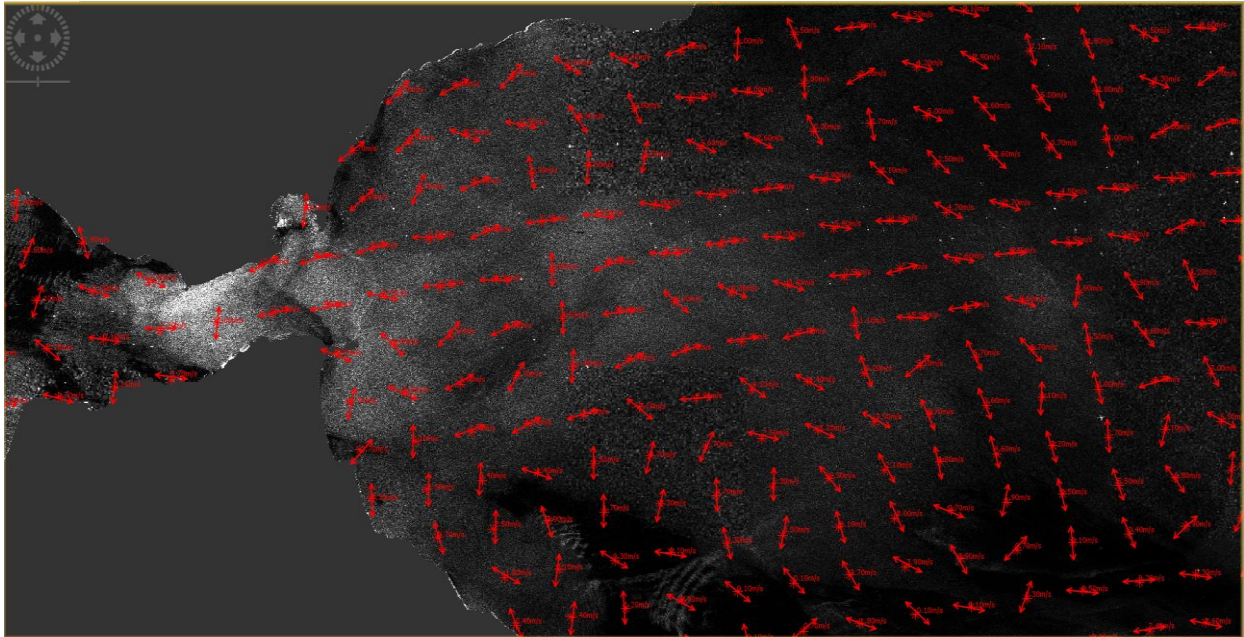


Figure 41: Wind direction and speed estimation data presented with red arrows and numeric values for the area of interest in SNAP

4.1.5 Vector data visualization in QGIS

The wind vector data was extracted from the product dataset and afterward was imported in the QGIS software for visualization and demonstration. The shapefile created during the extraction included values from the wind speed, direction and geocoded information. On QGIS toolbar we selected **Layer -> Add Layer -> Add Vector Layer** and we chose the file that was saved as **.shp**. The second layer that was activated during the simulation included a Google Satellite map of the Strait of Gibraltar (Figure 41).



Figure 42: Vector points projected on a Google Satellite map

Points were modified using wind direction data as a rotation factor and an arrow as a wind direction symbol to better represent the wind field. The wind speed was classified in 8 classes and graduated from 0 to 13.5 to show the variations in Figure 42. Depending on the value, arrows take a different shade of red. The higher the wind speed, the redder the arrow, that means stronger wind presence around the spot. Fortunately, there was no evaluation failure during the wind field estimation and all of the data was successfully estimated.

Symbol	Values	Legend
<input checked="" type="checkbox"/>	0.1000 - 1.0000	0.1 - 1
<input checked="" type="checkbox"/>	1.0000 - 2.2000	1 - 2.2
<input checked="" type="checkbox"/>	2.2000 - 3.3000	2.2 - 3.3
<input checked="" type="checkbox"/>	3.3000 - 4.6000	3.3 - 4.6
<input checked="" type="checkbox"/>	4.6000 - 5.9000	4.6 - 5.9
<input checked="" type="checkbox"/>	5.9000 - 7.4000	5.9 - 7.4
<input checked="" type="checkbox"/>	7.4000 - 9.4000	7.4 - 9.4
<input checked="" type="checkbox"/>	9.4000 - 13.5000	9.4 - 13.5

Figure 43: Classified wind speed values

The values of wind speed and the different directions are shown in Figure 43. We could also use the Sentinel-1 Level-2 OWI component of the ocean surface wind vector (speed and direction) and skip the whole simulation design and save a lot of time. However, Level-2 OCN products are processed by the Level-2 Instrument Processing Facility (IPF) and sometimes values are miscalculated or missing. Also, during the processing, a job order is read by the processor retrieving high level information required for processing a particular product. The land is not masked out and as a result, the algorithms for each component, as well as the workflow for the Level-2 OCN product generation, generates wind fields for the land area.

Therefore, we cannot rely on the Level-2 OCN data but a better approach would be to prepare the first level data manually and extract the vector fields.



Figure 44: The wind field estimation (speed and direction) in QGIS

4.2 4th Scenario: Ship and object detection

4.2.1 Data download – Onda Dias

In the 4th scenario, Sentinel-1 SAR data was used again for the data processing which is Level 1 SAR image of the Saronic Gulf (Figure 44). Search filters include Sentinel-1A or Sentinel-1B products, remote sensing period from 01/07/2022 to 3/07/2022, GRD product type and IW sensor function. The image ID is:

S1A_IW_GRDH_1SDV_20220702T162338_20220702T162403_043924_053E5E_4618.

The most important industrial, port, naval and shipbuilding facilities of the country were created on the shores of the Saronic. Together with the Argolic Gulf, they administratively and geographically form the ArgoSaronic region. The Argosaronic Islands are administratively under the Prefecture of Piraeus, (one of the four prefectures into which the Region of Attica is divided) which also includes the islands particularly remote from Attica: Kythira and Antikythera located south of the Peloponnese.

The Saronic Gulf is of particular maritime importance both for the maritime transports of which it is the starting point for many, but also from the fact that it connects the Aegean Sea with the Ionian Sea through the Isthmus of Corinth.

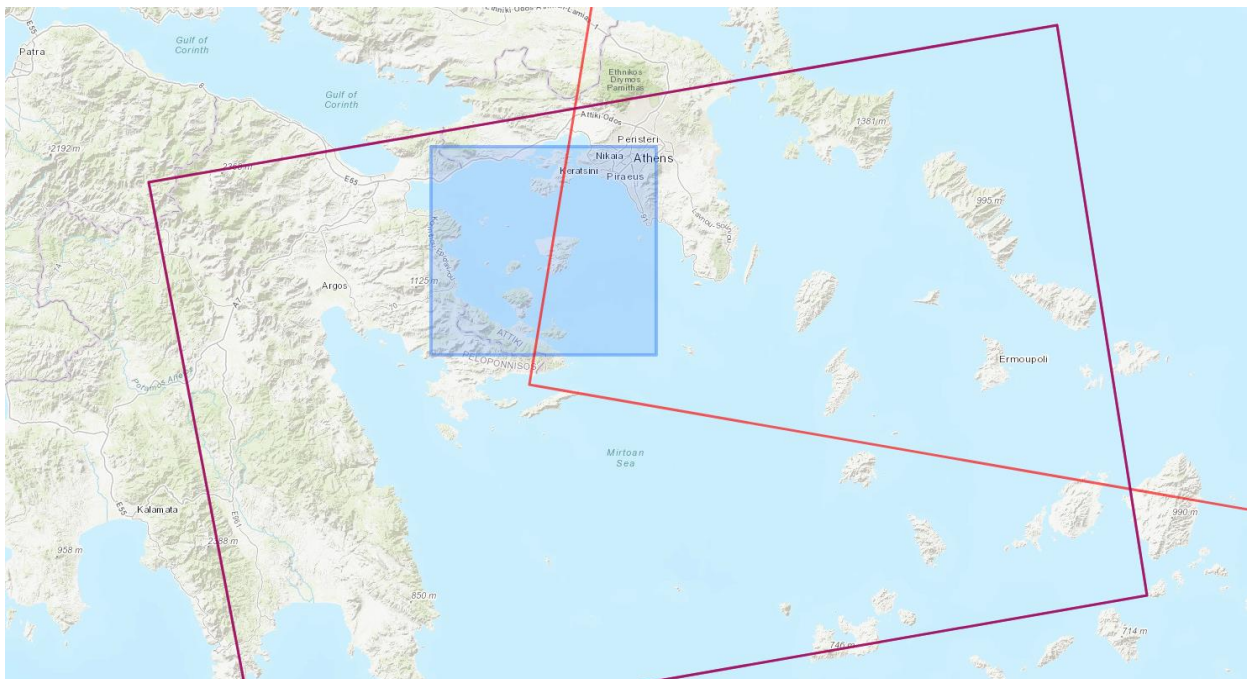


Figure 45: Saronic Gulf as the main area of interest of the wider region of Central Greece

Our initial object was to study the presence of dangerous cargoes transported by ships through the sea. SNAP can locate ships of small or large size and in combination with optical data, images can be analyzed to identify vessels that carry dangerous cargoes. This can be done either by thorough texture analysis or by a machine learning algorithm adapted to primarily detect flammable materials that are not secured and sealed in containers. Such combustible materials are coal, sulfur, cotton and fish meals which are heated due to the oxidation process. In this thesis we will create a simulation model specialized only in ship detection. Unfortunately, SNAP and QGIS alone cannot contribute further to the specific study without the use of python and machine learning

libraries. To do so would require expanding the research and going beyond the scope of this thesis into different scientific fields that are not our primary target.

4.2.2 Data pre-processing

We chose the ground and ranged detected product type, the standard GRD product consisting of two radar bands in VH and VV polarization separated by amplitude and intensity bands as shown in Figure 45.

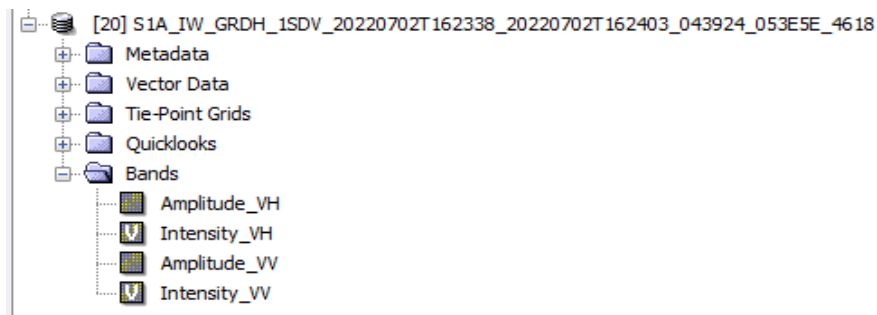


Figure 46: Four bands available for pre-processing, 2 amplitude VH and VV and 2 Intensity VH and VV respectively

The whole scene look was subset since we did not need to process the entire image and the land area was not of our interest. Thus, we only focused on certain area to reduce the processing time. In our case we used the spatial subset by manual definition as shown in Figure 46

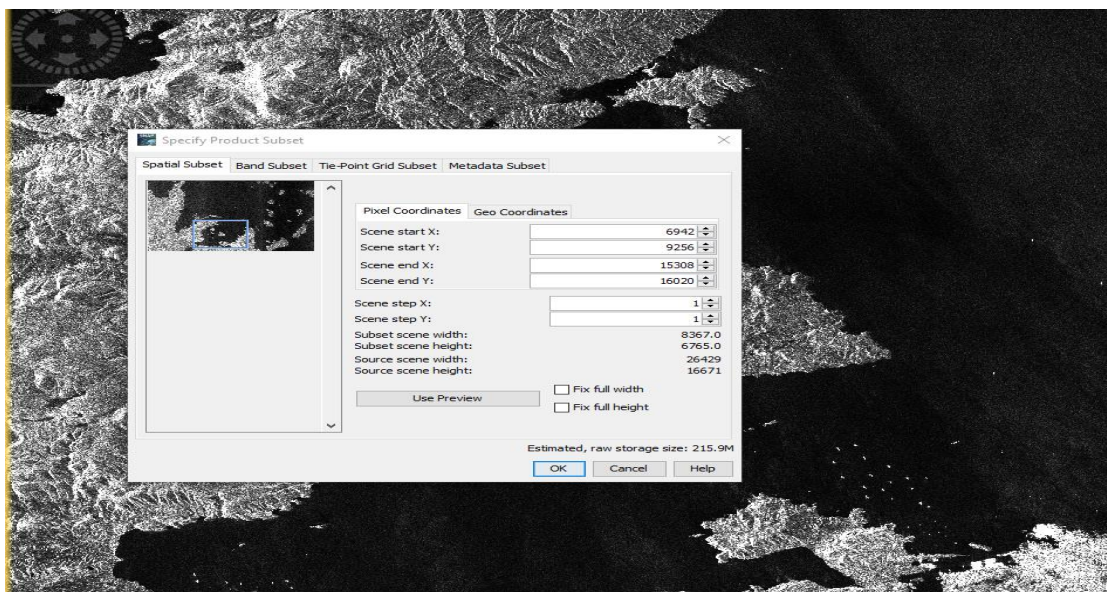


Figure 47: Specified product subset is selected due to the large processing time that would be needed

After the subset, we applied an **orbit file** so each sentinel product includes orbit state vectors provided in the meta data and to make sure the geocoding process will bring accurate results. Generally, the ones provided with the data are not accurate and can be refined with the precise orbit files that are available days to weeks after the generation of the product. The orbit file provides accurate satellite position and velocity information and based on this we can use the orbit file function to update the meta data.

The next step was optional. We performed a **speckle filtering** at first to reduce the noises in the ocean water body. About the processing parameters, we used Lee filter with 3x3 window size. We tested different speckle filter algorithms, noise in the ocean had been reduced and the image was a lot clearer. However, speckle filtering was softening the sharp values in certain areas quite a bit and as a result the ocean object algorithm mentioned below, did not classify the ships correctly. In our case, we did not include the speckle filtering function.

4.2.3 Ocean object detection algorithm

The snap **ocean object detection** includes land masking function by default. Land masking function is performed by looking at the SRTM digital elevation model, selecting area and masking out those with positive elevation. However, this method can sometimes introduce false targets along with complicated coastlines. Therefore, we could import and use our own vector mask but that requires to be loaded into the product as an ESRI shapefile. For the land sea mask, we followed the default setting.

The SAR data such as these needs to be calibrated because the pixel values can be directly related to the radar backscatter of the scene and though uncalibrated SAR imagery is sufficient for qualitative use, calibrated SAR images are essential for quantitative use.

The next step was an **adaptive thresholding** which was the main function of the ocean object detection. We defined the target window size which should be in this case set to 30 (smallest target such as ships, or cargos), since it should be the size of the smallest detectable object and it is mostly dependent on data resolution. Although pixel spacing is ten by ten meters, the resolution is twenty by twenty meters and therefore to avoid excessive number of false alarms, we set larger detectable target window size to thirty meters. The guard window (largest target size to detect) is set to 500 meters and the background window (background area to differentiate the target with the background, this should be wide enough to cover the guard window) is set to 800 meters.

The **PFA** or the probability of false alarm was set to minus 10. The exponent here could have been changed, however for our purposes the value was enough.

The **object discrimination** was the next step, so once we performed the adaptive thresholding, we then filtered all the detected targets and checked their sizes. Any target smaller than the minimum target size was eliminated and any target largest than the maximum target size was also thrown away. The result of the ocean object detection algorithm can be seen in Figure 47.

The imagery was geocoded and terrain corrected after the object discrimination using range-doppler algorithm. The input was the final detection product. As processing parameters were used the default ones and also, we unchecked the "Mask area with no elevation" box. The final image with the output detected ships was geocoded and terrain corrected following the true map projection. These detections would be later on exported to a shaped file and be processed further in QGIS software. A complete graph builder window is shown below in Figure 48.

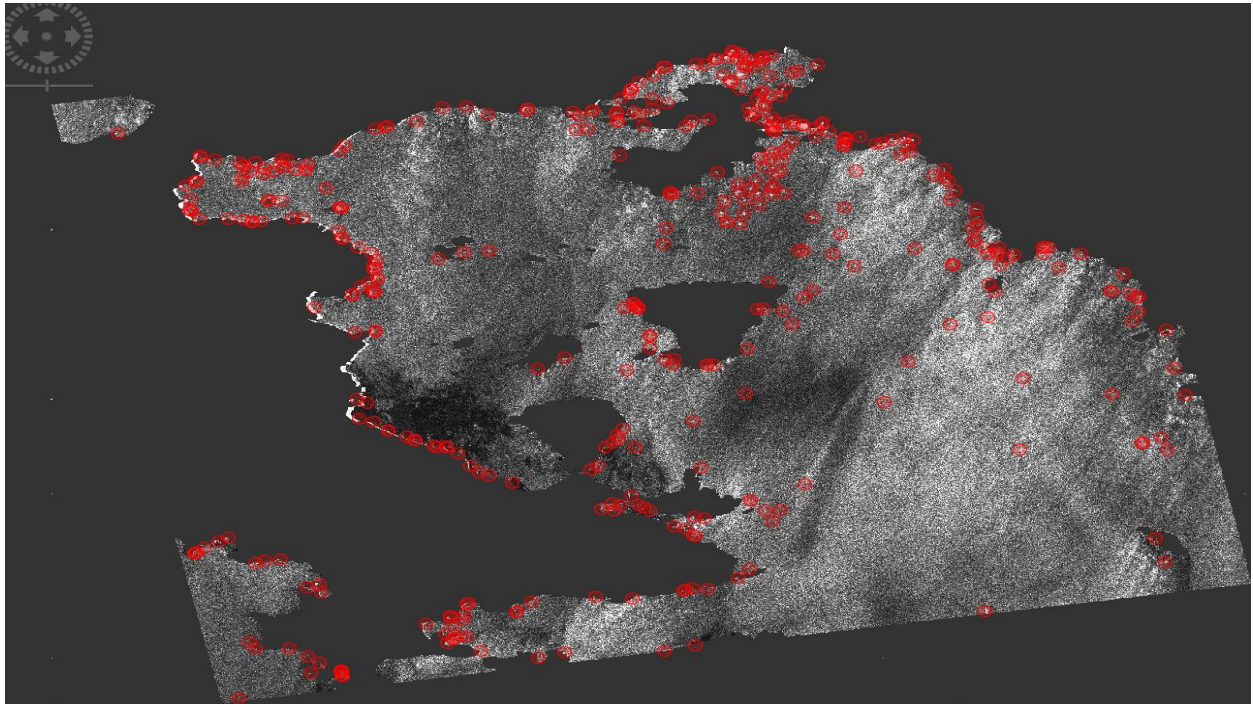


Figure 48: The result of the ocean object detection algorithm along with the terrain-correction. The red circles represent ships or boats with a target window size of 30. The ship detection points are available only after we add them through the layer manager tool window on the right.

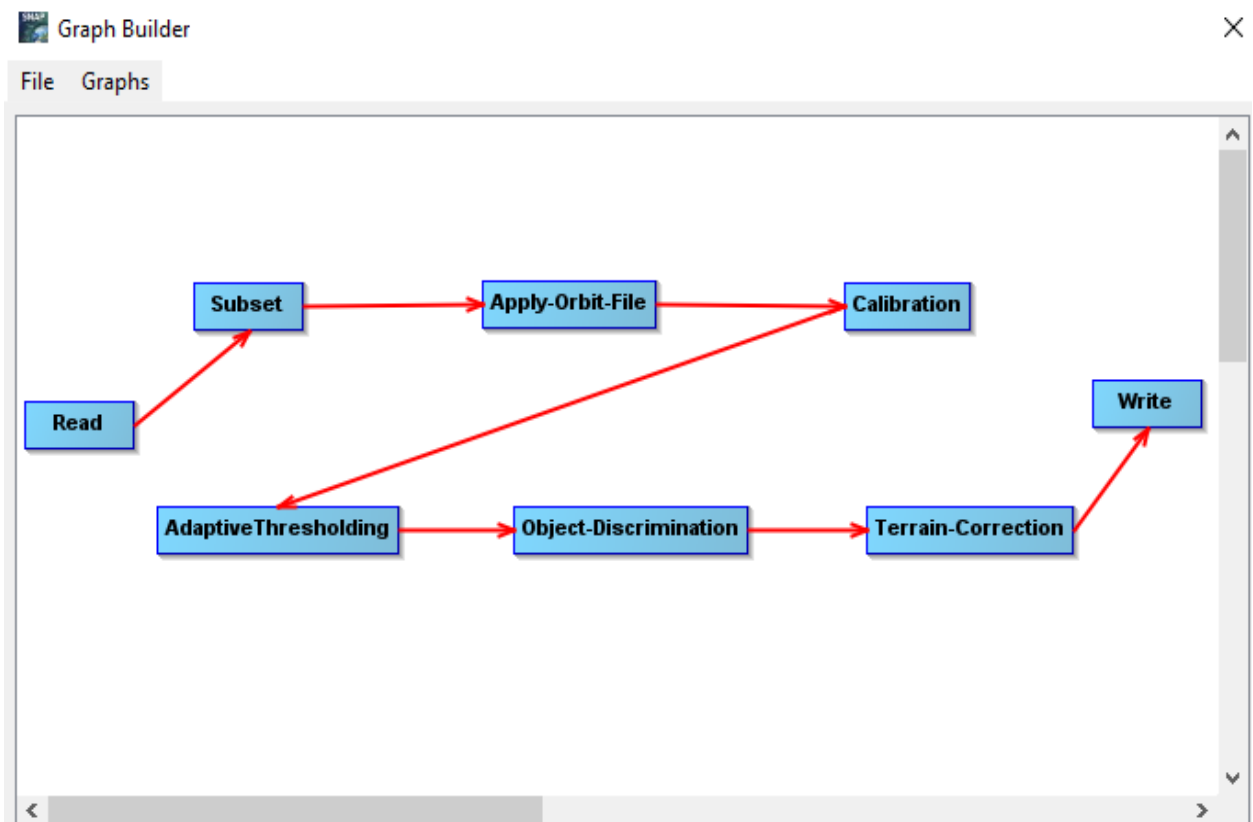


Figure 49: The graph builder tool illustrates the steps and the functions that were used in object and ship detection simulation

4.2.4 Vector data visualization in QGIS

The vector data was extracted from the product dataset and afterward was imported in the QGIS software for visualization and demonstration. The shapefile created during the extraction included values of the position of the circle marks, each one representing a ship and geocoded information. On QGIS toolbar we selected **Layer -> Add Layer -> Add Delimited Text Layer** and we chose the file that was saved as **.shp**. The second layer that was activated during the simulation included a Google Satellite map of the Argosaronic region (Figure 49).

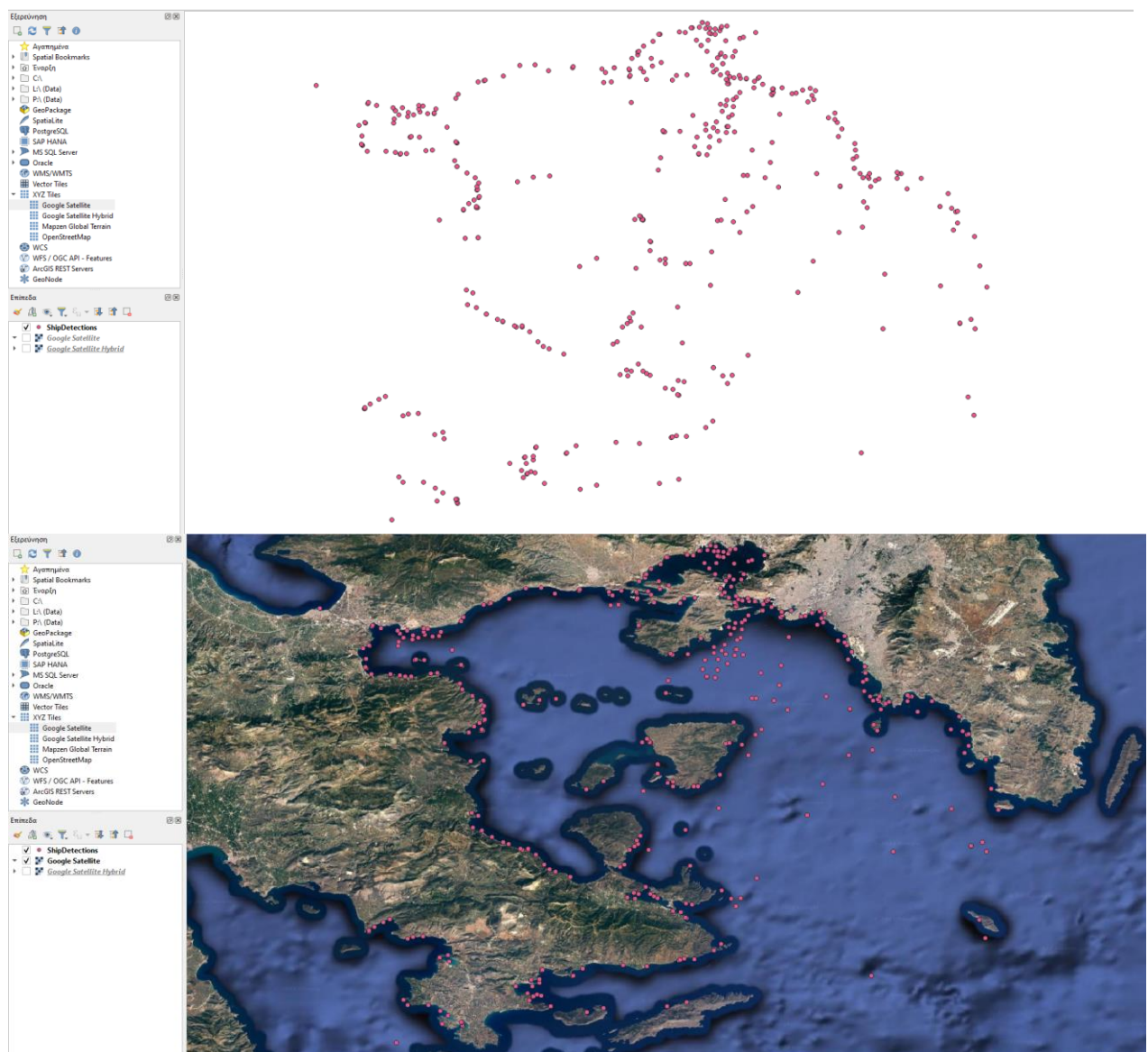


Figure 50: Vector points projected in QGIS on a Google Satellite map. Upper image shows the layer of vector points in a terrain corrected way while the bottom image is a combination of the google satellite map and the vector points.

Points were modified using the detected length values and were classified in 8 classes graduated from 0 to 290 to show the variations of each ship size in Figure 50 and Figure

51. Depending on the value, points take a different shade of red. The larger the ship, the redder the mark.

✓	○	10,00 - 30,00	10 - 30
✓	○	30,00 - 50,00	30 - 50
✓	○	50,00 - 80,00	50 - 80
✓	○	80,00 - 120,00	80 - 120
✓	○	120,00 - 160,00	120 - 160
✓	○	160,00 - 210,00	160 - 210
✓	○	210,00 - 260,00	210 - 260
✓	○	260,00 - 290,00	260 - 290

Figure 51: Classified ship size values

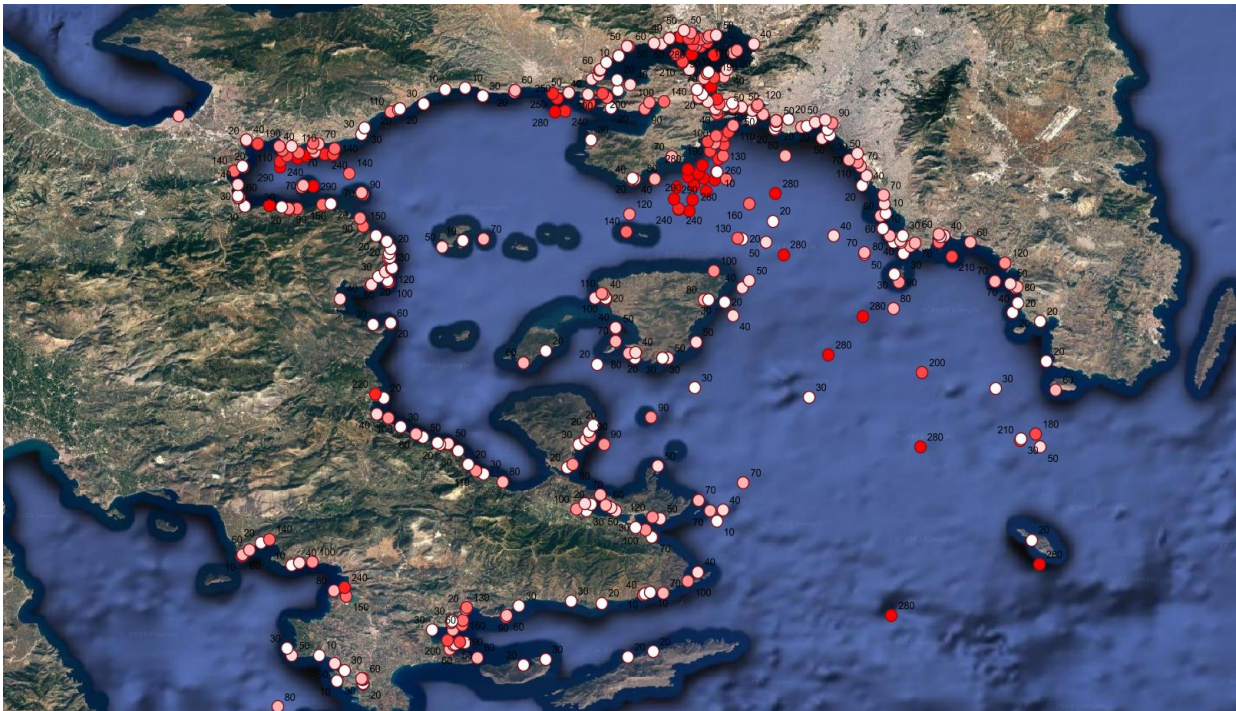


Figure 52: The graduated points were added in the Google Map Terrain to provide the best possible visualization of the detected ships.

However, to adjust the points and replace them with real ships through a visual representation, we will need to add Sentinel-2 visual data. This would help to later implement a machine learning algorithm that would detect any ship carrying dangerous cargo and categorize it as we mentioned previously.

5. CONCLUSION

5.1 Results

In this current thesis, EO has been highlighted and tested whether can be used for maritime surveillance for different operations. Sentinel-1 and Sentinel-2 marine data were used, as well as the SNAP and QGIS software for image processing and visualization of the results on the Earth map. Parameters and variables related to the procedures were implemented and adjusted according to the needs of each thematic area. Table 8 below presents a complete summary of the advantages and disadvantages of each scenario.

The processing of oil spill detection was performed based on internet references, theses and published articles in scientific journals. Two images of the Persian Gulf with a time difference of one month (April-May 2022) were used. There were some difficulties in using the automated function for oil spill detection as the image had a huge extension of dark spots. The algorithm was time consuming and did not complete due to low graphics card and processor performance. It was tested on 3 computers, 2 of them did not manage to complete the process. Unfortunately, it was not possible to limit the image size into a small subset, because valuable information would be lost and a large area of interest would be discarded. Instead, texture analysis was applied and a math band equation was incorporated for a threshold value equal to -23 dB as more efficient and secure. A variety of filters were used to smooth and homogenize the image pixels. A 5x5 arithmetic mean filter was preferred to reduce the false alarms of oil spill pixels due to the low backscatter. The results were very encouraging because the image included the true positive values and rejected several of the false positives. The chain process from the beginning to the visualization of the image to QGIS takes about 15 minutes, and this is due to the large number of pixels that had to be rendered. On a different computing system with increased capabilities, oil spill detection would take less time.

Optical data of Sentinel-2 were used in the second simulation for the Gulf of Bothnia with a sensor date of February 22, 2022. The preprocessing steps took less time than the first simulation design because many functions did not need to be performed. However, the bands did not have the same resolution and a resample was applied and in addition a simple mathematical equation was needed to reduce the effect of clouds that had disoriented the classifier and complicated the clustering. The classification took 10 minutes on a simple desktop computer and was successful with satisfactory results thanks to the three classification algorithms KD, KNN and RF present in SNAP. Of the unsupervised classification, only K-means with 5 or 7 classes managed to adequately group the different classes which were: water, soil, new ice, thin ice and thick ice. The most successful classification was supervised when the user fed training data to the algorithm. The best performing classifiers were KNN, KD and RF, because visually they gave almost even results without many wrong registrations of pixels in the different classes. Each type of ice was divided into layers that were placed in QGIS along with the Google map and gave a very neat visualization.

In the case of the third simulation scenario, a SAR image taken on 25 May 2022 depicting the Strait of Gibraltar was selected. The process of calculating the wind direction and speed followed an automated processing flow that is widely performed on the SAR images. The results were unexpected as the wind direction at the top and bottom follows an irregular course with extreme speed differences. We do not know if there were extreme weather conditions in the area during that period that disrupted the strait. The most likely

scenario is that some values during the calibration and application of the wind-field-estimation contain errors regarding direction and speed. The second logical explanation is that the window size used to calculate the wind field was quite small resulting in many values in a small square space, which as a result, reduced the efficiency of the algorithm. However, it is a very good representation quite close to the actual wind field.

The last scenario was ocean object detection. The product was once again, a SAR image of the Argo Saronic Gulf in Attica taken on July 2, 2022. The processing was performed based on a chain process that included, apply orbit file, calibration, land sea mask, adaptive thresholding, object discrimination and terrain correction functions. The size of the target window, guard window and background window were adjusted several times to end up with the fewest false alarms we could achieve which was close to 30%. The PFA was also changed and tested at 10 and 12.5 but we settled on 10 as optimal. The last parameter in object discrimination worked better for a minimum target size of 30 than for 20. The objects it detected for a target size of 20 were usually consecutive pixels of the sea which, due to backscatter, considered them as objects, increasing the false alarm to 50%. In this simulation and the above, the vector points were imported as layers in QGIS along with the Earth map, for visual representation.

Table 8: Advantages and disadvantages of each EO scenario

Subject	Advantages	Disadvantages
Oil Spill Detection	<ul style="list-style-type: none"> • Easy to apply algorithms on SAR images • Texture analysis without complicated methods • Huge amount of SAR data available • Overly useful for navigation, processing in real time possible 	<ul style="list-style-type: none"> • Sea often appears to be dark in SAR images making oil detection hard • Needs experience to detect false alarms • Satellite sensors cannot distinguish biogenic oil from mineral oil
Sea Ice Classification	<ul style="list-style-type: none"> • Overly useful for navigation, processing in real time possible • Products can be derived from satellites images, aerial photographs or videos on board • The different types of ice can be detected in the visible and near-infrared spectrum 	<ul style="list-style-type: none"> • Data and photographs must be taken during the same flight to cover the same ice • Difficult to analyze ice types in SAR due to thermal noise • Cloud coverage interacts in optical data • Optical data is harder to obtain due to longer revisit time of satellites

<p>Wind Speed and Direction</p>	<ul style="list-style-type: none"> • Satellite wind mapping is a useful tool for quick assessments of wind conditions • Easy to apply on SAR images • Microwave sensitivity to surface roughness allows SAR images to be exploited for accurate estimation of surface wind (speed and direction) 	<ul style="list-style-type: none"> • Thermal noise can saturate image and disorient mathematical models of wind speed estimation • Real time processing not possible • Needs to be further analyzed on a GIS software • SAR images can only predict wind speed and direction
<p>Ship Detection</p>	<ul style="list-style-type: none"> • Continuous and all-weather, ship information and motion can be provided from the surface of the sea • SAR technology can be used in areas with intense weather conditions or in areas with heavy cloud cover • Tools for ocean object detection are suitable for rapid mapping • Rapid ship extraction produces less false alarm with minimal time-consuming process 	<ul style="list-style-type: none"> • Needs experience to perform sufficiently ship extraction without machine learning algorithm • Needs to be further analyzed on a GIS software • SAR and optical data may need to be combined to increase performance of ship detection • Real time not possible • Ships in highly cluttered area are hard to detect

5.2 Future studies and analysis

To verify the above results, more research and studies should be done on SAR images and mainly texture analysis. Machine learning algorithms combined with big data are capable of extracting verified data. Other applications in oil spill detection can exploit wind fields and prevent an environmental disaster. Challenges lie on finding how satellites will be able to distinguish crude oil from other biogenic oils. Therefore, obtaining reliable information about the location, extent, and movement characteristics of ocean oil spill is required to mitigate oil pollution risks and damages.

Many future applications in space missions are possible when exploring the temporal dimension of new datasets. For example, there is potential to use the higher temporal resolution of Sentinel-2 (in conjunction with other satellites such as Landsat 8) to monitor glaciers and ice sheets.

Further experiments and simulations are needed to make a ship detection system fully operational. Combined with the use of an AIS, it offers maintenance of sea traffic, protection against illegal fishing, maritime border activity or protection against maritime piracy. In that case, individual images only provide information about the situation at a specific point in time. To be able to track the progression and development of the event, a time series of images is needed. This cannot be achieved with single satellites and to

persistently monitor an area, multiple satellites are required to ensure fast data acquisition with high revisit capabilities.

In summary, the applicability of the toolboxes to future space missions may be considered sufficient to a point. Acquiring more SAR and optical data, with the help of machine learning, can produce accurate and timely results. Thus, the simulation's design can be extended by taking into account the above assumption and can be used to examine additional scenarios or even combinations of the implemented scenarios.

TABLE OF TERMINOLOGY

Ξενόγλωσσος όρος	Ελληνικός Όρος
Applicability	Εφαρμοστικότητα
Atmospheric forcing	Ατμοσφαιρική επιβολή
Automated Identification System	Αυτοματοποιημένο σύστημα αναγνώρισης
Backscattering	Οπισθοσκέδαση
Cloud coverage	Ατμοσφαιρική κάλυψη
Dispersal patterns	Μοτίβα διασποράς
Earth observation	Γεωπαρατήρηση
False alarm	Ψευδές σήμα ανίχνευσης
Homogeneous areas	Ομοιογενείς περιοχές
Interferometry	Συμβολομετρία
Maritime shipping	Ναυτιλία
Multitemporal observations	Πολυχρονικές παρατηρήσεις
Neural network	Νευρωνικά δίκτυα
Pixel	Εικονοστοιχείο
Polarized	Πολωμένος
Principal component analysis	Ανάλυση κυρίων συνιστωσών
Probability of detection	Πιθανότητα ανίχνευσης
Propagation	Διάδοση
Radiometric characteristics	Ραδιομετρικά χαρακτηριστικά
Remote sensing	Δορυφορική τηλεπισκόπηση
Revisit time	Χρόνος επανεπισκεψιμότητας
Simulation model	Μοντέλο προσομοίωσης
Spatial resolution	Χωρική ανάλυση
Spectral	Φασματικός
Surveillance	Επιτήρηση
Synthetic Aperture Radar	Ραντάρ συνθετικού ανοίγματος
Texture analysis	Ανάλυση υφής
Threshold	Κατώφλι
Training data	Δεδομένα εκπαίδευσης
Un/supervised classification	Μη/επιβλεπόμενη ταξινόμηση
Variability	Μεταβλητότητα

ABBREVIATIONS – ACRONYMS

3C2N	Cascade Coupled Convolutional Neural Network
AIS	Automatic Identification System
AOT	Aerosol Optical Thickness
BOA	Bottom-Of-Atmosphere
CNN	Convolutional Neural Network
DEM	Digital Elevation Model
DFT	Discrete Fourier Transform
DL	Deep Learning
ECC	European Commission initiative Copernicus
EEA	European Environment Agency
EO	Earth Observation
ESA	European Space Agency
FDA	Fisher Discriminant Analysis
GDP	Gross Domestic Product
GLRT	Generalized Likelihood Ratio Test
GMES	Global Monitoring of Environment and Security
GOCE	Gravity field and steady-state Ocean Circulation Explorer
GRD	Ground Range Detected
HOG	Histogram of Oriented Gradient
IMSBC	International Maritime Solid Bulk Cargoes
ISA	Italian Space Agency
MIF	Maritime Interdiction Forces
NN	Neural Network
NRCS	Normalized Radar Cross-Section
OOS	Ocean Oil Spill
ORSS	Ocean Remote Sensing Systems
QGIS	Quantum Geographic Information System
SAR	Synthetic Aperture Radar
SCL	Scene Classification
SDG	Sustainable Development Goal

SI	Sea Ice
SMOS	Soil Moisture and Ocean Salinity
SNAP	Sentinel Application Platform
SRTM	Shuttle Radar Topography Mission
TCI	True Color Image
TCR	Target-to-Clutter Ratio
TEU	Twenty-foot Equivalent Unit
TOA	Top-Of-Atmosphere
UAV	Unmanned Aerial Vehicle
UVNS	Ultra-violet, Visible and Near-infrared
VGG	Visual Geometric Group
VH	Vertical Horizontal
VHF	Very High Frequency
VTS	Vessel Traffic Services

REFERENCES

- [1] Wikipedia, «History of navigation» 25 July 2022, Available on: https://en.wikipedia.org/wiki/History_of_navigation. [Accessed on 20 April 2022]
- [2] Alan P. Trujillo, Harold V. Thurman, «Essentials of Oceanography», 7th edition, California: Prentice Hall, 2001.
- [3] Jeff Toghil, «Celestial Navigation», Reprint edition, New York: W. W. Norton & Company, 1988.
- [4] Dava. Sobel, «Longitude: the true story of a lone genius who solved the greatest scientific problem of his time», New York: Penguin Books, 1996.
- [5] E. Commision, «The EU Blue Economy report 2020» Press release, Brussels, 2020.
- [6] International Chamber of Shipping, «Shipping and world trade: driving prosperity» 2021, Available on: <https://www.ics-shipping.org/shipping-fact/shipping-and-world-trade-driving-prosperity/>
- [7] Magirou Evangelos, Psaraftis Harilao, Christodoulakis Nikolaos, Thesis(Bachelor) «Quantitive methods in shipping: A survey of current use and future trends» Athens, 1992
- [8] Wikipedia, «2021 Suez Canal obstruction», last edit on 31 August 2022. [E-source]. Available on: https://en.wikipedia.org/wiki/2021_Suez_Canal_obstruction. [Accessed on 20 April 2022].
- [9] Wikipedia, «Prestige oil spill» last edit on 26 June 2022. Available on: https://en.wikipedia.org/wiki/Prestige_oil_spill. [Accessed on 20 April 2022].
- [10] T. Soukissian και M.-A. Sotiriou, «Long-Term Variability of Wind Speed and Direction in the Mediterranean Basin,» *Wind*, Volume 2, pp. 513-534, 2022.
- [11] Stein & Johannessen, Ola & Kloster, K. Sandven, «Sea Ice Monitoring by Remote Sensing» 2006.
- [12] Nasa, Earth Observatory «Ice on the St Lawrence River, Canada», 2010.
- [13] Hamid & Mahdianpari, Masoud & Homayouni, Saeid & Mohammadimanesh, Fariba & Daboor, Mohammed Jafarzadeh, «Oil spill detection from Synthetic Aperture Radar Earth observations: a meta-analysis and comprehensive review» *GIScience & Remote Sensing*, 2021.
- [14] Benjamin Holt, Kan Zeng, Werner Alpers, «Oil spill detection by imaging radars: Challenges and pitfalls», *Remote Sensing of Environment*, Volume 201, pp 133-147, 2017
- [15] Meisam & Ghorbanian, Arsalan & Asgarimehr, Milad & Yekkehkhany, Bahareh & Moghimi, Armin & Jin, Shuanggen & Naboureh, Amin & Mohseni, Farzane & Mahdabi, Sahel & Farsad, Layegh, Nasir Amani, «Remote Sensing Systems for Ocean: A Review (Part 1: Passive Systems)», *Journal of Selected Topics in Applied Earth Observations and Remote Sensing*, pp. 1-1, 2021.
- [16] Matthias Grote, Nicole Mazurek, Carolin Gräbsch, Jana Zeilinger, Stéphane Le Floch, Dierk-Steffen Wahrendorf, Thomas Höfer, «Dry bulk cargo shipping — An overlooked threat to the marine environment?», *Marine Pollution Bulletin*, Volume 110, pp. 511-519, 2016.
- [17] Ping Huang, Jingyan Zhang, «Facts related to August 12, 2015 explosion accident in Tianjin, China», Volume 34, pp. 313-314, 2015.
- [18] Αστάρας Θεόδωρος Αλεξάνδρου, «Τηλεπισκόπηση - φωτοερμηνεία στις γεωεπιστήμες», Θεσσαλονίκη: Γκιούρδας, *Edition 1*, 2010.
- [19] Randolph H. Wynne, James B. Campbell, «Introduction to Remote Sensing», New York, London, 5th ed., The guildford press, 1996.
- [20] Prashant K. Srivastava, Ramandeep Kaur M. Malhi, Prem Chandra Pandey, Akash Anand, Prachi Singh, Manish Kumar Pandey, Ayushi Gupta, «Revisiting hyperspectral remote sensing: origin, processing, applications and way forward», Elsevier, pp. 3-21, 2020.
- [21] «Astron, delivering environemntal intelligence», Available on : <http://www.astron.com.au/news/remote-sensing-platforms-which-will-work-for-your-/>
- [22] Marco Reggiannini, Marco Righi, Marco Tampucci, Angelica Lo Duca, Clara Bacciu, Luigi Bedini, Andrea D' Errinco, Claudio Di Paola, Andrea Marchetti, Massio Martinelli, Costanzo Mercurio, Emanuele Salerno and Bruno Zizi, «Remote Sensing for Maritime Prompt Monitoring», *Journal of Marine Science and Engineering*, Institute of information science and technologies, national research council of Italy, 2019.

- [23] ESA'S Gravity Mission, «www.earth.esa.int» Available on: <https://earth.esa.int/eogateway/documents/20142/37627/GOCE-ESAs-Gravity-Mission.pdf>, [Accessed on 25 April 2022].
- [24] Ν. Καλαμπόγιας, Μ. Καμποσούλη, Γ. Μπουμπάκης, Σ. Φαχουρίδη κ. Δ. Δεληκαράογλου «Χαρτογραφώντας το πεδίο βαρύτητας της Γης ... σε High Definition: Η δορυφορική αποστολή GOCE», ΓΕΩΔΑΙΣΙΑΣ Δείγματα & Παραδείγματα, 2012.
- [25] ESA, «Cryosat Mission», [E-source]. Available on: https://www.esa.int/Enabling_Support/Operations/CryoSat-2_operations. [accessed on 20 April 2022]
- [26] ESA, «Sentinel-1 mission», [E-source]. Available on: <https://sentinel.esa.int/web/sentinel/missions/sentinel-1>. [accessed on 20 April 2022]
- [27] ESA, «Sentinel-2 mission», [E-source]. Available on: <https://sentinel.esa.int/web/sentinel/missions/sentinel-2>. [accessed on 20 April 2022]
- [28] SA, «Sentinel-3 mission», [E-source]. Available on: <https://sentinel.esa.int/web/sentinel/missions/sentinel-3>. [accessed on 21 April 2022]
- [29] ESA, «Sentinel-5 mission», [E-source]. Available on: <https://sentinel.esa.int/web/sentinel/missions/sentinel-5>. [accessed on 21 April 2022]
- [30] Copernicus, «Copernicus Program», [E-source]. Available on: <https://www.copernicus.eu/en>, [Accessed on 21 April 2022]
- [31] Fingas, Merv and Carl E. Brown, «A Review of Oil Spill Remote Sensing», *Sensors, (Basel, Switzerland)*, Volume 18, p. 91, 30 Dec. 2017.
- [32] Werner Alpers, Benjamin Holt, Kan Zeng, «Oil spill detection by imaging radars: Challenges and pitfalls», *Remote Sensing of Environment*, Volume 201, pp. 133-147, 2017.
- [33] Solberg, A.H.S., Brekke C., «Oil Spill Detection in Northern European Waters: Approaches and Algorithms», Springer Science and Business Media Barale V., Gade M., Oslo, 2008.
- [34] Werner Alpers, Gade Martin, Christian Melsheimer, «Investigation of multifrequency/multipolarization radar signatures of rain cells over the ocean using SIR-C/X-SAR data», Issue 9, Volume 103, pp. 18867-18884, 1998.
- [35] Girard-Ardhuin, Fanny & Mercier, G. & Collard, Fabrice & Garello, René, «Operational Oil-Slick Characterization by SAR Imagery and Synergistic Data» *Journal of Oceanic Engineering*, Volume 30, pp. 487-495, 2005.
- [36] Government of Canada, «Oil Slick Detection» Canada, 2015, Available on: <https://www.nrcan.gc.ca/maps-tools-and-publications/satellite-imagery-and-air-photos/satellite-imagery-products/educational-resources/tutorial-radar-polarimetry/oil-slick-detection/9525>, [Accessed on 2 May 2022]
- [37] RUS Copernicus, «Oil spill mapping with Sentinel-1» 2018, Available on: <https://rus-copernicus.eu/portal/rus-webinar-oil-spill-mapping-with-sentinel-1/>, [Accessed on 2 May 2022]
- [38] Misra A., Balaji R., «Simple Approaches to Oil Spill Detection Using Sentinel Application Platform (SNAP)-Ocean Application Tools and Texture Analysis: A Comparative Study», *Indian Soc Remote Sens*, Volume 45, p. 1065–1075, 2017.
- [39] Renner A., Hendricks S., Gerland S., Beckers J., Haas C., & Krumpen T., «Large-scale ice thickness distribution of first-year sea ice in spring and summer north of Svalbard», *Annals of Glaciology*, pp. 13-18, 2013.
- [40] Josefino C. Comiso, Claire L. Parkinson, Robert Gersten, Larry Stock, «Accelerated decline in the Arctic sea ice cover», Volume 35, Issue1, 2008.
- [41] Angelika H.H. Renner, Marie Dumont, Justin Beckers, Sebastian Gerland, Christian Haas, «Improved characterisation of sea ice using simultaneous aerial photography and sea ice thickness measurements» *Cold Regions Science and Technology*, Volume 92, pp. 37-47, 2013.
- [42] Slater Thomas & Lawrence Isobel & Otosaka Inès & Shepherd Andrew & Gourmelen Noel & Jakob Livia & Tepes Paul & Gilbert Lin & Nienow P. «Review article: Earth's ice imbalance» *The Cryosphere*, Volume 15, pp. 233-246, 2021.

- [43] Huang, Wenfeng & Lu, P. & Lei, Ruibo & Xie, Hongjie & Li, Zhijun, «Melt pond distribution and geometry in high Arctic sea ice derived from aerial investigations», *Annals of Glaciology*, Volume 57, pp. 1-14, 2016.
- [44] Inoue, Jun & Kikuchi, Takashi & Perovich, Donald, «Effect of heat transmission through melt ponds and ice on melting during summer in the Arctic Ocean» *Journal of Geophysical Research*, Volume 113, 2008.
- [45] Lars Kaleschke, Anja Rösel, «Exceptional melt pond occurrence in the years 2007 and 2011 on the Arctic sea ice revealed from MODIS satellite data» *Journal of geophysical research*, Issue 5, Volume 117, pp. 37-47, 2012.
- [46] Christina A. Pedersen, Erin Roeckner, Mikael Lüthje, Jan-Gunnar Winther, «A new sea ice albedo scheme including melt ponds for ECHAM5 general circulation model» *Journal of Geophysical Research*, 2009.
- [47] Wright N. C. and Polashenski C. M., «Open-source algorithm for detecting sea ice surface features in» *The Cryosphere*, Volume 12, 2018.
- [48] T. Blaschke, «Object based image analysis for remote sensing», *Journal of Photogrammetry and Remote Sensing*, Volume 1, Issue 65, pp. 2-16, 2010.
- [49] Thomas Blaschke, Geoffrey J. Hay, Maggi Kelly, Stefan Lang, Peter Hofmann, Elisabeth Addink, Raul Queiroz Feitosa, Freek van der Meer, Harald van der Werff, Frieke van Coillie, Dirk Tiede, «Geographic Object - Based Image Analysis – Towards a new paradigm», *Journal of Photogrammetry and Remote Sensing*, Volume 87, pp. 180-191, 2014.
- [50] S. Khaleghian, H. Ullah, T. Kræmer, N. Hughes, T. Eltoft and M. A., «Sea Ice Classification of SAR Imagery Based on Convolution Neural Networks», *Remote Sens*, Volume 13, p. 1734, 2021.
- [51] Du Yong, Vachon Paris W., Wolfe John, «Wind direction estimation from SAR images of the ocean using wavelet analysis», *Canadian Journal of Remote Sensing*, 2002.
- [52] López, P. & Velo, R. & Maseda, F., «Effect of direction on wind speed estimation in complex terrain using neural networks» *Renewable Energy*, Volume 33, pp. 2266-2272, 2008.
- [53] Haoyu Jiang, «Wind Speed and Direction Estimation from Wave Spectra using deep Learnings», China University of Geosciences, 2022.
- [54] James S., «Using Sentinel-1 SAR satellites to map wind speed variation across offshore wind farm clusters», *Journal of Physics: Conference Series*, 2017.
- [55] Corazza Alexandre & Khenchaf Ali & Comblet Fabrice, «Assessment of Wind Direction Estimation Methods from SAR Images», *Remote Sensing*, Volume 12, 2020.
- [56] Wikipedia, «Automatic identification system», edited on 19 August 2022 [E-source] Available on: https://en.wikipedia.org/wiki/Automatic_identification_system. [Accessed on 22 April 2022].
- [57] J. Zhao, Z. Zhang, W. Yu, and. T. - K. Truong, «A Cascade Coupled Convolutional Neural Network Guided Visual Attention Method for Ship Detection From SAR Images», *IEEE Access*, Volume 6, pp. 50693-50708, 2018.
- [58] P. Iervolino, «Ship detection in SAR imagery: A comparison study», *IEEE International Geoscience and Remote Sensing Symposium (IGARSS)*, pp. 2050-2053, 2017.
- [59] M. Tsvetkova, N. Kolev, A. Hristov, and C. Alexandrov, «AIS Assisted Sentinel-1 SLC Image Ship Detection, Motion and Displacement Estimation», *EUSAR 2021, 13th European Conference on Synthetic Aperture Radar*, pp. 1-5, 2021.
- [60] Firdaus Hana & Pribadi Cherie & Filsa Bioresita H. Bioresita, «Ship detection in Madura Strait and Lamong Gulf using Sentinel-1 SAR Data», *Digital Press Physical Sciences and Engineering*, Volume 1, 2018.
- [61] No. 01-02: «Collision danger in the Persian Gulf and Strati of Hormuz Loss Prevention Circular», No. 01-02, [E-source] Available on: <https://www.gard.no/web/articles?documentId=7937>. [Accessed on 15 May 2022]